ALTERNATIVE TECHNOLOGIES FOR INLAND DESALINATION

by

Andrea F. Corral

_____

A Dissertation Submitted to the Faculty of the

DEPARTMENT OF CHEMICAL AND ENVIRONMENTAL ENGINEERING

In Partial Fulfillment of the Requirements

For the Degree of

DOCTOR OF PHILOSOPHY

WITH A MAJOR IN ENVIRONMENTAL ENGINEERING

In the Graduate College

THE UNIVERSITY OF ARIZONA

2014

THE UNIVERITY OF ARIZONA

GRADUATE COLLEGE

As members of the Dissertation Committee, we certify that we have read the dissertation prepared by Andrea F. Corral entitled Alternative Technologies for Inland Desalination and recommend that it be accepted as fulfilling the dissertation requirement for the Degree of Doctor of Philosophy

_____Date: 08/06/14

Wendell P. Ela

_____Date: 08/06/14

Robert G. Arnold

_____Date: 08/06/14

A. Eduardo Sáez

Final approval and acceptance of this dissertation is contingent upon the candidate's submission of the final copies of the dissertation to the Graduate College.
I hereby certify that I have read this dissertation prepared under my direction and recommend that it be accepted as fulfilling the dissertation requirement.

_____Date: 08/06/14

Dissertation Director: Wendell P. Ela

_____Date: 08/06/14

Dissertation Director: Robert G. Arnold

STATEMENT BY AUTHOR

This dissertation has been submitted in partial fulfillment of requirements for an advanced degree at the University of Arizona and is deposited in the University Library to be made available to borrowers under rules of the Library.

Brief quotations from this dissertation are allowable without special permission, provided that accurate acknowledgment of source is made. Requests for permission for extended quotation from or reproduction of this manuscript in whole or in part may be granted by the head of the major department or the Dean of the Graduate College when in his or her judgment the proposed use of the material is in the interests of scholarship. In all other instances, however, permission must be obtained from the author.

SIGNED: Andrea F. Corral

ACKNOWLEDGEMENTS

I would like to express my deep appreciation and gratitude to my advisors, Dr. Wendell P. Ela and Dr. Robert G. Arnold, for the patience guidance and mentorship they provided to me all these years throught the completion of this degree. Thank you for allowing me to develop critical thinking and challenge me to become a better researcher. I would also like to thank Dr. Eduardo Saez, for his direction as part of my dissertation committee, and the faculty at the Department of Chemical and Environmental Engineering for the contribution that each of them made to my intellectual growth during my years at the University of Arizona.

This work would not have been possible without the help and technical expertise from Philip Anderson and Steven Hernandez at the University Spectroscopy and Imaging Facilities (USIF) who conducted XRD and SEM-EDs analysis. Robert Seaman from the Environmental Research Lab who was instrumental in the pilot-plant operation of this work. A special thank you to the adminsitrative staff, Arla Allen and Debi Romero for their continuos dedication and help.

I would like to thank everybody in the Solar Membrane Distillation Group and the SALT group for all their help to make this work possible. Specially to Vicky Karanikola, Hua Jiang, Patrick Mette, Roy Strickle and Jason Decker for all their help duirng the pilot plant operation and to all my friends that in some way or another have may this possible.

I would like to thank my parents and siblings for their continuos support and encouragement during all these years. My sincere gratitude to Umur for all his love, patience, help and advise throughout these years.

Finally, I would like to acknowledge the Bureau of Reclamation and the Carson Scholar Program for the financial support provided during these years.

DEDICATION

To my Mom and the strong women in my life.

TABLE OF CONTENTS

LIST OF FIGURES

LIST OF TABLES

ABSTRACT

Water scarcity is one of the biggest issues we have to face as population and water consumption levels increase despite a fixed supply of renewable fresh water. Meeting the challenges that water scarcity poses to food production, ecosystem health, and political and social stability will require new approaches to using and managing water. Desalination already plays an essential role in water management. It constitutes a secure source of safe drinking water supply once demand management measures are fully implemented. Overcoming problems related to brine minimization and disposal is key to sustainable, efficient inland water desalination. The main focus of this was the investigation of technical limits and improvements for application in inland desalination.

The first part of the dissertation covers the study of Membrane Distillation (MD) for desalination of water. The second part provides a broad perspective of Reverse Osmosis (RO), pretreatments –comparison of slow sand filtration and microfiltration-, post-mortem study of membranes to determining fouling and scaling causes, and RO brine minimization via Vibratory Shear Enhance Processing (VSEP®) for use in RO brine minimization.

The study of Vacuum Membrane Distillation in a hollow fiber membrane was studied. Experimental work is supported by an original mathematical model to expose the physics of VMD and support predictions that extend VMD results beyond these generated in the laboratory. The advantages and disadvantages of each pretreatment, including their effects the effect on the performance of RO, a post-mortem membrane study and an economic analysis. The post-mortem study of membranes used during

Yuma Desalting Plant operation. This work was used to identify the best pretreatment and more suitable membrane to treat saline water in the lower Colorado River. The work performed during the brine minimization study using VSEP®. This study included experimental data and an extensive economic analysis comparing Ion Exchange (IX) as pretreatment and VSEP® as post-treatment for RO.

CHAPTER 1

INTRODUCTION

The first part of the dissertation covers the study of Membrane Distillation (MD) for desalination of water. The second part provides a comparison of Microfiltration (MF) and Slow Sand filtration as pretreatments for reverse osmosis (RO). Additional sections are devoted to a post-mortem study of membranes from the 2010 Yuma Desalting Plant Study and an investigation of Vibratory Shear Enhance Processing (VSEP®) for use in RO brine minimization. Sections have in common the investigation of technical limits and improvements for application in inland desalination for salt management in water.

This chapter introduces the challenging issue of water scarcity and the need to find efficient ways to desalinate water. Relevant technical literature for membrane distillation (MD) and RO pre-treatment technologies is reviewed. A description of the principles in which MD is based; advantages and disadvantages, configurations and application to desalination are covered.

Chapters Two describes the work performed with MD. The study of Vacuum Membrane Distillation in a hollow fiber membrane was studied. Experimental work is supported by an original mathematical model to expose the physics of VMD and support predictions that extend VMD results beyond these generated in the laboratory.

Chapters Three, Four and Five are devoted to various aspects of RO treatments. Chapter Three compares MF and SSF as pretreatments for RO. This chapter entitles the

advantages and disadvantages of each pretreatment, including their effects the effect on the performance of RO, a post-mortem membrane study and an economic analysis. Chapter Four covers the post-mortem study of membranes used during Yuma Desalting Plant operation. This work was used to identify the best pretreatment and more suitable membrane to treat saline water in the lower Colorado River. Chapter Five provides a short description of the work performed during the brine minimization study using VSEP®. This study included experimental data and an extensive economic analysis comparing Ion Exchange (IX) as pretreatment and VSEP® as post-treatment for RO. Finally, Chapter Six summarizes the findings of each study and point the way toward additional supportive work.

1.1. Water Scarcity

The term "water scarcity" could be defined as the depletion of freshwater sources, reducing volume of water remaining for further human use and ecosystem support or the extent to which water demand exceeds available water resources [1].

Nowadays, about 1.2 billion people live in areas where water is physically scarce, if the current model of consumption is followed it is estimated that by 2025 around 2.7 billion people will face water scarcity [2]. Most of the developed societies take water as granted, however pollution, over-consumption, lack of conservation and urban planning policies, and drought are contributing to increase this problem. Water scarcity will impact not only the way we live but also every economic activity around the world. The availability of freshwater and its quality are essential for agriculture, power generation and any other industry. It has been said that our economy runs on water [3].

Agriculture and food production withdraws 2.5 times more water than industry and consumes 70% of the total freshwater in the world and it is expected to increase by 19% by 2050 [4-6]. This value varies from 80% up to 90% for arid or semiarid countries [7]. Industry withdraws from the environment 23% of the total freshwater, this value might change as countries become more industrialized and divert greater amounts of their water to industrial use [4, 8]. Finally, only 7% of the water is used by households [8]. Figure 1.1 shows the water consumption for each use in billions cubic meter since 1900 to 2025.

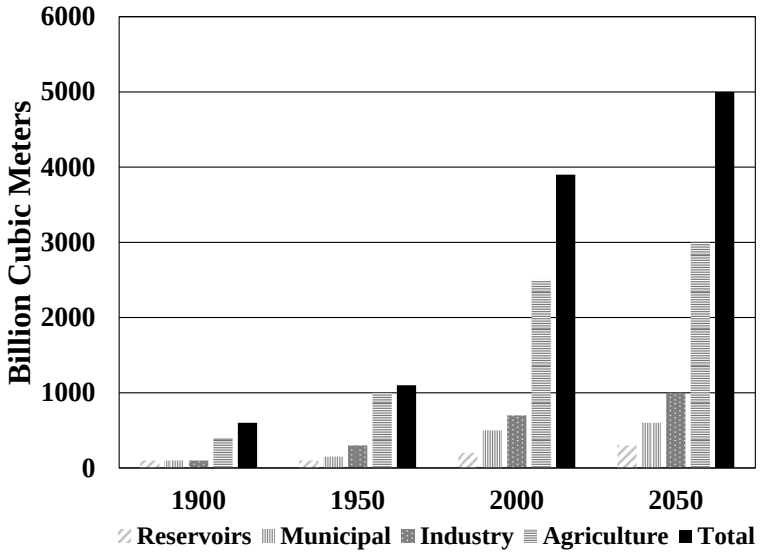

Figure 1.1. World water utilization from 1900 to 2025 in billions cubic meter. Adapted from [4]

Drought throughout the world has increased the threat of water scarcity. Drought intensity categories are based on temperature, precipitation, snowfall, dryness, and drought impacts among other indicators [9]. The drought monitor is consider a more versatile tool for determine drought conditions since is combines the best available data,

local observations and predictions from five different indicators (Palmer Drought Index, Climate Prediction Center Soil Moisture Model, U.S. Geological Survey's National Stream flow Information Program, Standardized Precipitation Index, and the Objective Short and Long-term Drought Indicator Blends). The Drought monitor summary map identifies drought areas by intensity:

- Abnormally Dry (D0), going into drought: short-term dryness slowing planting, growth of crops or pastures. Coming out of drought: some lingering water deficits; pastures or crops not fully recovered.
- Moderate Drought (D1), areas where some damage to crops, pastures; streams, reservoirs, or wells low, some water shortages developing or imminent; voluntary water-use restrictions requested.
- Severe Drought (D2), areas where signs of crop or pasture losses likely; water shortages common; water restrictions imposed.
- Extreme Drought (D3), Major crop/pasture losses; widespread water shortages or restrictions.
- Exceptional Drought (D4), Exceptional and widespread crop/pasture losses; shortages of water in reservoirs, streams, and wells creating water emergencies.

Figure 1.2 shows the drought intensity in the continental U.S. (including Hawaii, Alaska and Puerto Rico) from May 2011 to May 2014. During 2012, the United States underwent the worst drought since 1950.

Based on the Drought Monitor severe to extreme drought affected about 33% of the contiguous United States as of the end of June 2012. About 4% of the contiguous

U.S. fell in the severely to extremely wet categories and ~55% of the contiguous U.S. fell in the moderate to extreme drought categories (based on the Palmer Drought Index) at the end of June [9].

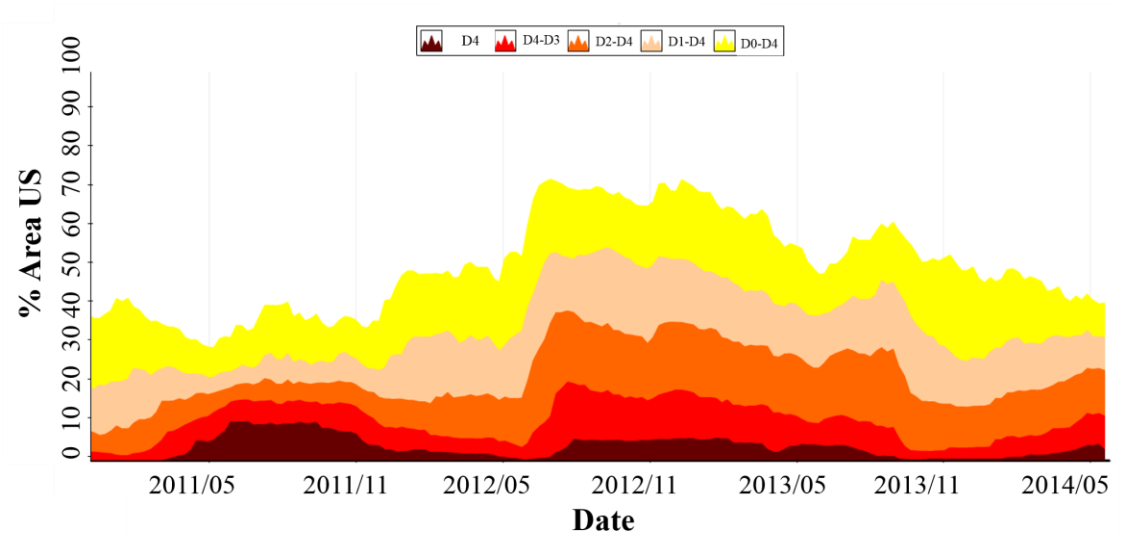

Figure 1.2. U.S. Drought monitor values for the last four years. This plot includes the Continental U.S., Hawaii, Alaska and Puerto Rico. The U.S. Drought Monitor is jointly produced by the National Drought Mitigation Center at the University of Nebraska-Lincoln, the United States Department of Agriculture, and the National Oceanic and Atmospheric Administration. Map courtesy of NDMC-UNL [9]

By the end of July 2013, more than 40% of the continental U.S. was in a moderate or worse drought, and more than 30% was in a severe or worse drought. The situation has improved compared with earlier in 2013 and 2012, as flooding rains have drenched the Northern Plains and Midwest. Meanwhile, drought has continued to expand in the Southwest, where dry conditions have fueled devastating wildfires. Scientists have warned that climate change can exacerbate the impacts of droughts [9]. During the first semester of 2014, 10% of the country is undergoing extreme drought and 3% exceptional

drought being the states California and Texas the most affected areas by the drought during this year. During the first trimester of 2014, ~62% of the state of California suffered from extreme drought [9].

1.2. Water Desalination as a Sustainable Solution to Water Scarcity

There are two primary technologies for water desalination: thermal processes, in which a phase change arises the separation of water from salt, and membrane processes, which are pressure driven. Energy cost, operational and maintenance cost, and capital investment are the main contributors to the water production cost of any of these processes. The energy cost is responsible for about 50% of the produced water cost. For thermal distillation processes, two energy forms are required for the operation: i) low-temperature heat, which represents the main portion of the energy input and is usually supplied to the system by a number of external sources (e.g., fossil fuel, waste energy, nuclear, solar) and ii) electricity, which is used to drive the system's pumps and other electrical components. For membrane processes, only electricity is required as an energy input [10].

Reverse osmosis (RO) is the most widely utilized membrane-based method for separating salt from water. RO treatment costs have become competitive with thermal desalination methods, even in seawater applications. Considering that the feed water quality is a critical design factor. A high or low total dissolved solids concentration determines the RO overall recovery rate, energy input and type of pretreatment, all of these variables influencing the cost of cubic meter of water treated [11]. However, both conventional thermal distillation processes and RO processes are energy intensive

processes, exhibit economies of scale that discourage decentralized or rural implementation, require enhanced expertise for operation and maintenance, and are susceptible to scaling and fouling when used to treat many impaired waters unless extensive feed pretreatment is employed [12].

Using renewable energy sources to power desalination technologies is a viable way to produce fresh water in many locations today. Particularly promising are renewable-energy-powered desalination systems for remote regions, where the connection to the public electrical grid is either not cost effective or not feasible, and where water scarcity is severe [10]. As technologies continue to improve, and as fresh water and cheap conventional sources of energy become scarcer, renewable energy powered desalination will become even more attractive. Several solar, wind, and geothermal or hybrid solar/wind desalination plants have been installed; most of them are demonstration projects and with limited capacity [10]. Membrane distillation processes, driven by low temperature thermal or vapor pressure gradients, can potentially overcome many of the drawbacks associated with conventional thermal distillation and RO desalination. This research focused on the study of vacuum membrane distillation configurations. A mathematical model was developed to describe the transport phenomena governing the process.

1.2.1. Membrane Distillation

Membrane distillation (MD) is a separation technology developed in the late 1960s but was not until the 1980s, with the development of membrane engineering, that it became more attractive for practical applications [13, 14]. MD is a non-isothermal separation process that involves a hydrophobic microporous membrane to support a

liquid-vapor interface at the entrance of the pores [15]. The membrane itself acts only as a barrier to hold the liquid/vapor interfaces at the entrance of the pores and it is not necessary to be selective as required in other membrane processes such as pervaporation [13, 15]. The driving force of this process is the gradient in the partial pressure of water vapor across the membrane [15]. As a result, liquid evaporates at the gas-liquid interface, crosses the membrane as vapor and condenses either inside at the cold side or outside with the aid of a condenser, resulting in a transmembrane permeate flux. [13, 16].

Since MD requires lower operation temperatures than conventional distillation technologies and is not a pressure driven process, it has become an attractive and promising separation technology because of its capability to utilize low-grade, waste and/or alternative energy sources, like solar, geothermal or nuclear energy [10, 13, 16-21]. Another advantage of MD is the ability to treat highly concentrated salt solutions with only a slight reduction on the permeate flux and high rejection rate [13, 22-24].

Amongst the potential applications of MD are water-reuse; food (e.g. juice concentration); medical; environmental clean-up; production of high-purity water; concentration of ionic, colloid or other non-volatile aqueous solutions and removal of trace volatile organic compounds (VOCs) from waste water [13, 15, 22, 23, 25-27].

1.2.1.1.MD Configurations

The main differences among MD configurations arise from the methods used to i) establish the transmembrane driving force for eater transport and ii) condense the water vapor as permeate [13, 15, 22]. The driving force in MD, the transmembrane vapor pressure difference, can be maintained in any of the following reactor configurations (Figure 1.3).

Direct Contact Membrane Distillation (DCMD): an aqueous solution colder than the feed solution is in direct contact with the permeate side of the membrane. As a result, water evaporates at the hot liquid/vapor interface, crosses the membrane in vapor phase and condenses at the cold liquid/vapor interface on the other side of the membrane (Figure 1.3a) [15].

Air Gap Membrane Distillation (AGMD): A stagnant air gap is interposed between the membrane and the condensation surface. In this case, the evaporated fluid or solute crosses both the membrane pores and the air gap to finally condense on a cold surface inside the membrane module (Figure 1.3b) [15].

Vacuum Membrane Distillation (VMD): The applied vacuum pressure on the permeate side is lower than the saturation pressure of volatile molecules to be separated from the feed solution. In this case, condensation occurs outside of the membrane module (Figure 1.3c) [15].

Sweep Gas Membrane Distillation (SGMD): An gas sweeps the permeate side of the membrane carrying the vapor molecules, and condensation occurs outside the membrane module (Figure 1.3d) [15].

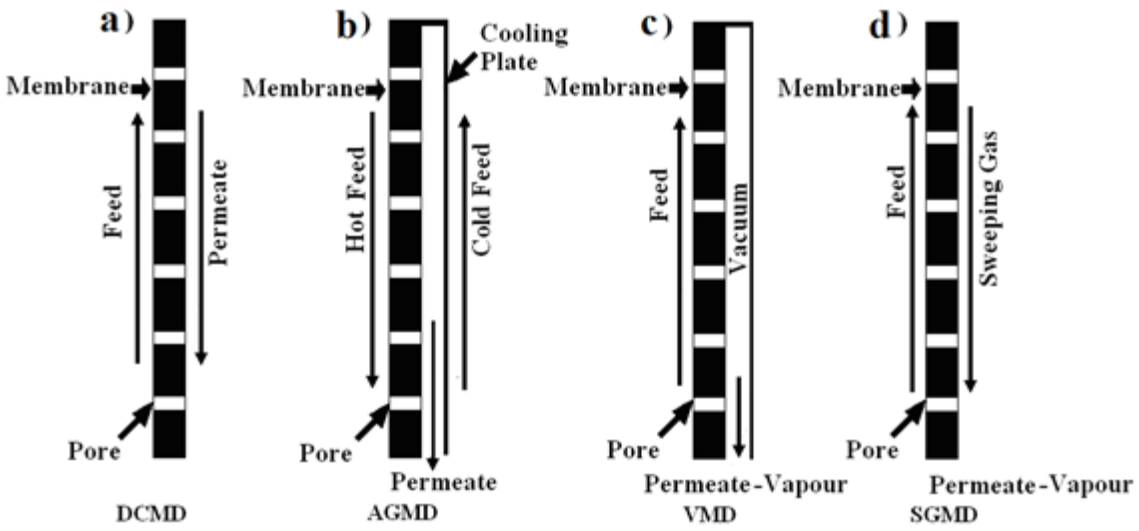

Figure 1.3. Membrane Distillation Configurations. Figure 1.3a. schematic for Direct Contact Membrane Distillation. Figure 1.3b. Schematic for Air Gap Membrane Distillation. Figure 1.3c. Vacuum Membrane Distillation and Figure 1.3d. Sweeping Gas Membrane Distillation [14]

1.2.1.2.Mass and Heat Transport Mechanisms

In membrane distillation mass and heat transfer simultaneously involved to drive water through the pores of the hydrophobic membrane. Mass transfer takes place through the pores of the membrane, while heat must be continuously transferred to the liquid-gas interface in order to provide the heat of vaporization and to raise the vapor pressure of water [28].

An electrical analogy of serial and parallel resistances may be used to describe heat and mass transfer in MD process (Figure 1.4). Mass transfer resistances within the membrane arise from Knudsen, molecular and surface diffusion mechanisms, and convective transport [22]. The contributions of the mass transfer boundary layers adjacent to the membrane to the overall mass transfer resistance can be neglected. The controlling step is the molecular diffusion across the membrane. When pure water is used as

condensing fluid or a vacuum is applied to the membrane side then the resistance to mass transfer on the permeate side can be omitted [22].

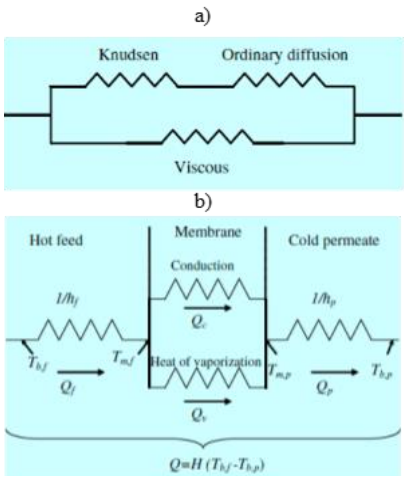

Figure 1.4. Serial and parallel arrangement of resistances to a) mass transport and b) heat transport in MD [15]

The mass transfer across a porous medium can be affected by Knudsen diffusion. Poiseuille or viscous flow due to the momentum transferred to the supported membrane, ordinary molecular diffusion and/or the combinations of these mechanisms. Generally, surface diffusion in assumed to be negligible [15, 22, 28].

The model used most frequently to describe the MD process is the dusty gas model [13, 15, 22, 23, 28, 29]. The dusty gas model is defined by equations 1.1 to 1.5:

$$\frac{J_i^D}{D_{ie}^k} + \sum_{j=1\neq 0}^{n} \frac{p_j J_i^D - p_i J_j^D}{D_{ije}^0} = \frac{1}{RT} \nabla p_i \tag{1.1}$$

$$J_i^v = \frac{\varepsilon r^2 p_i}{8RT\tau\mu} \tag{1.2}$$

$$D_{ije}^k = \frac{2\varepsilon r}{3\tau}\sqrt{\frac{8RT}{\pi M_i}} \tag{1.3}$$

$$D_{ije}^0 = \frac{\varepsilon}{\tau}\sqrt{\frac{8RT}{\pi M_i}} \tag{1.4}$$

$$J_i = J_i^D + J_i^v \tag{1.5}$$

where J^D is the diffusive flux, J^v is the viscous flux, D^k is the Knudsen diffusion coefficient, D^0 is the ordinary diffusion coefficient, P is the total pressure, μ is the viscosity of the gas mixture, r is the pore radius, ε is the membrane porosity, M is the molecular weight, τ is the pore tortuosity and the subscripts e and i refer to the effective diffusion coefficients and the transported compound i [15, 22].

The flux of water vapor across the membrane can be simplified and expressed as a linear function of the difference in vapor pressure across the membrane.

$$J = K\Delta p_i \tag{1.6}$$

where K is the membrane distillation coefficient and Δp_i is the difference in partial pressures of water vapor across the membrane. The membrane distillation coefficient is a function of the membrane characteristics, physical and chemical properties of the vapor transported across the membrane and the operational conditions [22].

The two mechanisms that dominate the total heat flux through the membrane are due to i) conduction across the membrane material and pores and ii) latent heat of vaporization, in this case of liquid water to water vapor. The energy balance would be defined by equations 1.7 and 1.8 [15].

$$Q_m = Q_c + Q_v \tag{1.7}$$

$$Q_m = k_m \frac{dT}{dx} + \sum_i J_i \Delta H_{v,i} \tag{1.8}$$

where, Q_m is the heat flux through the membrane, Q_c is the conduction across the membrane material and its gas filled pores and Q_v is the latent heat of vaporization. In Equation 1.8, $\Delta H_{v,\,i}$ is the evaporation enthalpy of species *i* at the absolute temperature, J_i is the transmembrane flux and k_m is the thermal conductivity of the membrane.

A detailed description of the mass and heat transport mechanisms and the related model development using experimental data are described in Chapter 2: Mass and Heat Transfer Mathematical Modeling for Vacuum Membrane Distillation in a Hollow Fiber Contactor.

1.2.2. Reverse Osmosis

Reverse Osmosis (RO) has been around since the 1960s when researchers at the University of California Los Angeles developed the first asymmetric RO membrane. Asymmetric membranes are made up of a support layer and an active layer. The active layer provides the separation capabilities. The development of this type of membrane led

to the commercialization of RO for desalination [30]. RO has become the most widely used membrane desalination technology [31, 32].

RO is a pressure-driven process that involves a semi-permeable membrane that rejects dissolved constituents present in the feed water relying, on the physical and chemical properties of the solutes for separation [30, 31].

A useful transport model to describe RO is the solution-diffusion model. This model assumes the existence of a permeable, non-porous, homogenous membrane surface layer. Water and solutes dissolve into the solid membrane material, diffuse though the solid, and reliquefy on the permeate side of the membrane [30-33]. The water flux through the membrane J_w is described by equations 1.9 – 1.10.

$$J_w = A\left(\Delta P_{NET}\right) \tag{1.9}$$

$$\Delta P_{NET} = \Delta P - \Delta\pi = \left(P_F - P_p\right) - \left(\pi_F - \pi_p\right) \tag{1.10}$$

where, J_w is the volumetric flux of water, is the net transmembrane pressure, ΔP is the pressure difference across the membrane, $\Delta\pi$ is the osmotic pressure differential across the membrane, and A is the water transport coefficient. Subscripts F and P refer to the feed and permeate, respectively. When $\Delta P > \Delta\pi$, water flows from the brine to the permeate side of the membrane against the osmotic pressure difference [33].

The salt fluxJ_s, across the membrane is described by equations 1.11 and 1.12.

$$J_s = B\left(\Delta C\right) \tag{1.11}$$

$$J_s = B\left(C_F - C_p\right) \tag{1.12}$$

where, B is the salt permeability constant and C_F and C_p, are the salt concentrations on the feed and permeate sides of the membrane, respectively. The concentration on the permeate side is usually much smaller that the feed concentration [33].

A RO treatment train usually consists of three separate sections i) pre-treatment of the feed water to meet the requirements of membrane manufacturers ii) RO treatment itself, and iii) post-treatment of the reject flow to increase recovery before brine disposal.

1.2.2.1.Pre-treatments for Reverse Osmosis

An efficient pre-treatment of the RO feed water is essential to avoid irreversible membrane damage, and maintain a stable flux through the membranes. Depending on the feed water quality it might be necessary to add antiscalant and/or acid for scale control. Pre-filtration may be necessary to remove particles. Brief descriptions of the two pre-filtration processes investigated during this study (microfiltration and slow sand filtration) are provided below.

1.2.2.1.1. Microfiltration

Microfiltration (MF) uses microporous membranes to sieve suspended particles between 0.1 and 10 microns from a fluid. It is a completely mechanical process in that no chemical or biological activity takes place. MF can effectively remove molecular weight particles in the 100,000 to 5,000,000 Dalton range such as algae, bacteria, some dyes and pigments, proteins, Cryptosporidium, Giardia, some viruses (if below 0.1 microns), and colloidal silica [30, 33].

In microfiltration driven by pressure difference through a membrane in either dead-end or cross flow configuration. Dead-end systems force raw water through the

membrane as the only outlet in the system. The flux declines at a rate that depends on water quality and until backwash is needed to restore the original permeability. Backwash water is usually sent to waste. A cross flow system allows water to permeate through the membrane while the water to be treated is passed along parallel to the membrane. The feed water becomes more concentrated along the membrane and before it is to another stage or to waste. The cross flow velocity decreases fouling but increases the volume of concentrate or waste. The type of system utilized depends on feed water constituents and desired filtrate quality.

1.2.2.1.2. Slow Sand Filtration

Slow sand filtration lies within the classification of media filters in which water is passed through a porous bed of filter medium that physically and biochemically, removes suspended particles. The concept of slow sand filtration was originally thought to be strictly physical removal of suspended particles in the water; however, after scientific examination and study of the schmutzdecke, it is now known that much removal comes from biological activity at the top of the sand layer [34-36]. Slow sand filters differ from other media filters in terms of the rate of filtration, and presence of a biological layer on top of the sand called the schmutzdecke. A typical slow sand filter is comprised of: a layer of raw water above the filter medium, the medium itself (sand), the schmutzdecke, and an under drain system to collect the filtered water.

There are two methods of cleaning SSFs: the traditional draining and scraping of the schmutzdecke, or the process of wet harrowing which can save time in the cleaning process. The traditional method requires the influent water supply to be stopped and the filter to be drained down to below the sand bed surface, which can be time consuming.

The schmutzdecke is then physically removed and discarded to waste. The filter is then refilled and run for 2-7 days to rebuild a schmutzdecke before the effluent can be used. The wet harrowing process drains down as well but stops 10-20 cm above the sand layer thus leaving some water in the filter and therefore decreasing the time required for draining. The water is then agitated slightly to suspend the settled particles on the schmutzdecke before it is drained to waste from above the sand. This process reduces drain down time, as well as maturation time, because the schmutzdecke is not completely removed.

1.2.2.2. Post-treatment for Reverse Osmosis: Vibratory Shear Enhance Processing (VSEP®)

Concentrate disposal can be a significant issue in the design of RO facilities, and the concentrate may require treatment before disposal. Methods for concentrate disposal include discharge to municipal sewer, deep well injection, estuary discharge, ocean or brackish river discharge, evaporation ponds, and other membrane technologies like Vibratory Shear Enhance Processing (VSEP®), the subject of this study.

VSEP® (New Logic Research, Inc.) is a membrane separation system in which high-pressure RO or nanofiltration is used to extract additional water from highly saline solutions. In a VSEP® system, the feed slurry remains nearly stationary, moving parallel to the membrane elements, which are vibrating. The shear waves produced by the membrane's vibration cause solids and foulants to be lifted off the membrane surface and remixed with the bulk material flowing through the membrane stack. This high shear rate and resultant pressure wave exposes the membrane pores for maximum throughput that is typically between 3 and 10 times the throughput of conventional cross-flow systems. The

VSEP® membrane filter pack consists of flat sheet membranes arrayed as parallel discs and separated by gaskets.

1.3. Conclusions

Water scarcity has rapidly spread to many parts of the world, as population and water consumption levels increase despite a fixed supply of renewable fresh water. Meeting the challenges that water scarcity poses to food production, ecosystem health, and political and social stability will require new approaches to using and managing water. Greater efforts will be needed to reserve water for the maintenance of ecological functions and, where necessary, to return water to natural systems to restore those functions. Desalination already plays an essential role in water management. It constitutes a secure source of safe drinking water supply once demand management measures are fully implemented. Overcoming problems related to brine minimization and disposal is key to sustainable, efficient inland water desalination.

CHAPTER 2

MASS AND HEAT TRANSFER MATHEMATICAL MODELING FOR VACUUM MEMBRANE DISTILLATION IN A HOLLOW FIBER CONTACTOR

2.1. Introduction

The need to find alternatives for water desalination that would increase utilization of renewable energy sources and water recovery has made membrane distillation (MD) attractive for desalination of brackish water and seawater. MD is a non-isothermal process in which the driving force is the partial water vapor pressure gradient across a hydrophobic microporous membrane [15]. MD enjoys several advantages over more traditional desalination technologies like reverse osmosis (RO) and conventional distillation. These include the ability to operate at lower pressures and temperatures, and be driven by solar, geothermal energies or low grade heat from other sources. MD can also treat water with higher feed total dissolved solids (TDS) concentrations without prohibitive membrane fouling and without expensive pretreatments [13-15, 22, 26, 37, 38].

There are four primary MD configurations differentiated by the method utilized to collect the permeate: i) Direct Contact Membrane Distillation (DCMD) wherein the permeate side of the membrane is in contact with liquid water, ii) Air Gap Membrane Distillation (AGMD) wherein an air gap is interposed between the permeate membrane

face and a condensing surface, iii) Sweeping Gas Membrane Distillation (SGMD) wherein a gas is swept through the permeate side to carry the vapor to an external condenser where the permeate is collected, and iv) Vacuum Membrane Distillation (VMD) wherein a vacuum in applied to the permeate side of the membrane to withdraw the vapor to an external condenser [13, 14, 22, 28].

The ease of operation and the fact that no external condenser is needed make DCMD and AGMD the most studied configurations [13, 28]. VMD and SGMD have been much less studied. The need for an external condenser to recover the permeate complicates the operation of these configurations; however, VMD yields a higher specific permeate production compared to DCMD [18, 39-41].

In this study, a mathematical model was developed to simulate the performance of hollow-fiber VMDs. The model was validated with experimental data obtained in this work. The mathematical model used coupled energy and mass balances to determine the incremental prediction temperature at the liquid-vapor interface along the hollow-fiber module, which affects the vapor pressure gradient and, in turn, the rate of water recovered. The model accounts for membrane characteristics, such as pore size, tortuosity, membrane thickness and porosity.

2.2. Material and Methods

The membrane module was a hollow fiber Liqui-cel® Extra-Flow Contactor (2.5-in x 8-in, polyvinylidene fluoride (PVDF), Separation Products Division, Hoechst Celanese Corporation, Charlotte, NC, USA). Module specifications are summarized in

Table 2.1. The hollow-fiber module contained ~7000; 0.2 m long, hydrophobic microporous membrane straws bundled in a cylindrical membrane housing.

Table 2.1. Membrane Module Specifications

Liqui-Cel Membrane Module	
Membrane material[a]	PVDF
Pore Size[a] [μm]	0.03
Area[a] [m^2]	1.4
Fiber length[a] [m]	0.2
Fiber inner diameter[a] [μm]	225
Fiber outer diameter[a] [μm]	315
Porosity[a] [%]	30
Tortuosity[b][--]	3
Number of Fibers[c]	~7000

a Manufacturer's data
b Fitted parameter in the model
c Calculated

The bench-scale apparatus consisted of a hot brine tank, membrane VMD module, condenser, cooling bath and a permeate collection tank (Figure 2.1). The hot brine solution was recirculated up-flow through the module, counter current to the direction of water vapor movement in the module. The volume of the brine tank was 7 L. The permeate side of the hollow fiber membrane was connected to a vacuum pump (Gast, ShopVac, 5.0 peak hp). Permeate was collected in a shell and tube counter-current condenser (Model # AB-404-85098, Thermal Transfer Products, interfacial area 0.57 m^2). K-type thermocouples were installed in the inlet and outlet of the module and condenser, and a rotameter was placed at the entrance of the module to measure the brine flow rate.

Vacuum pressure was measured at the top of the VMD module. The electrical conductivity in the feed and permeate solutions was monitored with a benchtop thermo conductivity meter (inoLab® Cond Level).

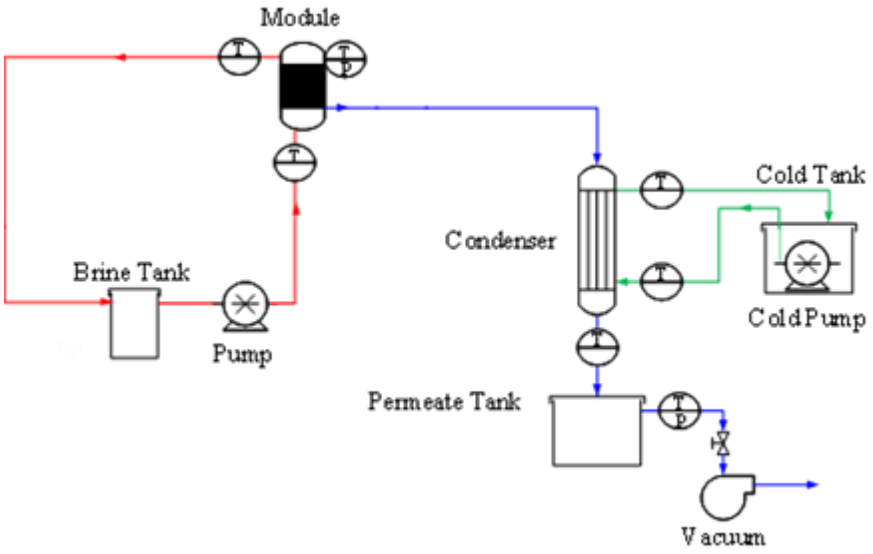

Figure 2.1. Lab-scale experimental VMD set up. Adapted from Karanikola et al. 2014. The red line represents the hot brine loop; the blue line represents the water vapor exiting the VMD module; and the green line represents the cold water loop flowing into the condenser. T represents the thermocouples and P the pressure gauges

2.3. Mass and Heat Transfer Model

A finite-difference, steady-state heat and mass transfer model was developed to predict the water production rate during VMD. The model is based on energy and mass balances through the VMD module during the distillation process. A resistance model (Figure 2.2) illustrates the resistances to mass and heat transfer in a VMD membrane module, where T_f, and T_i are the feed and the interface temperatures, respectively, $P_{sat}(T_i)$ and P_V are the pressures at the feed interface temperature and the vacuum channel.

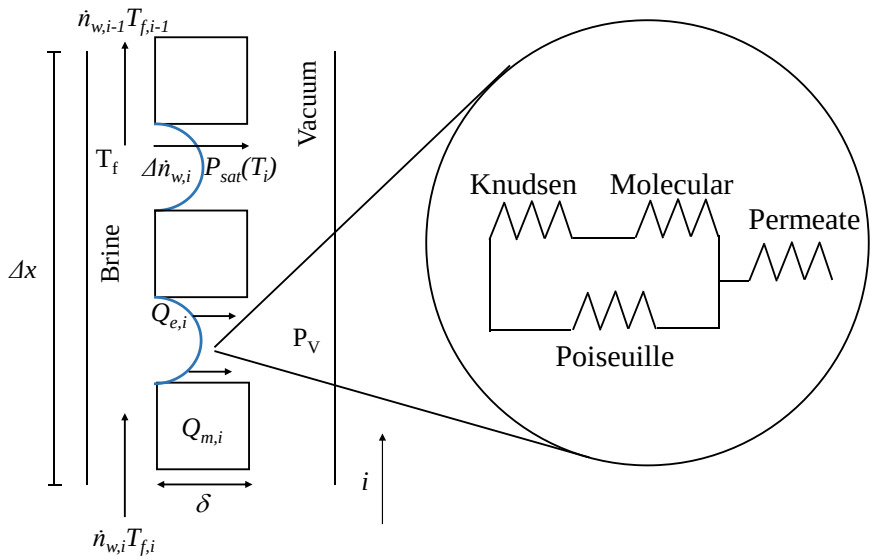

Figure 2.2. Resistances to transmembrane mass and heat transport in VMD

2.3.1. Mass Transfer Model

The mass balance in each section of the hollow fiber module is governed by equation 2.1.

$$\dot{n}_{w,i} = \dot{n}_{w,i+1} + \Delta\dot{n}_{w,i} \tag{2.1}$$

where $\dot{n}_{w,i}$ and $\dot{n}_{w,i-1}$ are the molar water vapor flow [mol.s^{-1}] at the inlet and outlet of each section and $\Delta\dot{n}_{w,i}$ is the molar water vapor rate of transport [mol.s^{-1}].

The molar water vapor rate of transport is related to the water vapor flux, J_i, across the membrane in each section by equation 2.2.

$$J_i = \frac{\Delta\dot{n}_{w,i}}{\Delta A_s} \tag{2.2}$$

where A_s is the membrane surface area [m^2].

The water vapor flux in each section is described by equation 2.3:

$$J_i = K \times \left(P_{sat,Ti} - P_v \right) \tag{2.3}$$

where $P_{sat,\,Ti}$ [Pa] is the saturation vapor pressure at interface temperature, $_{Ti}$ [C] (equation 2.4), *A*, *B*, and *C* are component-specific constants and *K* is the membrane distillation coefficient [$kg.m^{-2}.Pa^{-1}.s^{-1}$].

$$P_{sat,Ti} = 10^{A - \frac{B}{C+T_i}} \tag{2.4}$$

A resistance model approach was used to calculated the membrane distillation coefficient can be calculated is defined by equation 2.5 [42].

$$\frac{1}{K} = \frac{1}{k_f} + \frac{1}{k_m} + \frac{1}{k_p} \tag{2.5}$$

where K^{-1} is the overall mass transfer resistance [$s.m^{-1}$], k_f, k_m, and k_p are the mass transfer coefficients [$m.s^{-1}$] through the liquid feed boundary layer, the membrane, and the permeate, respectively.

The overall resistance to water vapor transport through the membrane, R_m, is defined by equation 2.6.

$$\frac{1}{R_m} = \frac{1}{R_{Kn} + R_{Mol}} + \frac{1}{R_{Poi}} \tag{2.6}$$

where R_{Kn}, k_{Poi}, k_{Mol} are the contribution to the resistance by the Knudsen, molecular diffusion and Poiseiulle flow [$s.m^{-1}$]. Rm can be calculated by equation 2.7 [43].

$$R_m = \frac{1}{k_m} = \frac{\delta}{D_{eff}} \frac{d_{outer}}{d_{mean}} \tag{2.7}$$

where δ is the thickness of the membrane d_{outer} is the outer diameter of the hollow fiber membrane, d_{mean} is the arithmetic mean diameter and D_{eff} is the effective diffusivity of water vapor in the membrane (equation 2.8).

$$D_{eff} = \frac{\varepsilon}{\tau} D \tag{2.8}$$

where D is the diffusion coefficient defined by equation 2.9.

$$\frac{1}{D} = \frac{1}{D_{Mol} + D_{Kn}} + \frac{1}{D_{Poi}} \tag{2.9}$$

The molecular diffusion, D_{Mol} [$m^2.s^{-1}$], was calculated using equation 2.10 [44].

$$D_{mol} = \frac{0.926}{10^{-6} P} \left(\frac{T^{2.5}}{T + 245} \right) \tag{2.10}$$

where P is the average pressure between $P_{sat,\,Ti}$ and P_v [kPa] and T [K] is the temperature of the feed side solution. The Knudsen diffusion coefficient, D_{Kn} [$m^2.s^{-1}$] was calculated by equation 2.11 [37].

$$D_{Kn} = \frac{2\varepsilon r}{3\tau} \sqrt{\frac{8RT}{\pi M_w}} \tag{2.11}$$

where ε is the porosity, r is the pore radius [m], τ is the tortuosity, R is the gas constant [m^3.Pa.mol^{-1}.K^{-1}], T is the temperature of the brine in the entrance of the module [K], and M_w is the molecular weight of water [kg.mol^{-1}].

The Poiseuille flow diffusion coefficient is defined by equation 2.12 [37].

$$D_{Poi} = \frac{\varepsilon r^2 P_{pore}}{3\tau\mu RT} \tag{2.12}$$

where the viscosity of water vapor is μ [Pa s], and P_{pore} is the average pressure between $P_{sat,\,Ti}$ and P_v [Pa], R is the ideal gas constant [Pa m^3.K^{-1} mol^{-1}], T_i is the temperature at the liquid-vapor interface [K]. The membrane characteristics were obtained from the membrane manufacturer, except for the tortuosity which is the only fitted parameter.

The Knudsen number (K_n) was used to determine the dominant mass transfer mechanism in the pores (equation 2.13). A large K_n number implies that the diffusional flow is strongly influenced by the interaction of the molecules with the wall of the membrane relative to the influence of intermolecular collisions. The K_n number at smaller pore sizes like the one used in this study (d_p = 0.03 μm) was calculated and suggested that Knudsen diffusion is the prevailing mechanism of mass transfer since K_n > 10 [14, 37, 45].

$$K_n = \frac{\lambda}{d_p} \tag{2.13}$$

where, λ is the mean free path defined in equation 2.14 and d_p is the mean pore size of 0.03 μm.

$$\lambda = \frac{k_B T}{\pi\left(\sigma_w + \sigma_a/2\right)^2 P_{pore}} \frac{1}{\sqrt{1 + M_w/M_a}} \tag{2.14}$$

where k_B is the Boltzmann constant (1.381×10^{-23} [$J.K^{-1}$], σ_w and σ_a the collision diameters for water vapor (2.641×10^{-10} [m]) and air (3.711×10^{-10} [m]), T is the mean absolute temperature at the pores [K], P_{pore} is the average pressure ($P_{sat,\ Ti}$ and P_v) [Pa] [14, 22].

The values for the molecular diffusion and Poiseuille resistances were calculated and proven to be negligible in comparison with the contribution by Knudsen diffusion (Figure 2.3). The vacuum applied on the permeate side of the membrane can increase the diffusion coefficient. As the mean free path increases, the flux from that position decreases, therefore as the vacuum is applied and increased, the diffusion gradient increases. That is why we as other authors, the mass transfer resistance on permeate side can be ignored when compared to the mass transfer resistances in the membrane and the liquid side [37, 46].

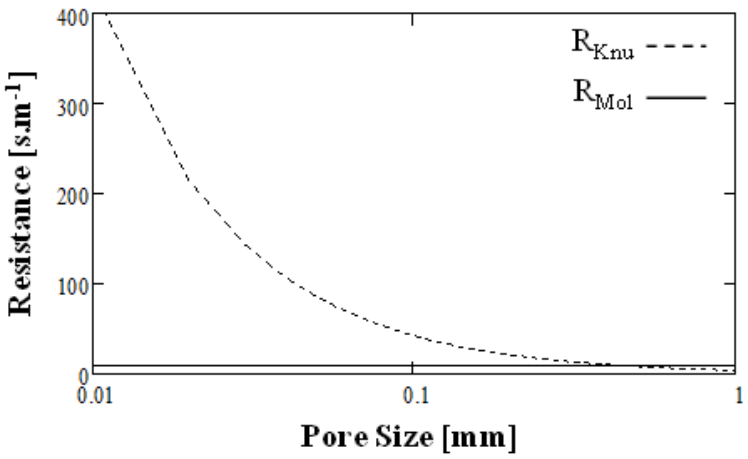

Figure 2.3. Mass transfer resistances, R_{Kn} and $R_{Mol,}$ as a function of the mean pore size. Vertical line shows d_p = 0.03 μm. Tf = 70 [°C] and v_f = 0.06 [$m.s^{-1}$] at a vacuum of 70 kPa

2.3.2. Heat Transfer Model

The equations that governed the energy balance are described from equations 2.15 to equation 2.18.

$$Q_f = Q_m + Q_{evap} \tag{2.15}$$

where Q_{evap} is the heat rate needed to evaporate liquid water from the brine stream [W], $Q_{m,}$ is the rate of heat transfer across the membrane [W], and $Q_{f,}$ is the heat transfer in the boundary layer formed on the brine-side of the membrane [W].

The heat needed to evaporate liquid water from the brine stream in each section is defined by equation 2.16.

$$Q_{evap,i} = \Delta A_s h_f \left(T_{f,i} - T_{i,i}\right) + \Delta \dot{n}_{w,i}\, \Delta H_v \tag{2.16}$$

where ΔH_v is the heat of vaporization [$J.kg^{-1}$] and is a function of $T_{i.i}$.

The rate of heat transfer across the membrane section [W] and is defined by equation 2.17.

$$Q_{m,i} = H \times \Delta A_s \times \left(T_{f,i} - T_{i,i}\right) \tag{2.17}$$

where Cp_f [J.mol^{-1}.K^{-1}] is the specific heat of the feed solution, and $T_{f,i}$ [K] are the outlet and inlet feed temperatures in section i. H is the overall transmembrane heat transfer coefficient [W.K^{-1}.m-^{2}], A_s is the total surface area of the module section [m^2], and $T_{i,i}$ is the interface temperature [K] at each section.

Including the change in state between the liquid and vapor phase to account for the phase transition at $T_{i,i}$, the heat balance at each section is given by equation 2.18.

$$\Delta \dot{n}_{w,i}\, Cp_f \left(T_{f,i} - T_{i,i}\right) + \Delta \dot{n}_{w,i}\, Cp_v \left(T_{i,i} - T_{v,i}\right) + \Delta \dot{n}_{w,i}\, \Delta H_v = h_f \left(T_{f,i} - T_{i,i}\right) \Delta A_s + \Delta \dot{n}_{w,i}\, \Delta H_v \left(T_{i,i}\right) \quad (2.18)$$

where Cp_v is the heat capacity for the vapor [J.mol^{-1}.K^{-1}] and $T_{v,i}$ is the temperature in the vacuum chamber [K]. $T_{v,i}$ is assumed to be equal to the temperature at $T_{i,i}$. Heat transfer for hollow fiber VMD process is determined by four separate processes: i) heat transfer by convection from the brine to the surface of the membrane; ii) heat transfer by conduction through the membrane; iii) energy required for water vaporization; and iv) heat transfer by convection from the surface of the membrane to the permeate. The overall transport coefficient, H, at steady state, can be expressed by a resistances model showed in equation 2.19 [37].

$$\frac{1}{H} = \frac{1}{h_f} + \frac{1}{h_m + J\Delta H_v} + \frac{1}{h_m} \quad (2.19)$$

where H is the overall heat transfer coefficient [W.m^{-2}.K^{-1}], h_f, h_m, and h_p are the individual heat transfer coefficients of the feed, membrane and permeate respectively.

The heat transfer coefficient for the membrane is given by equation 2.20.

$$h_m = \frac{\lambda}{\delta} \tag{2.20}$$

where λ is the thermal conductivity of the membrane [$W.m^{-1}.K^{-1}$] and is calculated using equation 2.21 [47].

$$\lambda = \varepsilon\lambda_{vapor} + (1+\varepsilon)\lambda_{solid} \tag{2.21}$$

where λ_{vapor} and λ_{solid} are the thermal conductivities of the vapor and the membrane material, respectively. The values for the λ_{vapor} are very low (0.016 $W.m^{-1}.K$) and for λ_{solid} (PVDF = 0.17 – 0.19 [$W.m^{-1}.K$] [22, 47].

The following simplifications has been applied to this analysis: i. compared to the other resistances (feed and membrane) the heat transfer resistance on the permeate side is negligible because of the low pressure applied on the permeate channel [13, 14, 37, 48], and ii. since the water vapor inside the permeate side of the membrane is removed from the pores of the membrane by the vacuum applied, the thermal conductivities of membrane contribution in VMD are further reduced. Therefore, the heat transfer by conduction through VMD membrane are usually neglected [14, 37, 39, 47, 49, 50].

An empirical correlation for an inside/out hollow fiber module was used by other authors to estimate the boundary layer heat transfer coefficient, h_f, is utilized in this study (equation 2.22) [39, 51-53].

$$h_f = \frac{Nuk_L}{d_h} \tag{2.22}$$

where d_h is the hydraulic diameter of the feed flow channel [m] and k_L is the thermal conductivity of the feed solution [W.m^{-1}.K].

The heat transfer coefficient for laminar flow and for a hollow fiber is calculated from the corresponding Nusselt number, *Nu*, given by equation 2.23 [39, 51, 54]:

$$Nu = 1.86\left(\frac{\mathrm{Re}\,\mathrm{Pr} d_h}{L}\right)^{1/3} \tag{2.23}$$

where *Re* is the Reynolds number, *Pr* is the Prandlt number and *L* is the length of the membrane fiber [m]. The Reynolds and Prandlt numbers are defined in equations 2.24 and 2.25.

$$\mathrm{Re} = \frac{v d_h \rho}{\mu_f} \tag{2.24}$$

$$\mathrm{Pr} = \frac{Cp\mu_f}{k_L} \tag{2.25}$$

where v, ρ, μ_f, and C_p are the velocity [m/s], density of [kg.m^{-3}], and heat capacity of the feed [J.kg^{-1}.K^{-1}], respectively.

2.4. Model Implementation

A finite difference model based on the heat and mass balance equations was developed to model the performance of the VMD process. The developed model accounts for the fact that the brine temperature will drop as water vapor diffuses vaporizes across the water/air interface and through the membrane.

From equations 2.2 and 2.3 we solve for the interface temperature, $T_{i,i.}$

$$\frac{\Delta \dot{n}_{w,i}}{\Delta A_s} = K \times \left(10^{A - \frac{B}{c+Tii}} - P_v \right) \tag{2.26}$$

Solving equation 2.26 for $T_{i,i}$ we get equation 2.27.

$$T_{i,i} = C - \frac{B}{A - \log\left(\frac{\Delta n_{w,i}}{A_s \times K \times \varepsilon} + P_v \right)} \tag{2.27}$$

Equation 2.18 is solved for Ti,i

$$T_{i,i} = \frac{\Delta \dot{n}_{w,i} \left(Cp_f T_{f,i} - Cp_v T_{v,i} \right) - \Delta A_s h_f T_{f,i}}{\left(\Delta \dot{n}_{w,i} Cp_f - \Delta \dot{n}_{w,i} Cp_v + \Delta A_s h_f \right)} \tag{2.28}$$

Equations 2.27 and 2.28 are equated and solved for $\Delta \dot{n}_{w,i}$. The value of $\Delta \dot{n}_{w,i}$ calculated until $T_{i.i} = T_{i.i}$. Once this takes place, and $\Delta \dot{n}_{w,i}$ has been calculated, $T_{f.i+1}$ is solved so the next section of the membrane module can be calculated. A script was developed in Python to account for the changes in brine temperature at each section of the membrane module. At each section, T_i, and m are solved based on the mass and heat transfer coefficients. Since, the temperature of the brine, T_f, changes within the longitudinal length of the module an incremental approach was used to solve for the solution (Figure 2.4).

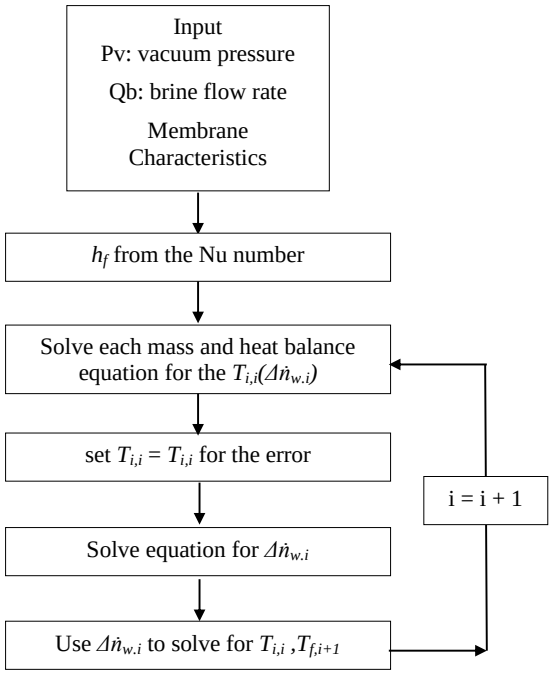

Figure 2.4. VMD Modeling Program Flow Diagram

2.5. Results and Discussion

The effects of brine temperature, vacuum pressure, brine velocity, and membrane pore size on the permeation rate were evaluated during this study. The brine consisted of 0.500 g/L NaCl (Fisher Scientific) in milli-Q (Merck Millipore) water. Salt rejection was monitored at the end of each experiment by conductivity measurement of the permeate, and always was > 99 %. All experiments were run several times to establish repeatability.

2.5.1. Temperature Effect on Permeate Flux

The permeate production increased with increasing influent brine (Figure 2.5). The relationship between flux predictions and observations was developed at a brine velocity v_b = 0.06 m/s and vacuum pressure of 70 kPa for the temperature range of 50 – 80 °C. The permeate flux increased by 10X for an increase of 20 °C in influent brine

temperature from 60 to 80 °C. This is anticipated since there is a direct relationship between temperature and vapor pressure. At higher temperature the saturated vapor pressure is greater, therefore there is an increase of the driving force in this process and an increase on permeate flux [38, 39]. It can be observed that operating below the boiling point of water at a set vacuum pressure (boiling temperature at 70 kPa vacuum 70.2 °C) results in zero permeate production. The steady state condition on the vapor side would be under-saturated due to the lower brine temperature relative to the maximum saturated temperature in relation to vacuum pressure. Due to the lower temperature state, the steady state temperature profile of the membrane would be flat and limiting the flux to forces of natural convection. Water vapor flow increases across the membrane in relation to the relative boiling point to the vacuum pressure, which occurs when the pressure in the permeate channel is reduced to the saturated pressure of water, the vapor present at the interface on the feed side becomes greater than the pressure at the pore interface on the permeate side [46]. In a vacuum environment, the permeate channel of the membrane only has the presence of air and water vapor. As the air leaves the permeate channel, the partial pressure of air approaches zero and the total pressure in the membrane channel is equal to the saturated vapor pressure of water at the interface. Once all the air has exited the permeate channel, it can be assumed that only water vapor is inside the channel. At this point, water transport across the membrane will continue as long as the temperature of the brine, T_f, is greater than the temperature of the interface, T_i. Water transport across the membrane will stop once $T_f = T_i$, this when the driving force (gradient of vapor pressure) that drives the water transports is null.

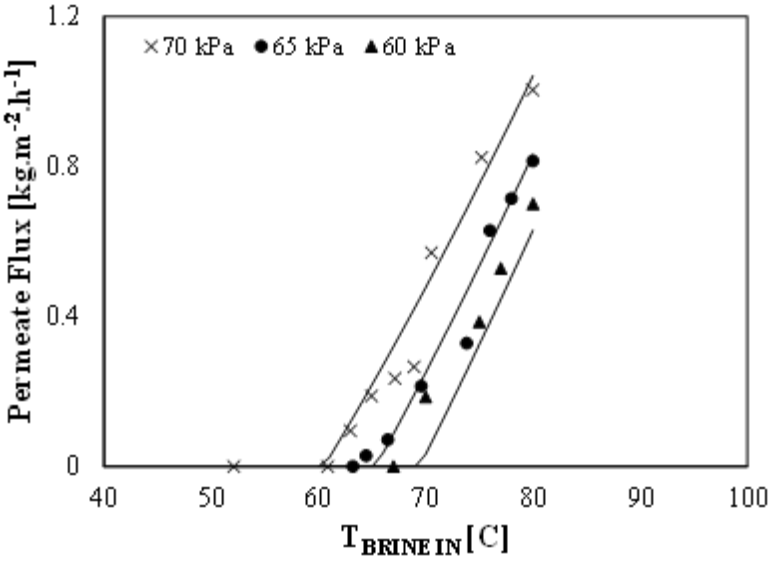

Figure 2.5. Permeate mass flow as a function of the feed brine temperature T_f. The continuous line depicts the model simulation. Data points are measured permeate fluxes. Experiments were run at 70 kPa of vacuum pressure and a brine velocity of 0.06 m/s

2.5.2. Permeate Flux vs. Gas Pressure

Increasing the vacuum on the permeate side of the membrane should increase the permeate flux because the driving force increases [55, 56]. There is a linear relationship between the difference the saturation pressure evaluated at the interface temperature and the vacuum applied to the permeate channel. Figure 2.6 shows experimental data and model results for influent brine temperatures of 80 and 65 °C and pressures from 60 – 70 kPa (vacuum). Due to experimental set-up limitation only these pressures were examined in this study. Literature showed that VMD with higher vacuums yields higher permeation rates [18, 38, 41, 46]. The brine approach velocity was constant at 0.06 m/s. In this case, it can be observed that the permeate production increases ~30% by an increase of the

applied vacuum applied on the permeate side by 10 kPa. The developed model well simulates with the measured data.

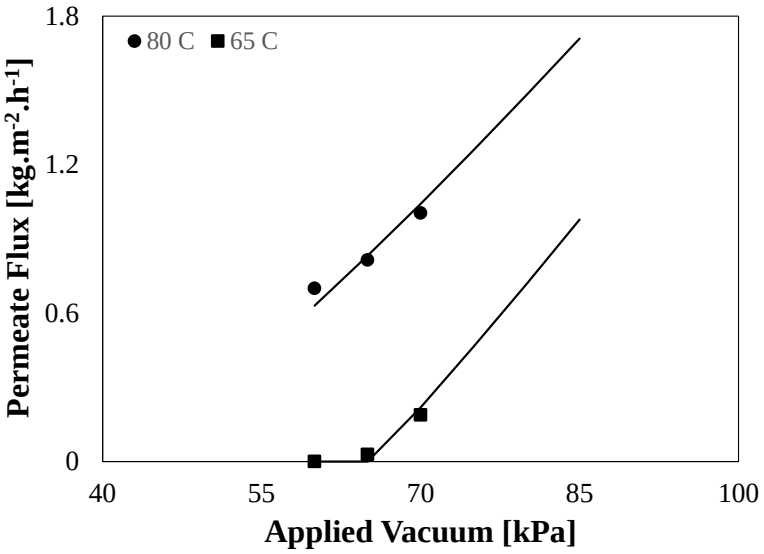

Figure 2.6. Effect of applied vacuum and influent brine temperature on permeate flux (v_b = 0.06 m/s) during VMD

2.5.3. Anticipated Effect of Independent Variables in Permeate Flux

Restrictions from the commercial hollow fiber membrane module design (pore size; hollow fiber dimensions; and inlet and outlet fittings) and experimental set-up (pump capacity) limited the range of variables that could be change for experimentation. However, the model developed was able to simulate the permeate flux as a function of pore size and brine velocity.

2.5.3.1. Pore size

The membrane characteristics (ε, τ, r, and δ) affect the mass transfer across the microporous membrane. In this case, the model was used to analyze the performance of the module for different pore sizes (Figure 2.7). Data are available for a pore size of 0.03

μm. For this case, the results show that an increase the pore size approximately by an order of magnitude (0.03 μm to 0.2 μm) results in an increase of ~40% on the permeate flux at 80 °C, for a vacuum of 70 kPa and a brine approach velocity of 0.06 m/s. When the pore size was increased to 0.45 μm, the permeate flux remains almost the same (3% increase in the flux) in comparison to a pore size of 0.2 μm. This increase in the permeate production with increasing membrane pore size may be related to the fact that the mass transport mechanisms depend on the pore size relative to the mean free path. Knudsen diffusion mechanisms prevail at smaller pore sizes, while at larger pore size while at larger pore size, the controlling mass transport mechanism is Knudsen-viscous. However, the increase of the membrane pore size is limited by the liquid entry pressure (LEP) that provides a relationship between the membrane's largest allowable pore size and the operation conditions (e.g. liquid pressure, vacuum applied). It is recommended for VMD a pore size smaller than 0.45 μm to avoid membrane pore wetting [13, 15, 37, 42, 48]. Membrane pore wetting occurs when the feed liquid penetrates inside membrane pores.

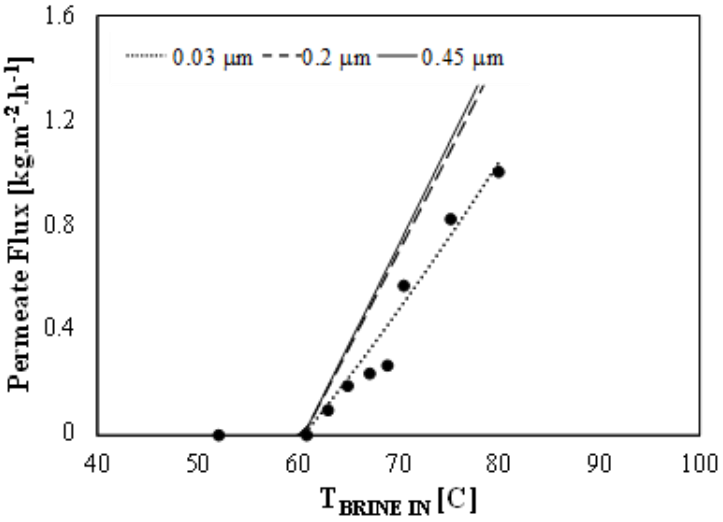

Figure 2.7. Pore size effect on the Permeate Flux

2.5.3.2.Brine Velocity Effect

The brine velocity effect in permeate rate was simulated using the model developed (Figure 2.8). The model simulates that the permeate production rate increases with the brine velocity. However, at higher brine velocities the permeate production reaches a plateau. An increase in the brine velocity decreases the residence time of the feed solution in the module and increases the temperature of the brine leaving the module [39, 47, 50, 57].

The effect of brine velocity (v_b) on the permeate flux was evaluated experimentally for brine velocities of 0.03 and 0.06 m/s through the range of 50 – 80 °C and a vacuum pressure of 70 kPa. For these cases, the permeate production rate increases by ~55% when the brine velocity increases from 0.03 to 0.06 m/s (data not shown). Higher fluxes were not examined experimentally due to experimental set-up limitations.

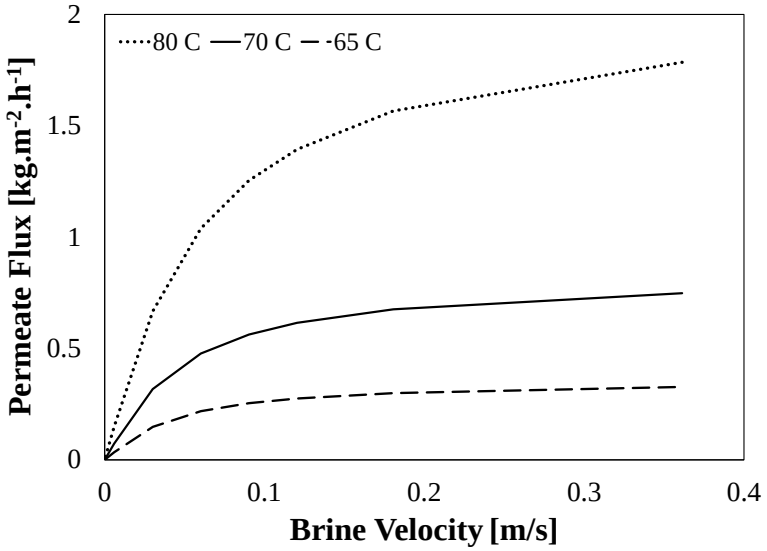

Figure 2.8. Effect of brine velocity on water production rate at a pressure of 70 kPa vacuum

2.6. Conclusions

A finite difference mathematical model was developed to simulate the VMD process in a hollow fiber membrane. The model coupled heat and mass balances to calculate the temperature at the interface and the permeate production. The following conclusions can be drawn from this study.

- Numerical simulations are in excellent agreement with experimental data.
- Knudsen diffusion is the prevailing mass transfer mechanism.
- Results for the model and experiments show no production below the boiling point.
- As temperature increase feed temperature and applied vacuum the water production rate increases since there is an increase in the driving force.
- Increase in pore size and temperature increase the flux.
- Brine velocity increase increases the flux up to an asymptotic maximum value.

CHAPTER 3

COMPARISON OF SLOW SAND FILTRATION AND MICROFILTRATION AS PRETREATMENTS FOR INLAND DESALINATION VIA REVERSE OSMOSIS

3.1. Abstract

A pilot study was conducted from October 2007 to November 2010 to establish the long-term feasibility of using reverse osmosis (RO) treatment to manage salt levels in Central Arizona Project water. Pretreatments consisting of microfiltration (MF) and slow sand filtration (SSF) were compared based on performance—turbidity removal, silt density index (SDI), volume treated between cleaning events and protection of downstream RO—during side-by-side operation over a yearlong period. SSF always produced feed water that was suitable for RO treatment (SDI < 5). However, MF consistently provided filtrate with SDI < 3, and long-term RO performance improved significantly with MF as pretreatment. Although the economic costs of MF and SSF pretreatments are similar; MF is preferred based on the quality of treated water and stability of downstream RO operation

3.2. Introduction

The lower Colorado River basin is the only major United States watershed in which annual water consumption exceeds regional runoff. Regional demands for water

are satisfied, at least for the time being, by importing and conserving water, treating waters of initially impaired quality and water marketing [58, 59]. Regional water resources that are of impaired initial quality, e.g. municipal wastewater and brackish ground water, will play an increasingly important role in southwestern water management.

The importance of the Colorado River to the water resources portfolios of southwestern states has become axiomatic. With an average annual flow of roughly 1.9 x 10^{10} m^3 (15 million acre-feet), the Colorado River is the most important source of water in the southwestern United States, providing water for tens of millions of people from San Diego to Denver [58]. Forty percent of Arizona's water supply is taken from the Colorado River. In all southwestern water supply scenarios, effective utilization of Colorado River water is among the keys to regional water resources sustainability. In some respects, however, water quality in the lower Colorado River already fails to meet sustainability objectives. In the lower Colorado River basin, the average total dissolved solids (TDS) level is approaching 750 mg/L [60], so that the Central Arizona Project (CAP) canal transports about 200,000 metric tons of salt into the Tucson, AZ, area each year. Only a small percentage leaves as surface flow or groundwater underflow. Consequently, the average TDS concentration in major aquifers serving the Tucson municipal area is expected to increase at a rate of 5 mg/L·yr [61], leading to long-term salinity and soil fertility issues. As a point of reference, the secondary MCL for TDS in drinking water is 500 mg/L [62], and waters with TDS concentrations greater than 1000 mg/L are considered brackish [63].

Salinity management in CAP water has been seriously considered in central and southern Arizona [63]. Reverse osmosis (RO) and nanofiltration (NF) are commonly used to separate salts from water when initial TDS levels are below those of seawater. Both RO and NF processes, however, require pretreatment of the feed water to remove membrane foulants and limit membrane scaling. Of the several available methods, slow sand filtration (SSF) and microfiltration (MF) were chosen here for comparison. Previous work by utility and agency partners (Tucson Water, Northwest (Tucson) Water Providers, and Bureau of Reclamation (BOR)) indicated that both pre-treatments controlled fouling during RO treatment of CAP water and that, land permitting, SSF was significantly less expensive [64]. This conclusion arose from a test performed over seven months of continuous operation that did not include comparisons based on contemporary operation of pretreatment alternatives or investigation of seasonal factors. Slow sand filtration has not been extensively used for RO pretreatment, but was studied previously as a pretreatment for ultrafiltration. SSF improved the performance of ultrafiltration by delaying the normal loss of permeate flux [65, 66]. When used for RO pretreatment, SSF consistently produced water with silt density index (SDI) values below membrane manufacturers' recommendation of 5.0 %/min for RO [64, 67, 68]. On the other hand, MF has been widely studied as a pretreatment for RO [69-76].

Typical design/process parameters for SSF and MF are as shown (Tables 2 and 3). In SSF, sand supports the development of a schmutzdecke, a biologically active surface layer in which suspended particles and dissolved organics can be biochemically degraded [34-36]. Biological growth in the schmutzdecke eventually impedes infiltration to a degree that requires the filter surface to be renewed by removing a thin layer of sand.

MF uses micro-porous membranes to strain particles from suspension. This is a completely mechanical process in that no chemical or biological activity is involved. MF utilizes the largest pore size range of the pressure membrane family, from 0.1µm-10µm, and operates at the lowest pressure [72, 77]. At filter pore sizes < 0.2 µm, microfiltration removes bacteria, some viruses and colloidal silica as well as larger particles that might foul RO membranes.

Here we describe the results of a pilot study in which SSF and MF were used as pretreatments for RO treatment of CAP water in the Tucson, AZ area. Pretreatment effectiveness was compared in terms of year-long pre-RO water quality characteristics, sustained (downstream) RO performance and cost.

3.3. Experimental

Calcium sulfate, calcium carbonate and barium sulfate solubilities will be exceeded in brines derived from RO treatment of CAP water at 80 % RO water recovery (Table 3.1). CAP water arrives in Tucson oversaturated with respect to barium sulfate, and it has been suggested that $BaSO_4$ precipitation limits recovery during RO treatment [78].

The pilot-scale desalination facility was located 20 miles northwest of Tucson, adjacent to the CAP Canal. Unit operations (Figure 3.1) consisted of slow sand filtration (SSF) or microfiltration (MF); chemical addition—15 mg/L of sulfuric acid, to maintain the RO feed water at pH ~6.8, commercial antiscalant (Flocon 135, 3.5 mg/L), NaOCl (1.4 mg/L) plus $(NH_4)_2SO_4$ (2.0 mg/L) for disinfection—and reverse osmosis. Free chlorine concentration was maintained at <0.1 mg/L, and combined chlorine was 1.5 – 2

mg/L (as chlorine). The RO brines were used locally to grow salt-tolerant plants. The pilot-scale RO unit consisted of 6 pressure vessels containing a total of 18 membrane elements in a two-stage, 2:2:1:1 array (Figure 3.1). Membrane elements were 2.5-inch diameter by 40-inch length polyamide thin film composite membranes (ESPA2-2540, Hydranautics and later Koch TFC ULP). RO pressure requirements ranged from 80 to 110 psi, adjusted to maintain constant recovery (80%). The average permeate flux was 0.5 m/d. The feed water temperature varied from 15 to 28° C.

Table 3.1. Concentration/solubility data for CAP water ion pairs that may contribute to membrane scaling

Precipitate	**Ion concentration in CAP water**	**log (ion product) in CAP water**	**log K_{S0}[(b)]**	**Degree of super saturation following RO treatment[(c)]**
$BaSO_4(s)$	$[Ba^{+2}] = 1.11 \times 10^{-6}$ M $[SO_4^{-2}] = 2.66 \times 10^{-3}$ M	-7.13	-9.96	673.20
$CaSO_4(s)$	$[Ca^{+2}] = 1.87 \times 10^{-3}$ M	-3.91	-4.85	8.81
$CaCO_3(s)$	$[CO_3^{-2}] = 6.88 \times 10^{-6}$ M[(a)]	-6.49	-8.48	97.19

(a) based on 118.05 mg/L carbonate alkalinity as HCO_3^- and pH = 7.88.
(b) [79] & [80]
(c) calculated as Q_{SO}/K_{SO}. The value represents the approximate degree of oversaturation in the RO brine produced from CAP water at 80% recovery.

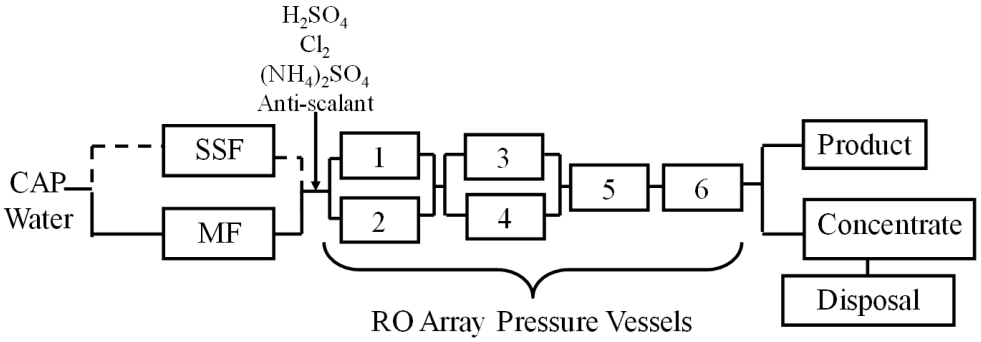

Figure 3.1. Schematic of the Science and Technology Pilot-Scale Desalination Facility in Marana, AZ. The pilot scale facility was used to desalinate CAP water from 2007 to 2010

Two SSF units (north and south) were operated in parallel. The North Slow Sand Filter (NSSF) and the South Slow Sand Filter (SSSF) were filled with silica sand (ES) from OgleBay Norton Industrial Sands, Inc. (Colorado Springs, CO) [81]. Both sands had a d_{10} of 0.34 mm, and uniformity coefficient (d_{60}/d_{10}) of 1.7. Particle size distributions, as determined by sieve analyses, were similar. SSF design parameters were as shown (Table 3.2). Filtration rates were 1.6, 3.1, 4.7, and 6.3 m/d (0.027, 0.053, 0.080, and 0.107 gal/ft^2/min; 1.7, 3.3, 5.0, and 6.7 million gal/day/acre) during constant flow operation. These values provided a range of operational conditions covering most of the SSF range of operation recommended by the Arizona Department of Environmental Quality—1.9 to 9.4 m/d (0.032 to 0.159 gal/ ft^2/min; 2.0 to 10.0 million gal/day/acre) [27]. Excess pretreated water was wasted as necessary to produce a steady RO feed of ~18 L/min.

Table 3.2. SSF design parameters; comparison to parameter values used in the pilot-scale application

Slow Sand Filters		
Parameters	Pilot Plant	Design[(a)]
Initial depth of filter sand bed [m]	0.91	0.9 – 1.5
Minimum depth of filter sand bed [m]	0.46	0.4 – 0.5
Sand uniformity coefficient, d_{60}/d_{10}	1.7	1.5 – 2.0
Height of the under drains, including gravel layer [m]	0.91	0.3 – 0.6
Height of water above the sand [m]	1.52	0.9 -1.5
Product flow per filter [m^3/d]	43.6	NA
Maximum Filtration rate [m^3/m^2.d]	6.3	9.4[(b)]
Total filter area per filter [m^2]	7	NA
Number of filters [-]	2	NA

(a) [30]
(b) [82]

SSF operations were interrupted for filter cleaning when constant flow operation could no longer be maintained due to filter head loss. At that point, 1.5 cm of sand containing the schmutzdecke was manually removed from the top of the filter. The sand was dried, sieved and subsequently used to re-sand the SSFs. After cleaning, filters were run in recirculation mode for ~3 days to rebuild a schmutzdecke. Before SSF filtrate was again used as RO influent, turbidity measurements were < 0.3 NTU and SDI values were < 5.

The MEMCOR 3M10C Continuous Microfiltration (CMF) unit contained three hollow fiber filtration modules. The MEMCOR 3M10C operates in a dead end mode. Membranes had a nominal pore size of 0.2 µm. Water passed through the membranes from shell to lumen side. Specifications for the unit were as shown (Table 3.3) [83]. Backwash was automatic at 50-minute intervals and dumped to waste. When the transmembrane pressure (TMP) reached 103.4 kPa, the membrane modules were cleaned in place (CIP) using a caustic commercial solution, Memclean® C (Siemens, Colorado). CIP consisted of a 24-hour extended soak followed by a thorough rinse, which normally restored the TMP to the clean-membrane value (~30 kPa).

Samples were taken from the SSF and MF units on the same days, within 3 hours of one another. The frequency of sampling varied from daily to every other day depending on the filtration rate.

Table 3.3 - Microfiltration unit specifications in comparison to typical design values

MEMCOR CMF Unit		
Parameters	**Pilot Plant[(a)]**	**Design[(b)]**
Membrane material [-]	Polypropylene	Polypropylene
Nominal membrane pore size [μm]	0.2	0.1 - 5
Maximum filtration rate [$m^3/d\ m^2$]	1.8	0.7 – 4
Maximum transmembrane pressure [kPa]	103.4	20 – 100
Flow regime	Dead end	Dead end
Membrane area of each filtration module [m^2]	15	NA
Total membrane area [m^2]	45	NA
Operation filtration rate [$m^3/d\ m^2$]	1	NA
Number of filtration modules [-]	3	NA
Coagulation	No	In some cases

(a) [83]
(b) [30]

3.3.1. Analytical

To measure the SDI, samples were passed at constant pressure (207 kPa) through a 0.45-μm pore size membrane filter. The water temperature was constant (± 1°C) throughout the test. Time-dependent flow data were used to calculate a plugging factor (PF), the percentage decrease in flow through the filter over a specified period—here 15 min [77]. Then,

$$SDI = \frac{PF}{t} = \frac{\left[1 - \frac{t_i}{t_f}\right]}{t} \tag{3.1}$$

where, *SDI* is the silt density index [%/min], *PF* is the plugging factor [%]; the percent decrease in filtration rate after *t* min; t_i, the time [minutes] required initially to filter 0.5 L; t_f, the time required to collect a 0.5-L sample at the end of the test period, *t* [15 minutes].

Following convention, SDIs are reported here without units, although a unit of %/min is appropriate, per equation 3.1. If PF reached 75% prior to the end of the 15-min test, the apparatus stopped automatically without providing a useful SDI value. SDI values < 5.0 are recommended to protect RO membranes from influent particle accumulation and fouling [77, 84]. However, SDI values < 3.0 in RO feed water are recommended in order to obtain runs of several months without cleaning [77, 85]. SDI measurements were performed with a Chemetec Model FPA-3300 and MILLIPORE Millex® -HA MF-Millipore Membrane (mixed cellulose esters) syringe driven filters. A relationship between the SDI and the modified fouling index (MFI), an alternative method to measure the fouling potential of feed water for reverse osmosis, was used to compare literature values to our data [85, 86].

Sample turbidities were measured on a model 2100P IS Portable Turbidimeter on the day of sample collection. A Hitachi S-3400N Type II / ThermoNORAN with NORAN Systems Six software (NSS) was used for energy dispersive X-ray spectroscopy (EDS), and variable pressure Scanning Electron Microscopy with EDS (SEM-EDS) was used to analyze material deposited on RO membranes. X-Ray Diffraction (XRD) analyses were performed with the Scintag XDS 2000 PTS Diffractometer to determine

the composition of the material scraped from the membrane. SEM-EDS and XRD analyses were performed at the University of Arizona Spectroscopy & Imaging Facilities.

3.4. Results and Discussion

3.4.1. Extended SSF Performance

Independent variables for the study included the identity of the pretreatment reactor (NSSF, SSSF), season and the SSF filtration rate. Dependent variables were the filtrate quality, as indicated by the SDI value, and the length of filter runs or volume of water treated between cleanings. The raw CAP water had a mean turbidity of 2.14 NTU (σ = 1.5, n = 217). Both SSFs consistently reduced the turbidity to less than 0.3 NTU (Table A.2). Values were unrelated to influent water turbidity, which varied considerably. Results were comparable to those of previous studies using SSF for turbidity removal [65, 66, 87]. However, insensitivity of the turbidity parameter led to selection of SDI as indicator of filtrate quality.

The turbidity of raw CAP water did not change appreciably during 15 months of operation (August 2009 – November 2010). Around 85% of the samples measured had turbidities $\leq$ 3.3 NTU (Figure A.1). During the same period, both SSFs produced filtrate with SDI values < 5 in 99% of effluent samples (NSSF n = 122 and SSSF n = 125; Figure 3.2) at overflow rates from 1.6-6.3 m/d. Direct comparison of mean SDI values in contemporary NSSF and SSSF filtrates suggests that the NSSF outperformed the SSSF throughout the study. That is, SDI values in NSSF effluent were generally lower than those measured in SSSF effluent (Figure 3.3) despite the fact that water production between cleaning events was equivalent in the two reactors (Figure 3.4). SSF pretreatment for RO treatment of Rhine River water produced filtrate with an average

membrane fouling index (MFI) 1.23 ±0.51 [68]. This is equivalent to an SDI of 3.7±1.53 [85, 86]. When SSF was used previously to treat lower Colorado River water, the average filtrate SDI varied seasonally from 3.1 to 4.5 [64, 67].

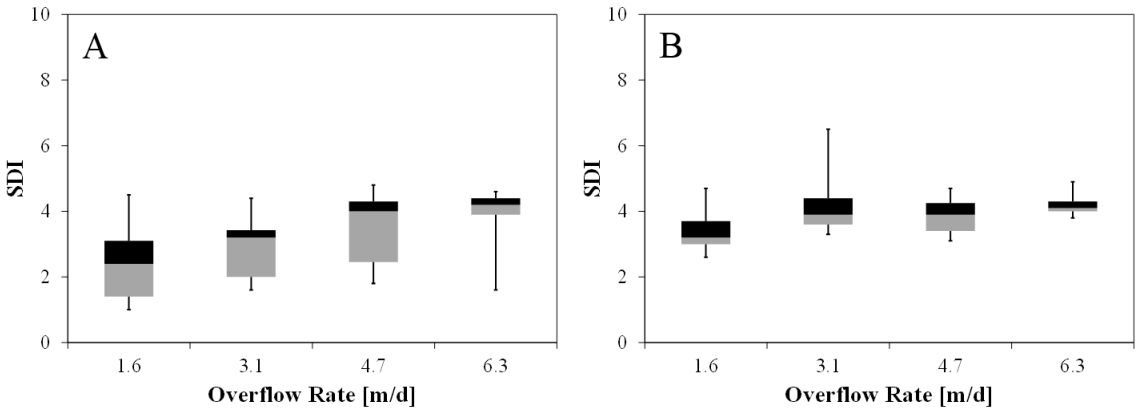

Figure 3.2. Box-plots for NSSF (a) and SSSF (b) SDI values at different overflow rates. SDI values are shown in %/min. SDI values for the raw CAP water could not be obtained since the PF routinely exceeded 75% prior to the end of the 15-min test. Mean and standard deviation values are in %/min

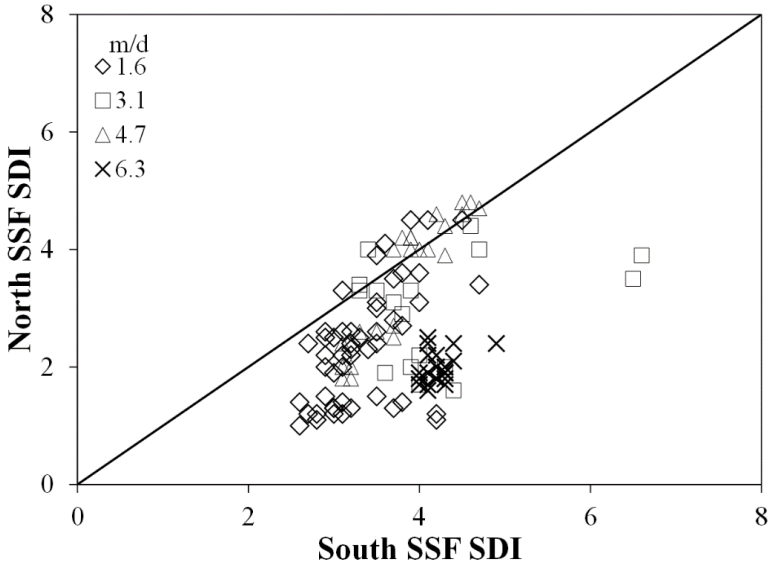

Figure 3.3. Comparison of north and south SSF performances in terms of contemporary SDI values at the overflow rates (m/d) indicated Filled markers show the filters production during summer and the open markers show the operation during winter

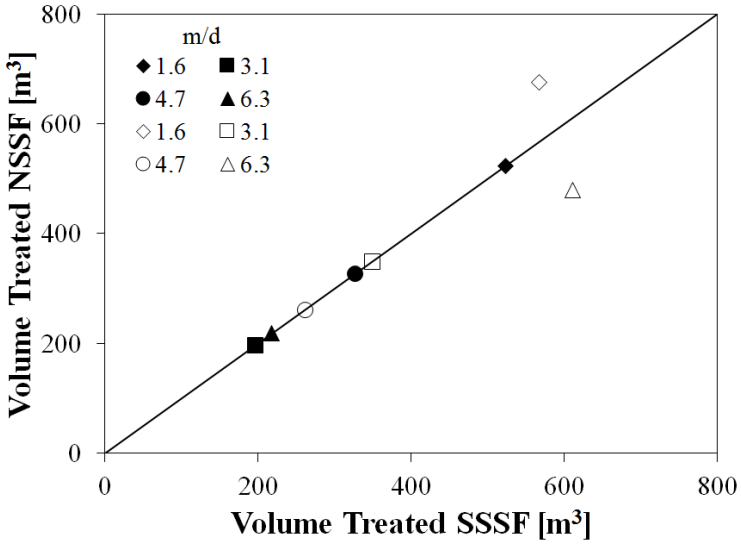

Figure 3.4. Comparison of NSSF and SSSF performance in terms of the volume of filtrate produced between cleanings in contemporary studies. The overflow rates indicated are in units of m/d. Filled markers show the filters production during summer and the open markers show the operation during winter

Table 3.4 shows results of one-way ANOVA involving NSSF and SSSF effluents at each of the filtrate rates. The null hypothesis—that the NSSF SDI mean value was equivalent to that of the SSSF was rejected at filtration rates $\leq$ 3.1 m/d ($p << 0.05$), indicating that performance of the NSSF was significantly better than that of the SSSF, particularly at low filtration rates (Figure 3.3). It is also apparent that lower SDI values in NSSF filtrate did not result from abbreviated filter runs (Figure 4). The expected length of SSF runs between filter cleaning operations is $\geq$ 14 days under the least favorable conditions [88]. In this study, the time between cleanings varied from 6 to 62 days and was sensitive to overflow rate and season.

Table 3.4 One-way ANOVA results for comparison of SSSF and NSSF filtrate SDI values. In each case, the null hypothesis was that there was no difference between SDI measurements for the north and south filters

Overflow Rate [m^3/m^2 d]	**Mean (south/ north)**	**Variance (south/ north)**	**F-observed**	**P-value**	**F-critical**	**Df**
1.6	3.35 / 2.42	0.25 / 1.09	32.72	$1.11x10^{-7}$	3.94	100
3.1	4.21 / 2.97	0.96 / 0.81	14.7	$5.57x10^{-4}$	4.15	32
4.7	3.84 / 3.45	0.26 / 1.21	2.43	0.13	4.06	45
6.3	4.16 / 3.80	0.04 / 1.03	3.77	0.06	4.01	56

3.4.2. MF Performance

MF is generally accepted as a stable, reliable pretreatment for RO [72-74], providing permeate SDI values ≤ 3 in seawater applications [69, 70, 74-76]. Here, mean values for MF permeate SDIs during the summer and winter were 2.07 (SD = 0.35, n = 97) and 1.68 (SD = 0.33, n = 98) (Figure 3.5). The seasonal difference was statistically significant, one-way ANOVA, p = 8.97 E-14. This difference could be explained based on the fact that warmer temperatures during summer promoted algal growth and activity in the source water.

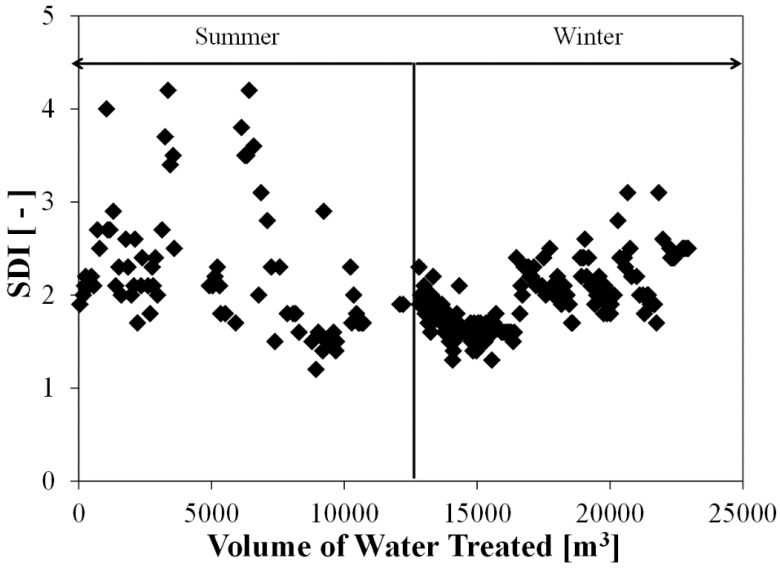

Figure 3.5. SDI as a function of filtrate volume produced and season during the one-year overall period of MF operation.

MF fouling was completely reversed during CIP (Figure 3.6). Each CIP restored TMP to about 30 kPa. Time between cleanings was a function of the quality of the influent. In summer, when influent was particularly turbid due to high irrigation withdrawals and rapid algal growth, CIP was necessary after treatment of ~2000 m^3, compared to ~5000 m^3 during the winter months.

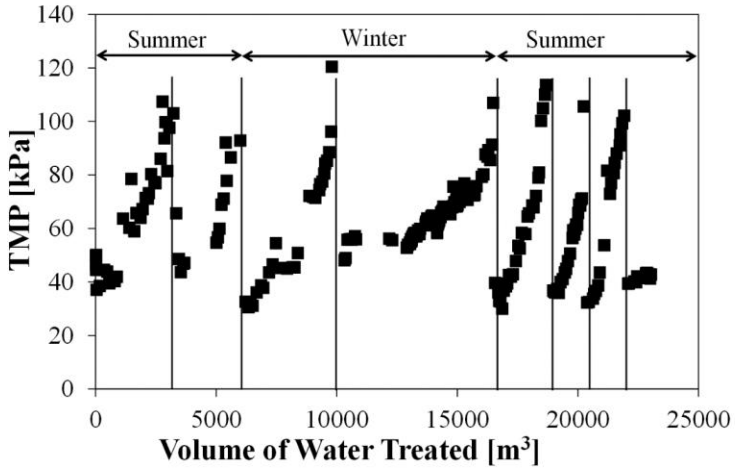

Figure 3.6. TMP as a function of volume of water treated by microfiltration. Vertical lines represent timing of CIP events

3.4.3. MF vs. SSF

The best SSF performance observed was specific to the NSSF at an overflow rate of 1.6 m/d, where the mean SDI was 2.42 (SD = 1.04, n = 52). That case was selected as a basis for comparing SSF and MF performances. The MF unit operated at a filtration rate of 1.0 m/d (40 gal/ft^2/day) throughout the study. One-way ANOVA was used to test the null hypothesis—that SDI values were statistically indistinguishable in the NSSF (overflow rate 1.6 m/d only) and MF filtrates during the period of parallel operation. Mean values for filtrate SDIs for the NSSF and MF units were 2.42 (SD = 1.04, n = 52), and 1.89 (SD = 0.38, n = 193), respectively. The test indicated that the MF unit outperformed SSF in terms of SDI values in pretreated water, p = 1.81 E-08, despite the fact that only the best SSF data set obtained (the more effective filter at the lowest filtration rate) was considered.

The cumulative SDI frequency distributions in the MF and NSSF (1.6 m/d) filtrates illustrate relative process performances. About 95% of the MF effluent samples had SDI values < 3 while only 71% of the SDI values for the NSSF were < 3 (Figure 3.7).

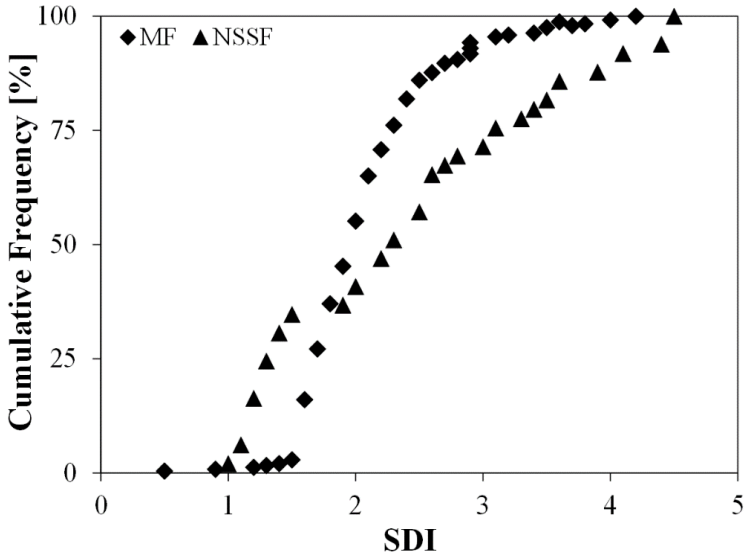

Figure 3.7. Cumulative Frequency vs. SDI for MF filtrate and NSSF at an overflow rate of 1.6 m/d

3.4.4. Pretreatment as Determinant of RO Performance

The effect of alternative pretreatments on RO performance is illustrated by comparing time-dependent profiles of the RO membrane transport coefficient (A) and the salt passage coefficient (B) [30] for both pretreatments (Figure 3.8). The temperature-corrected water transport coefficient is given by:

$$A=\frac{F}{P_{avg}-P_p-\left[\pi_{avg}-\pi_p\right]}\times 1.033^{(25-T)}=\frac{\left[\frac{m}{s}\right]}{Pa} \quad (3.2)$$

where F is the permeate flux, P_{avg} and P_P are pressures in the unit feed and permeate streams, π_{avg} and π_p are the osmotic pressures in the unit feed and permeate and T is the temperature of the sample (^{O}C).

The temperature-corrected salt transport coefficient (B) is defined in equation 3.3.

$$\text{B}=\frac{\text{F}\times TDS_p}{TDS_{avg}-TDS_p}\times 1.033^{(25-T)}=\frac{m}{\text{s}} \tag{3.3}$$

where *TDS* is the total dissolved solids for the permeate, *p* stands for the permeate and *avg* is the average feed concentration.

From October 2007 through March 2010, the RO feed water was pretreated via SSF. The SSFs operated at an average filtration rate of 3.1 m/d. Profiles of the water transport coefficients for the head and tail elements of the 2:2:1:1 RO unit over the entire three-year period are provided (Figure 3.8). Over the first six months of continuous operation, the A coefficient in the downstream RO element decreased by 80%. Each time the RO unit was chemically cleaned (NaOH solution, pH 12, 26^{o}C) the A coefficient was restored to approximately its original value. The cleaning process consisted of four steps: (i) a low-flow flush with the basic solution in recycle mode; (ii) soak; (iii) a high-flow flush with the basic solution, again in recycle mode and (iv) a neutral pH flush, without recycle. After new membranes were installed in the tail elements in August 2008, membrane permeability again deteriorated—by >80% in the tail elements within 2.5 months.

Causes of time-dependent reductions in the water transport coefficient remain speculative. The head RO element experienced the slower decline in membrane permeability, suggesting that scaling, as opposed to fouling, was responsible for rapid reduction in A values in the tail elements. The concentrate HPC data (Figure A.17), while interesting, are conflicting. During SSF pretreatment, fifty percent of the measured RO concentrate HPCs were < 100 CFU/mL and 90% of the values were <500 CFU/mL. After MF pretreatment was implemented, only 21% of the HPC data were < 100 CFU/mL and 50% were < 500 CFU/mL. Thus high HPC data were not unique to the period of SSF pretreatment, undermining to an extent arguments relating reduction in water transport to a fouling mechanism. Membrane autopsy data (not shown) indicated that HPC values in material scraped from the membrane surfaces accounted for low fractional membrane coverage.

After November 2008, A values also declined rapidly in the upstream RO elements, suggesting that the mechanism for loss of membrane permeability may have shifted abruptly toward fouling. All values were considerably larger than the 23% decline of the A coefficient observed over an 11-month period in a study in the Rhine River [11]. In that investigation, the RO unit was not chemically cleaned at any time.

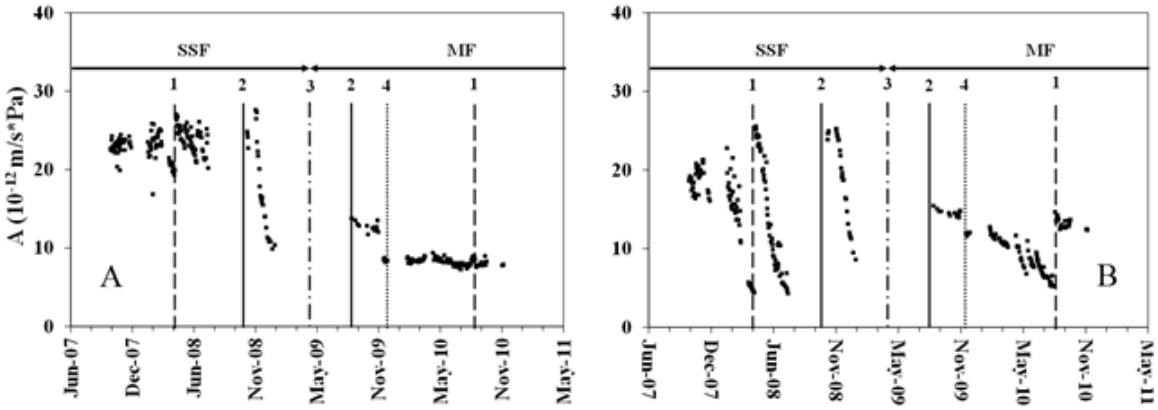

Figure 3.8. Time-dependent trajectories of the water permeation coefficient (A) during RO treatment of pretreated CAP water. Left: Lead elements. Right: Tail elements. (1) The dashed lines (~ April 08 and November 10) mark the times of chemical cleaning of the entire RO unit. (2) Solid vertical line indicates when new membranes (Hydranautics ESPA2) were installed in the tail elements (~October 08) and new membranes were installed (Koch Membranes TFC ULP) in all pressure vessels (~August 09). (3) The dashed-dotted line shows when MF was installed as pretreatment for RO and the vertical dotted line shows when MF backwash valve failed (4)

In August 2009, new membranes were installed in the RO unit, and thereafter the RO feed water was pretreated by MF. Lower values of the permeation coefficient after August 2009, were a direct result of the clean membrane characteristics of the Koch TFC ULP membranes installed at that point. Koch TFC ULP membrane performance was relatively stable for a period approaching six months in vessels 5 and 6 and for more than a year in vessels 1 and 2 (Figure 3.8). The abrupt decrease of the A coefficient in November 2009 was due to a failure in the MF unit backwash effluent valve that produced a one-time, irreversible loss of permeability in all vessels.

Figure 3.9 shows the fouling resistance (equation 3.4) for the head and tail elements of the RO unit. The membrane resistance due to fouling (R_f) is the difference between the measured resistance to water passage (R_{obs}—the inverse of the water transport coefficient) and the clean membrane resistance (R_m—the inverse of the clean membrane water transport coefficient).

$$R_f = R_{obs} - R_m \tag{3.4}$$

$$R_f = {A_{obs}}^{-1} - {A_m}^{-1} \tag{3.5}$$

where A_{obs} is the water transport coefficient measured and A_m is the clean membrane water transport coefficient.

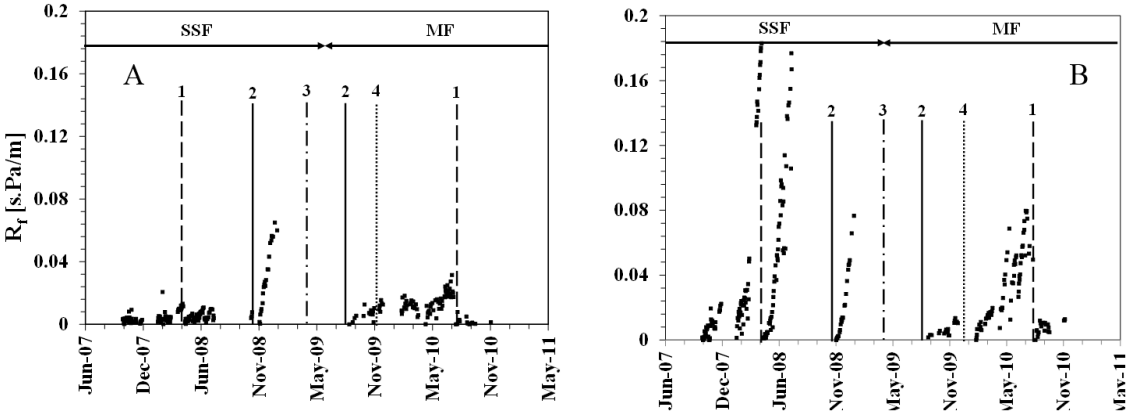

Figure 3.9. Rate of change of fouling resistance, R_f, for a) head elements and b) tail elements in RO skid. (1) The dashed lines (~ April 08 and November 10) mark the times of chemical cleaning of the entire RO unit. (2) Solid vertical line indicates when new membranes (Hydranautics ESPA2) were installed in the tail elements (~October 08) and new membranes were installed (Koch Membranes TFC ULP) in all pressure vessels (~August 09). (3) The dashed-dotted line shows when MF was installed as pretreatment for RO and the vertical dotted line shows when MF backwash valve failed (4)

In the head membrane elements (Figure 3.9a), membrane resistance increased sharply after a 9-month period of near-steady performance. The only operational period in which membrane resistance increased continually may have arisen after a brief period of operation at 85% recovery (Aug – Nov 08). After MF pretreatment was initiated, the only increase in fouling resistance was due to the MF backwash failure described previously, and this was reversed via subsequent membrane cleaning. The tail elements (Figure 3.9b) provide a significantly different picture. Throughout the period of SSF pretreatment, membrane fouling resistance in the tail elements increased continuously. Discontinuities correspond to cleaning events and membrane replacement. After MF pretreatment was initiated, membrane resistance was consistently near zero for a period

of three months. At that point, the MF backwash failure occurred, and R_f increased steadily over the next six months of operation. After the membranes were cleaned in July 09, R_f remained steady (near zero) for the remainder of the study (4 months). Taken together, Figure 3.8 and 9 results suggest that the shift from SSF to MF pretreatment improved RO performance, mitigating fouling as a mechanism for loss of membrane permeability. The accelerated rate of decline in the permeation coefficient in the tail RO elements with SSF as pretreatment suggests that both scaling and fouling contributed to the time-dependent loss of RO performance. These observations are supported by the results of SEM and EDS analyses that were part of the membrane autopsy procedure. See below. For perspective, representative R_m values were 0.04 s.Pa/m and 0.07 s.Pa/m for the ESPA2 membranes and Koch TFC ULP membranes respectively. It is evident that membrane fouling contributed significantly to overall membrane resistance after relatively long periods of use between cleanings.

The salt passage coefficient (B) increased continuously throughout the period in which SSF treatment was provided (Figure 3.10). This may have been a consequence of progressively lower water fluxes coupled with minor membrane abrasion during cleaning. The rate of increase in B values was much less dramatic during the period in which MF pretreatment was provided.

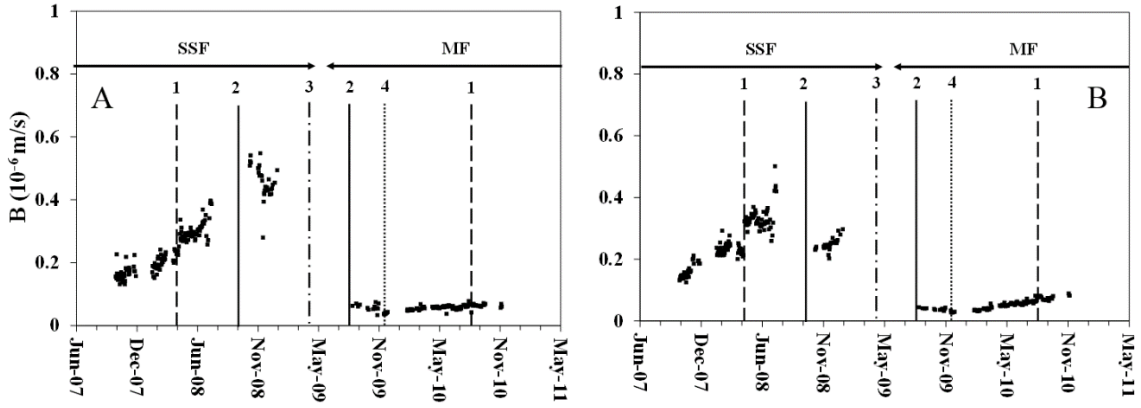

Figure 3.10. Time-dependent trajectories of the salt transport coefficient (A) during RO treatment of pretreated CAP water. Left: Lead elements. Right: Tail elements. (1) The dashed lines (~ April 08 and November 10) mark the times of chemical cleaning of the entire RO unit. (2) Solid vertical line indicates when new membranes (Hydranautics ESPA2) were installed in the tail elements (~October 08) and new membranes were installed (Koch Membranes TFC ULP) in all pressure vessels (~August 09). (3) The dashed-dotted line shows when MF was installed as pretreatment for RO and the vertical dotted line shows when MF backwash valve failed (4)

3.4.5. Membrane Post-Mortem Analyses

Material accumulation on the surface of the ESPA2 membranes was examined by visual inspection, SEM imaging, and EDS. After material was removed from a representative section of membrane, it was analyzed using XRD. The membrane shown (Figure 3.11(a)) was in operation for a total of 6 months, during which pretreatment was exclusively via SSF. Material accumulation was obvious in SEM images (Figure 3.11(a)). It was easily collected by scraping with a soft spatula, visually restoring the membrane surface to almost its original appearance. Elemental analysis of deposits indicated that the light material in Figure 3.11(a) is enriched in barium and sulfur (Supplemental Information Figure A.3.), suggesting the presence of precipitated barium sulfate. This was expected based on the degree of barium sulfate saturation in the CAP

brine following RO treatment (Table 3.1). EDS analysis of the darker material showed enrichment of aluminum and silicon, suggesting that the material consists of a mixture of silica clays. XRD produced strong peaks corresponding to silicon oxide, hydrated sodium magnesium aluminum silicate hydroxide, sodium calcium aluminum silicate and phosphorus oxide sulfate (Figures A.4-A.9). Together, results of the analysis suggest that the ESPA2 membranes experienced a combination of scaling by barium and calcium sulfate and fouling with a mixture of clays. It is possible that clay particles on the membrane surface originated in the sand filters (silicon oxide) [71].

In contrast, the (Koch TFC ULP) RO membranes that were fed MF-pretreated water for 12 months exhibited little material build-up on the membrane surface (Figure 3.11(b)). EDS results suggested that the light-colored deposits (upper right quadrant) consisted of barium and calcium sulfates. XRD analysis of the material on the surface of the Koch TFC ULP membranes produced peaks for barium sulfite and sulfate, silicon oxide and barium strontium sulfate (Figure A.12).

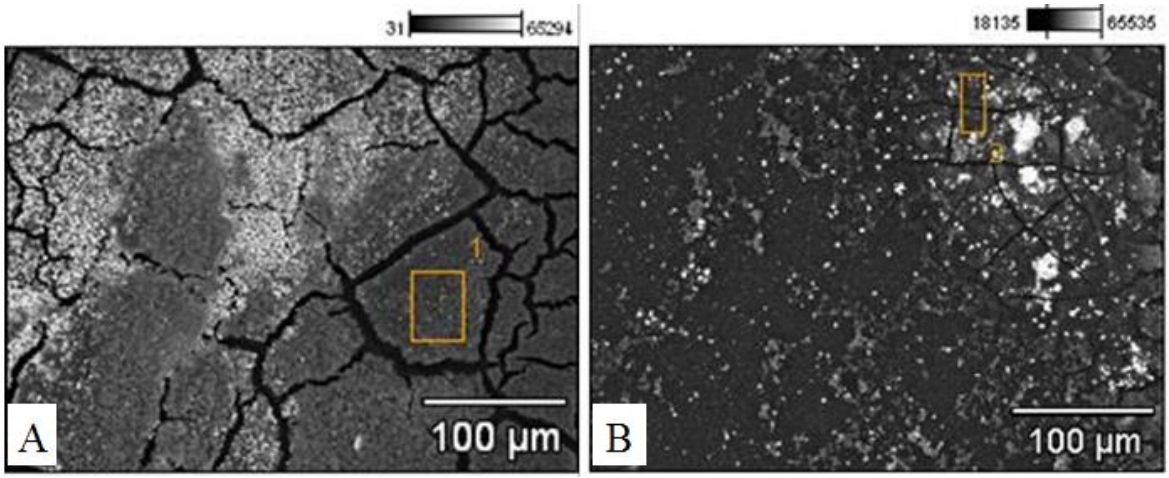

Figure 3.11. Scanning Electron Microscope (SEM) images of the surface of the (a) Hydranautics ESPA2 and (b) Koch TFC ULP membranes recovered from the tail of RO vessel 6. While the ESPA2 membranes were in use, pretreatment was provided by SSF.

MF pretreatment was is place during use of the Koch membranes. Areas indicated by rectangles were further analyzed to determine elemental composition (Supplemental Information Figures A.2 and A.11)

3.4.6. Economic Analysis

The costs of MF and SSF as pretreatments for RO desalination of CAP water were compared for a hypothetical RO desalination plant that treats 57,000 m^3/day (15 MGD). The period of the economic analysis was 30 years, the assumed service life of the RO pressure vessels and non-mechanical infrastructure, and the discount rate was 0.06 yr^{-1}. Reported costs are in October 2012 dollars (ENR CCI 9375.52) [89]. Table 3.5 summarizes the economic analysis for the MF unit and SSFs at all overflow rates tested during this study.

The annualized cost of SSF per volume of RO product over the 30-yr economic analysis ranged from \$0.25/m^3 (\$0.94/1,000 gallons) at a filtration rate of 3.1 m/d to \$0.14/m^3 (\$0.53/1,000 gallons) at a filtration rate of 6.3 m/d (Table 3.6). The amortized cost for MF pretreatment was estimated at \$0.21/m^3 (\$0.81/1,000 gallons) at a filtration rate of 1.0 m/d (40 gal/ft^2/day). This value includes the cost of land, but the footprint of the MF technology was less than 10% of the land needed for SSF operating at 6.3 m/d. The unit cost for un-subdivided, undeveloped rural land used for this analysis was \$1.24/m^2 (\$5000/acre) [37]. Incremental costs attributable to SSF pretreatment were estimated at \$0.21/m^3 although a study treating lower Colorado River concluded that only 0.04 \$/m^3 was required. In that analysis, it was assumed that SSFs would operate continuously for 22 days between cleanings at an overflow rate of 6.5 m/d [7]. The maximum filter run length observed here at a similar overflow rate (6.3 m/d) was 8 days.

The economic analysis did not include RO costs, which were common to all scenarios but might differ significantly based on the quality of water produced during pretreatment. Thus, although the direct economic costs of MF and SSF pretreatments were similar, MF may be preferred economically based on differential RO operation and maintenance costs that were not considered here.

Table 3.5. Cost components for the economic analysis of SSF and MF in 2012 dollars

Item	Basis of Calculation [a]	Assumptions/Explanations
Capital Costs		
MF units	$(3.01\times10^6 \times (Q_{TP})^{0.872} + C_L \times A_{MF}) \times F_{30}$	**Capital Cost for MF construction** [88] Q_{TP} = RO feed flow = 56,775 m^3/day (15 MGD) C_L= \$1.24/m^2 [89] A_{MF} = 840 m^2 F_{30}= 0.0726 A_{SSF} = area of filter in m^2 dependent on overflow rate
SSF Units	$(C_c + C_L + C_S + C_G) \times F_{30}$	**Capital Cost for SSF construction** [90] C_S= \$45.46 / ton [79] Thickness of gravel layer = 0.5 m (equal thickness layers of 3 different gravel sizes: 2.54 cm, 1.9 cm and 0.9 cm) [91] $C_c = 1{,}270 \times A_{SSF} + 10^6$ [90] C_G= \$26.5/ton, \$24.5/ton and \$24.75/ton [92] ρ_S = 1602 kg/m^3 [93] ε_S = 0.4 [94] ρ_G = 1682 kg/m^3 [93] ε_G = 0.2 [94]
O&M Costs		
MF	$4.44\times10^5 \times (Q_{TP})^{0.4323} \times F_{30}$	**Operation and Maintenance for MF** [88] $M = 2.7\times10^6 (Q_{TP})^{0.875}$ [88] r = 6% Assuming a new set of modules is purchased every 10 years.
Annualized Module Replacement Cost	$[(M10 \times 1/(1+r)^{10}) + (M20 \times 1/(1+r)^{20})] \times F_{30}$	
SSF	Cost for cleaning + Cost for Resanding $[(T_{CSSF} \times A_{SSF} \times f_C) + (T_{RSSF} \times A_{SSF} \times f_R)] \times P_W$	**Operation and Maintenance for SSF** T_{CSSF} = 2.5 h/100 m^2 [95] f_C = frequency of cleaning based on overflow rate [#/year] [(b)] f_R= resanding frequency based on overflow rate [year][(c)] T_{RSSF} = 50 h/100 m^2 [95] P_W = \$19.60/h [96]

a) All costs are annualized
b)

Overflow rate [m/d]	f_C [#/year]	f_R [#/year]
1.6	8	0.26
3.1	20	0.67
4.7	34	1.11
6.3	43	1.43

c) When half of the sand depth in bed has been removed, resanding is required.

Table 3.6. Comparison of economic costs for SSF and MF pretreatments for a hypothetical 15 MGD desalination facility

Unit	Land [m^2]	Capital Cost M$/yr	O&M Cost M$/yr	Total Cost M$/yr	Cost $/$m^3$
SSF @ 1.6 m/d	42,000	9.0	0.3[(a)]	9.3	0.45
SSF @ 3.1 m/d	22,000	4.8	0.4[(a)]	5.2	0.25
SSF @ 4.7 m/d	15,000	3.3	0.5[(a)]	3.8	0.18
SSF @ 6.3 m/d	11,000	2.5	0.4[(a)]	2.9	0.14
MF	840	2.5	1.9	4.4	0.21

[(a)]The sand scraped from the SSFs is sieved and used to re-sand the filters when needed.

3.5. Conclusions

Slow sand filtration and microfiltration were compared as pretreatments for RO. RO performance was more stable when MF pretreatment was provided. Post-mortem membrane inspections, confirmed by SEM-EDS images, showed that significantly more material accumulated on the membrane surface during SSF pretreatment, reducing the water transport coefficient due to a combination of fouling and scaling reactions. To reduce the likelihood of biological fouling, future work of this nature should regulate free chlorine contact time and chloramine residual in the RO feed to maintain HPCs below 100 CFU/mL in the RO reject. Economic analysis suggests that the costs of MF and SSF

pretreatments are comparable, but MF pretreatment should be economically preferred when RO membrane cleaning and replacement costs are considered.

CHAPTER 4

POST-MORTEM ANALYSIS OF MEMBRANES FROM THE YUMA DESALTING PLANT POLYAMIDE MEMBRANES ASSESSMENT STUDY

4.1. Abstract

Fouled membranes used between 2010 and 2012 from the United States Bureau of Reclamation's Water Quality Improvement Center (WQIC) undertook a study of the effect of feed water and pretreatment method on performance of RO polyamide membranes. The two sources of water used during this study were the Main Outlet Drain Extension (MODE) and the Yuma Mesa Conduit (YMC). Partial lime softening-gravity filtration, direct filtration, manganese oxide-amended anthracite filtration and greensand filtration were evaluated as options to pretreat the two water supplies prior to desalination by reverse osmosis. Analytical techniques used in the study included scanning electron microscope (SEM), SEM equipped with energy-dispersive X-ray spectroscopy (SEM-EDX), Fourier Transform Infrared Spectroscopy (FTIR) and attenuated total reflectance-FTIR (ATF-FTIR), X-ray diffraction (XRD), and heterotrophic plate counts (HPC).

Post-mortem results for membranes showed biofouling, deposition of inorganics (clays, silicon oxides, and traces of iron) and organic fouling were much greater with lime softening than microfiltration as pretreatment. For the YMC water pre-treatment

alternatives, microfiltration (MF) and cartridge filtration (CF), there was significantly greater material build-up with CF pre-treatment, particularly on the tail element in the high recovery array.

4.2. Introduction

Agricultural drainage water from the Wellton-Mohawk Irrigation and Drainage District (WMIDD) is currently collected in a canal system that bypasses the Colorado River and drains into wetlands located in Ciénega de Santa Clara (Santa Clara Slough) in Mexico. The drainage water contains greater than 1,400 mg/L and total dissolved solids (TDS) and is thus unsuitable for direct potable or most agricultural use. The bypassed water does not contribute to water deliveries to Mexico that are required by international agreement between Mexico and the United States [90]. Desalting the drainage water and returning it to the Colorado River, where it can be counted among the treaty-mandated deliveries to Mexico, would free additional Colorado River water for upstream use within the U.S. In its original configuration, the YDP could, in theory, treat and recover the entire bypassed WMIDD flow (an annual average of ~132 million m^3 of water). The plant is capable of treating water with TDS in the range 2,850-3,450 milligrams per liter (mg/L) [Reference]. Operation of the YDP could extend Colorado River water supplies to alleviate protracted drought, over allocation of supply and increased demand.

Reverse osmosis (RO) is the most widely used inland desalination technology. RO uses a semipermeable membrane and external pressure to overcome the osmotic pressure in order to extract low salinity water from brackish water or seawater. RO has proven to be a reliable, efficient way to desalinate water [91]. However, RO membranes

are prone to scaling and fouling. Membrane fouling due to the accumulation of rejected species at the membrane surface is the major cause of long-term flux decline, poor quality permeate, premature membrane replacement, frequent membrane chemical cleanings, and increased operation and maintenance costs [92, 93].

There are four major types of foulants i) soluble inorganic compounds; ii) colloidal or particulate matter; iii) dissolved organics; and iv) microorganisms [71, 92, 94]. The mechanism of fouling depends on the type of foulant. Scaling occurs if the concentration of soluble components exceeds their solubility limit and soluble inorganic compounds precipitate on the membrane surface. Accumulated particulate matter may form compact cakes, which adds resistance to water transport. Blockage of membrane pores may be caused by adsorption of low molecular weight solutes. Irreversible gel formation on the membrane surface can be caused by polymerization of inorganic compounds such as silica, the adsorption of organic macromolecules or the entrapment of inorganic colloids or crystals. Irreversible membrane damage can be caused by chemical reaction of solutes at the membrane boundary layer or with the membrane polymer. Microbial growth and attachment to the membrane surface can lead to the formation of a biofilm, providing a nucleation site for crystals of inorganic compounds [92, 95, 96]

Traditionally membrane performance and the fouling effect is characterized by a decline in the pressure-normalized flux with time. This method does not identify the origin or nature of the foulants. Post-mortem studies of fouled membranes have been carried out when fouling is complex in order to better understand the responsible physicochemical processes [71, 95, 97-102]

The United States Bureau of Reclamation (USBR), the Central Arizona Water Conservation District (CAWCD), the Metropolitan Water District of Southern California (MWD) and the Southern Nevada Water Authority (SNWA) motivated a study at USBR's Water Quality Improvement Center, located adjacent to the Yuma Desalting Plant (YDP) to identify possible alternative YDP operating scenarios that could improve plant performance and reduce costs. The overall goal of that work was to provide data on the use of polyamide (PA) membranes and alternative operating processes to increase operational reliability and cost effectiveness relative to operation in YDP's current configuration.

This paper discusses the autopsy results for four different spiral wound RO membranes that were employed in desalination studies at the United States Bureau of Reclamation's Water Quality Improvement Center (WQIC). The membranes were autopsied after 3-5 months of operation during screening tests and about 9 months in the case of full-array testing phase. To provide information on the condition of the test membranes prior to use at the WQIC and their original physical and chemical properties, a new membrane of each type was autopsied, as well. Analytical techniques used in this study included inspection via scanning electron microscopy (SEM) supplemented with energy-dispersive X-ray spectroscopy (SEM-EDX), Fourier transform infrared spectroscopy (FTIR) and attenuated total reflectance-FTIR (ATF-FTIR), X-ray diffraction (XRD), and heterotrophic plate counts (HPC).

The goal of the screening tests (Rounds 1 and 2) was to (i) evaluate the effectiveness of alternative pretreatment strategies for preventing fouling on several membrane types and (ii) measure the response of the several membrane element types to

the water sources and pretreatment alternatives evaluated. That is, screening tests were used to identify the RO element types that are best suited for long-term YDP operations. The goals for the full-array testing phase (Round 2, Full-Array) of the project were evaluate the long-term cost effectiveness and reliability of the treatment alternatives.

4.3. Experimental

4.3.1. RO Testing Units

4.3.1.1. Membrane Evaluation Research Units (MUs)

MUs are pilot scale, full recovery, mobile testing units that use 6.4 cm (2.5-in) diameter membrane elements. These units were custom made for the Bureau of Reclamation's Water Quality Improvement Center (WQIC). They are fully instrumented and electronically controlled units that can be used for high-recovery testing (up to 85%). MUs incorporate a 2-1 array that contains 21 spiral wound, 6.4 cm (2.5 in) by 101.6 cm (40-in) elements. RO recovery percentage (80%) was selected for the study based on the chemistry of water to be treated using antiscalant and dosage recommended by the membrane manufacturer.

The two-stage MUs ran at a water flux of 4.2 $L/m^2.d$ (12 gfd). Each RO unit operated with a feed flow of 20.7 L/min, a product flow of 16.6 L/min, and a reject flow of 4.1 L/min (80% recovery). MU 1, like all the other MUs, was initially operated at 80% recovery. However, from early November 2011 until the test termination, MU 1 (Pretreatment 1a) ran at a recovery of 85% and average water flux of 5.3 $L/m^2.d$ (15 gfd), which produced a reject flow of 3.8 L/min from the Hydranautics LFC elements.

4.3.1.2.Element Test Apparatus (ETA)

ETA pilot-scale screening units are fully instrumented and electronically controlled. They are used for testing individual membrane elements, either 2.5-in or 4-in in diameter, before they are taken to pilot-scale, full-recovery systems. The test apparatus consisted of two 6.4 cm (2.5-in) and two 10.2 cm (4-in) pressure vessels (203 cm (80-in) long and each holding two elements) mounted on a metal frame skid.

Four ETA units (ETAs 1-4) were used for this research study to evaluate seven different types of membranes in two different rounds. Round 1, which lasted almost 3000 hours (4 months), tested four different types of membranes. Round 2, which lasted more than 3500 hours, tested three more membrane types. The Toray TML10 was used for both rounds for the purpose of direct comparison.

4.3.2. RO membrane elements

Seven different types of polyamide RO membranes—Hydranautics ESPA2 and LFC3, Toray TML10, Koch/Fluid Systems ULP-TFC, Dow Filmtec BW30-XFR, and CSM Woongjin RE-FE and RE-CE—were tested on two different brackish water sources: (1) MODE water – surface canal agricultural drainage from the Wellton-Mohawk Irrigation & Drainage District – and (2) groundwater from the YMC, which collects agricultural drainage pumped from wells located on the Yuma Mesa and in the Yuma Valley. Testing was carried out in two sequential stages. Round 1 comparatively evaluated the performance of four RO membrane types (ESPA2, LFC3, TML10, and ULP-TFC) at low recovery to select the best performing element for treatment of each source water/pretreatment combination. The selected membrane, LFC3, was then operated for long-term, high recovery testing in Round 2. Round 2 Full-Array testing

lasted about nine months and used a 2 x 1 staged, 21 element array to achieve 80% recovery. This paper will focus on post mortem studies on ESPA2, LFC3, TML10, and ULP-TFC due to the large amount of data.

4.3.3. Source Waters

The two water sources selected for the research program are distinct and unique to the Yuma region. One is the Main Outlet Drain Extension (MODE) water consisting of agricultural drainage water from the Wellton-Mohawk Irrigation & Drainage District (WMIDD). The second is brackish ground water from the nearby Yuma Mesa Conduit (YMC), which collects agricultural drainage pumped from the Yuma Mesa and Yuma Valley. Table 4.1 shows average water quality characteristics for a year for each water source.

4.3.3.1. Main Outlet Drain Extension (MODE)

The MODE is an open canal that is exposed to environmental events that might change the water quality during transport. The operation of the canal (e.g., the flow rate), the source of water flowing in the canal, the season, etc. can affect water quality. MODE water, which represents the current source water for the YDP, served as the feed to Pretreatment 3 and Pretreatment 1a treatment trains throughout the period of experimentation (describe in section 4.5). MODE water, being a surface supply, was expected to have a higher fouling potential due to higher levels of particulate and organic matter. It is susceptible to the annual fluctuations in the temperature and sunlight. The biological activity in the MODE canal affects both organic and inorganic contaminant levels.

4.3.3.2.Yuma Mesa Conduit (YMC)

The YMC is a closed pipe conveyance. YMC water served as the feed to Pretreatment 1b and Pretreatment 2 treatment trains. The levels of particulate and organic matter are lower in the YMC water compared to MODE water (Table 4.1). On the other hand, the YMC water contains elevated levels of iron and manganese that require removal prior to RO treatment.

Table 4.1. Water Quality Data for MODE and YMC Source Waters

Parameter	**Units**	**MODE**	**YMC**
pH	-	8.0	8.0
Conductivity	μS/cm	3,923	2,438
Total Dissolved Solids	mg/L	2,400-2800	1,400-1,700
Barium	mg/L	0.032	0.046
Calcium	mg/L	170.1	132.4
Iron	mg/L	0.063	0.142
Magnesium	mg/L	76.7	43.5
Manganese	mg/L	0.074	0.048
Potassium	mg/L	7.2	5.2
Sodium	mg/L	606.6	354.9
Strontium	mg/L	2.4	1.7
Bicarbonate	mg/L	364.5	285.8
Chloride	mg/L	621.9	322.5
Nitrate as N	mg/L	4.5	ND
Silicon Dioxide	mg/L	18.9	25.3
Sulfate	mg/L	857.7	537.5
Total Alkalinity as $CaCO_3$	mg/L	299.0	238.5
Total Organic Carbon	mg/L	2.4	1.0

4.3.4. Pretreatments

In all cases, the pretreated water was pH adjusted with sulfuric acid, chlorinated and dosed with ammonia (to form chloramines) and anti-scalant before being pumped to the RO membranes.

4.3.4.1.Pretreatment 1

Pretreatment 1a and Pretreatment 1b were running on MODE and YMC waters, respectively, with direct gravity filtration (silica sand and anthracite) and microfiltration used as pretreatment for RO operation.

4.3.4.2.Pretreatment 2

YMC water is treated with direct gravity filtration (switched to greensand and manganese oxide-amended anthracite with an addition of cartridge filtration later on).

4.3.4.3.Pretreatment 3

Lime-softened (with Ferric Sulfate) gravity-filtered MODE water. Quicklime (CaO) is mixed with water to make a lime slurry, a thick solution with lime ($Ca(OH)_2$), before being pumped in to the units together with ferric sulfate. This process was designed to remove the hardness ions as well as suspended particles from the water. The formation of sludge and the settling process are improved by the addition of ferric sulfate.

4.3.5. Post-mortem Analysis Procedure

The post-mortem analysis involved the dissection of each membrane element. The procedure followed is described below:

i. The membrane element's case (fiberglass or tape) was removed and the membrane was unrolled carefully.
ii. Visual inspection was documented and supported with pictures.
iii. The membrane area was measured and calculated.
iv. Fractions (4 cm^2) were collected for scanning electron microscope (SEM-EDs) and x-ray diffraction (XRD).

v. Fractions ($4cm^2$) were collected for heterotrophic plate count (HPC) analysis and kept in a sterile container at 4 °C.

vi. For the Fourier Transform Infrared Spectroscopy (FTIR) two samples were collected for analysis. For the first sample, rectangular fractions (6 cm^2) was collected as it is. For the second sample, the material over the membrane was scraped with a plastic spatula.

4.3.6. Analytical Methods

A Hitachi S-3400N Type II / ThermoNORAN NSS EDS: a variable pressure scanning electron microscope with Energy Dispersive X-Ray Spectrometer (SEM-EDS) was used to analyze material deposited on RO membranes. X-Ray Diffraction (XRD) analyses were performed with a Scintag XDS 2000 PTS Diffractometer to determine the composition of the material scraped from the membrane. SEM-EDS and XRD analyses were performed at the University Spectroscopy & Imaging Facilities at the University of Arizona. HPCs were performed at the Department of Soil, Water and Environmental Science at the University of Arizona. FTIR analyses were carried out in the same department utilizing a Nicolet Magna 560 Fourier Transform Infrared Spectrometer.

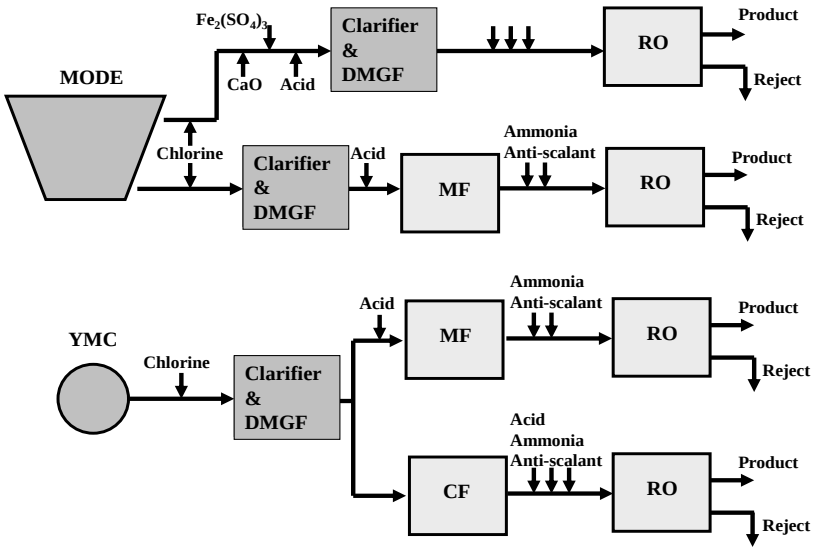

Figure 4.1. Pretreatment Options for the YDP Optimization Study

4.4. Results and Discussion

4.4.1. Relationship Between Bacterial Removal and Pretreatment Efficiency

Heterotrophic plate counts (HPC) were conducted using scrapings from a measured area of surface for each membrane element autopsied. In general for the MUs running on MODE water, it was found that the HPC was highest in the tail rather than lead elements for each treatment train (Table 4.2). This suggests that (i) viable bacteria were not filtered out in the feed spacer passages as feed/concentrate progressed through the elements in series and (ii) the bacterial population was largest where the feed solution and presumably organic substrates were most concentrated. In addition, the Pretreatment 1a (microfiltration) tail elements had much higher HPCs than the analogous elements in Pretreatment 3 (partial lime softening). This confirms conjecture that bacterial growth occurred in Pretreatment 1a RO units during the time when the total chlorine in the feed

decreased to 1.5 mg/L. In response, the total chlorine was increased to 2.0 mg/L in the feed solution.

Table 4.2. Heterotrophic plate counts (HPCs) for lead and tail elements of MUs operated on MODE water. HPCs are expressed in units of [cfu/in^2]

Pretreatment 1a	HPCs	Pretreatment 3	HPCs
MU3, Vessel 1, Element 1	4.62E+01	MU4, Vessel 1, Element 1	8.39E+02
MU3, Vessel 2, Element 1	0.00E+00	MU4, Vessel 2, Element 1	1.38E+03
MU3, Vessel 3, Element 7	1.10E+05	MU4, Vessel 3, Element 7	1.18E+02
MU1, Vessel 1, Element 1	4.46E+02	MU2, Vessel 1, Element 1	5.33E+01
MU1, Vessel 2, Element 1	4.85E+03	MU2, Vessel 2, Element 1	3.78E+01
MU1, Vessel 3, Element 7	1.61E+06	MU2, Vessel 3, Element 7	1.80E+02

4.4.2. Partial Lime Softening vs. Microfiltration Pretreatment of MODE Water

Figures 4.2a and 4.2b show scanning electron microscope (SEM) images of the surface of TML and LFC membranes used in round 1, to treat partial lime softened MODE water (Pretreatment 3, ETA 4). Material build-up was also observed also on ULP and ESPA 2 membranes, but to a lesser degree (not shown).

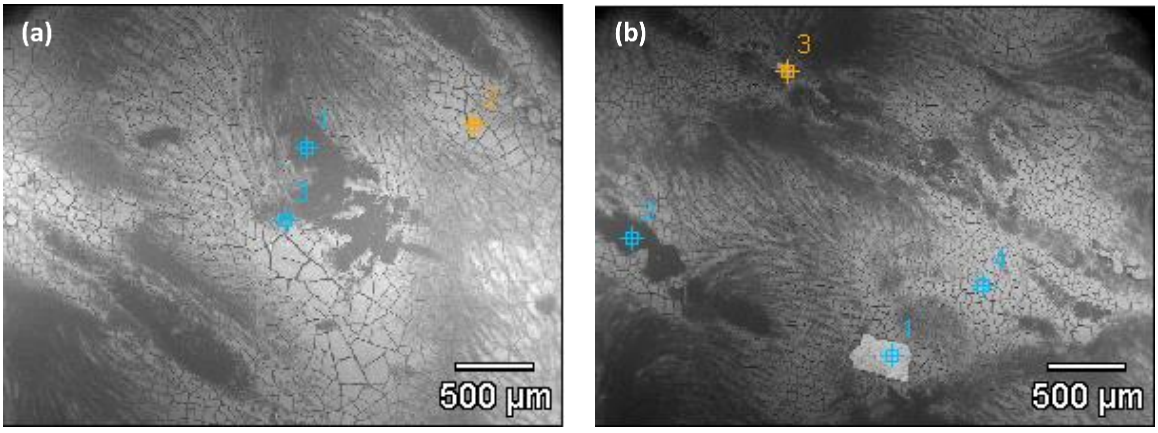

Figure 4.2. Scanning Electron Microscope (SEM) images of the surface of (a) Toray TML10 and (b) Hydranautics LFC3 membranes used in Round 1 to treat partial lime softened MODE water (Pretreatment 3, ETA 4)

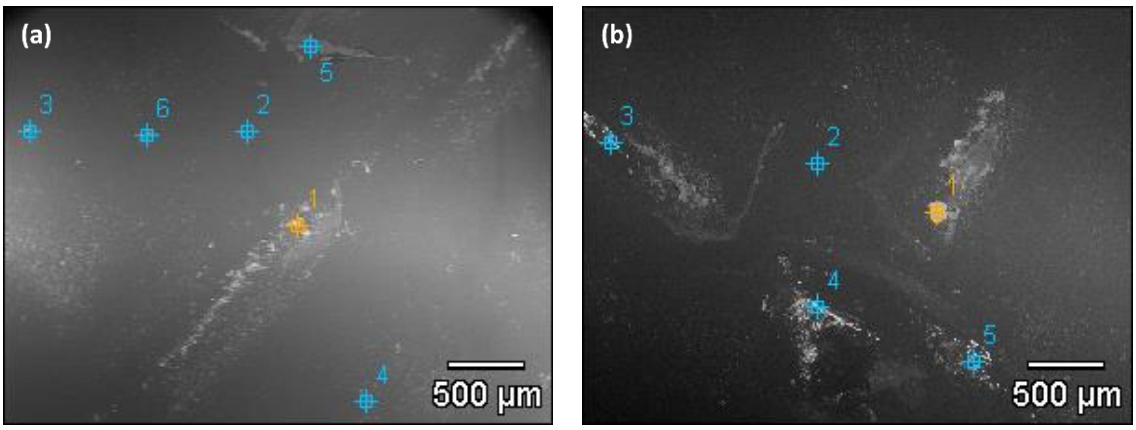

Figure 4.3**.** Scanning Electron Microscope (SEM) images of the surface of (a) Toray TML10 and (b) Hydranautics LFC3 membranes used in Round 1 on microfiltered MODE water (Pretreatment 1a, ETA 1)

In contrast, the membranes receiving microfiltered MODE over the same period showed no or very little material build-up. Figure 4.3a shows an SEM image of the TML membrane and the representative amount of build-up observed on pretreatment 1a round 1 membranes (ETA 1). The FTIR spectra of round 1 MODE water elements support the visual and SEM observations of greater material build-up following partial lime softening than after microfiltration. Figures 4.4a and 4.4b show FTIR spectra of round 1 TML10 and LFC3 membranes after air drying.

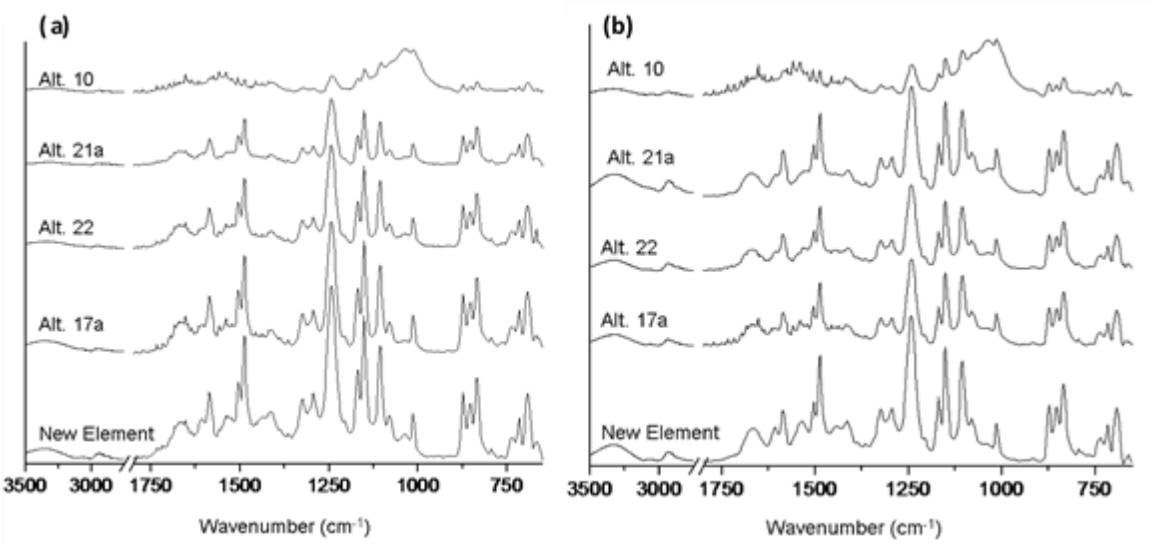

Figure 4.4. Fourier transform infrared spectroscopy (FTIR) spectra of (a) Toray TML10 and (b) Hydranautics LFC3 membranes used in Round 1 after air drying. Y-axis on the graphs presented is "absorbance"

Both Pretreatment 3 membranes show clear evidence of biofouling with polysaccharide build-up (wavenumber 1,150-950 cm^{-1}) and/or abiotic fouling with silicon-oxide materials (e.g. alumina silicates) (1,040 cm^{-1}), and general attenuation (by surface coating) of the polyamide and polysulfone structures of the membrane in the 1,700-1,500 cm^{-1} and 1,350-1,100 cm^{-1} ranges, respectively. In contrast, the pretreatment 1a (microfiltered water) membranes show little if any polysaccharide or general surface build-up in the FTIR spectra. SEM-EDS (energy dispersive spectroscopy) and XRD (x-ray diffraction spectroscopy) of the material on the surfaces of both Pretreatment 3 and 1a membranes identified aluminum-silicates (anorthite clay), silicon oxide and iron oxide as the primary inorganic constituents of the foulants. The Pretreatment 3 SEM revealed a number of diatoms on the membrane (Figure 4.5), and SEM-EDS measured high

fractions of silicon (in the range of 30% by weight) in surface particles, likely representing either biotic (diatoms) or abiotic (clays) origin.

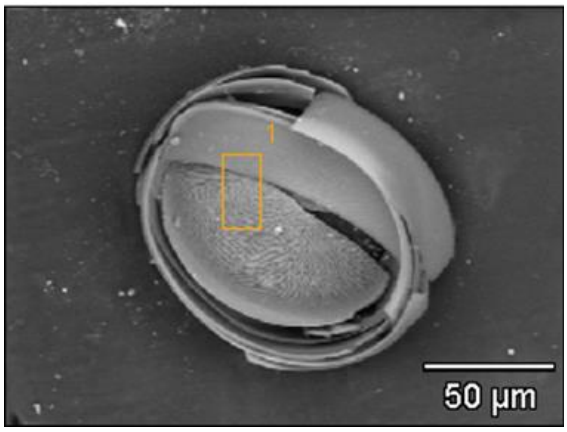

Figure 4.5. SEM image of a diatom on ESPA2 membrane used in Round 1 lime softened MODE water (Pretreatment 3, ETA 4)

After round 2, high recovery testing, material accumulations were similar to those (both pretreatments) shown for round 1. During round 2 high recovery tests, the feed/concentrate passed through 14 elements in series, as opposed to the round 1 use of low recovery testing with 2 elements in series. High recovery testing provided insight into lead versus tail element foulant accumulation that was not possible in the round 1 and 2 low-recovery testing. Figures 4.6a and 4.7a show that both lead and tail RO elements following pretreatment 1a accumulated very little polysaccharide (wavenumber 1,150-950 cm^{-1}) compared to RO membranes that followed Pretreatment 3. Although there was a slight decrease in polysaccharide accumulation between the lead and tail elements, there was a very substantial increase in spectra that are indicative of palmitate salts (e.g., $Ca(CH_3(CH_2)_{14}COO)_2$, particularly after Pretreatment 3. Palmitic acid is the most common fatty acid in biological tissue and indicates the presence of organisms or

their residual tissues. The spectra for palmitate include peaks at 2,920 and 2,850 cm^{-1} (CH_2 stretching), 1,470 cm^{-1} (CH_2 bending), and 1,575 and 1,540 cm-1 (COO^- stretching).

It should be noted that the material deposited on the high recovery membranes was easily removed by simply scraping the surface with a soft plastic spatula, allowing the near-original surface features to reappear (Figures 4.6b and 4.7b). This supports speculation that foulants might be removed from membrane surfaces *in situ* without aggressive cleaning, although this was not verified. Cleaning studies were beyond the scope of work.

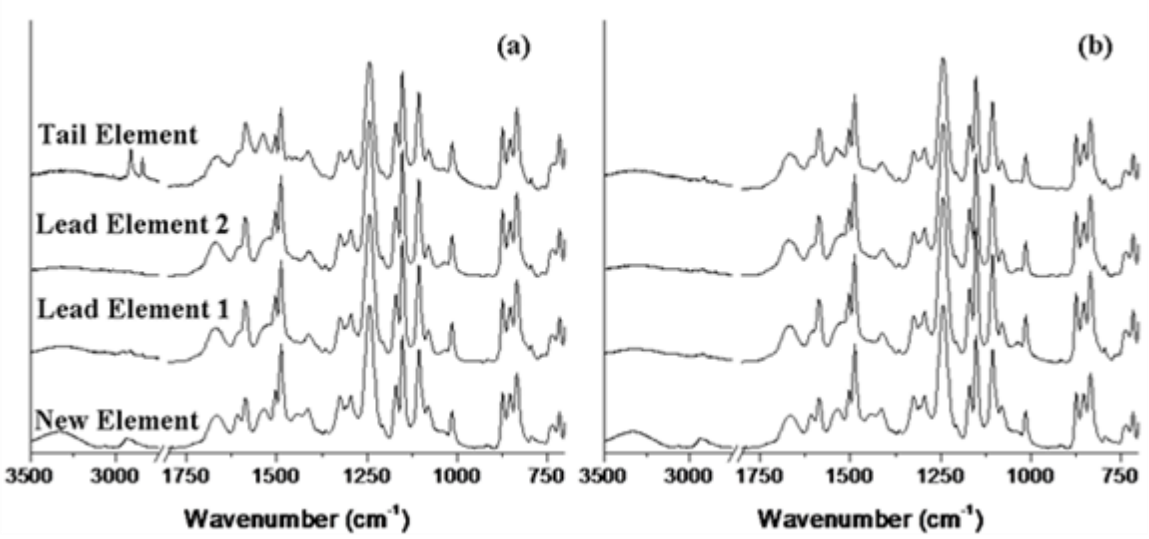

Figure 4.6**.** Fourier transform infrared spectroscopy (FTIR) spectra of LFC3 elements retired from MU 3 operated with microfiltered MODE water (Pretreatment 1a); (a) original elements and (b) surface precipitate removed from elements by scraping with a soft plastic spatula. Y-axis on the graphs presented is "absorbance"

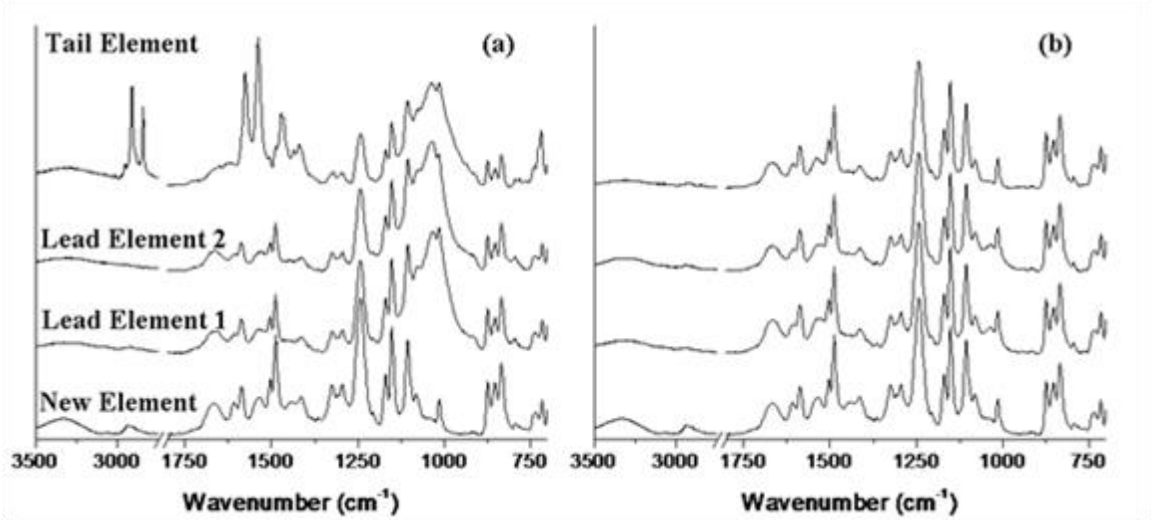

Figure 4.7. Fourier transform infrared spectroscopy (FTIR) spectra of LFC3 elements retired from MU 4 operated with lime softened MODE water (Pretreatment 3); (a) original elements and (b) surface precipitate removed from elements by scraping with a soft plastic spatula. Y-axis on the graphs presented is "absorbance"

4.4.3. Effect of High Flux and High Recovery

For 3 months, a second 21-element high recovery unit (MU1) was operated in parallel with the original high recovery unit (MU3). MU3 was in operation for 5 months using microfiltered MODE water when the second reactor was added. MU1 also contained Hydranautics LFC membranes, but was operated at a higher average flux of 5.3 $L/m^2.d$ (15 gfd) (25% above the normal average flux of 4.2 $L/m^2.d$ (12 gfd)) for the full three months in order increase recovery to 85% (rather than 8+0%) for 1.5 months. Despite the abbreviated period of operation, the high flux/recovery (HFR) elements showed considerably greater accumulation of surface material than the flux/recovery (NFR) elements operated at 80% recovery (Figure 4.8a and Figure 4.8b). SEM-EDS and XRD analyses indicated that a large proportion of material on the HFR membrane surface consisted of elemental sulfur with smaller amounts of aluminum silicate clays.

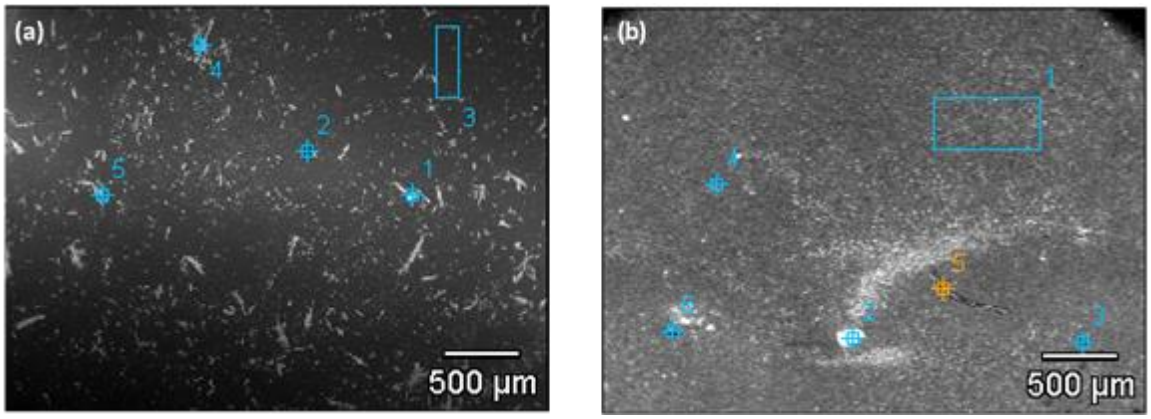

Figure 4.8. Scanning Electron Microscope (SEM) images of the surface of LFC3 elements retired from (a) MU 1 (Round 2 Phase 2 – HFR) and (b) MU 3 (Round 2 – NFR). Both units received microfiltered MODE water (Pretreatment 1a). Both micrographs represent the conditions of tail elements

The surface accumulation is further evidenced in the FTIR spectra (Figure 4.9a). Comparing the HFR FTIR spectra to that of the NFR FTIR spectra (Figure 4.6a), the tail element exhibits a general coating over the entire HFR spectra and the appearance of distinct palmitate peaks between 3,000 – 2,500 cm^{-1}. The fouling is pronounced in the HFR tail element, but biofouling is also evident in the lead elements in the 1,200 – 1,000 cm^{-1} range. As observed for membranes operated on MODE water, foulants on the HFR membranes were readily removed using a spatula (Figure 4.9b).

As previously discussed with respect to the fouling observed with the partial lime softened MODE water, FTIR peaks in the 1,200 – 1,000 cm^{-1} range are indicative of polysaccharides (biofouling). However, the silicon-oxygen stretching peak also occurs at about 1,040 cm^{-1}. The 1,040 cm^{-1}peak in the HFR tail element is qualitatively more singular (sharper) than that for tail and lead elements in the partial lime softened case (compare Fig 4.9a to Fig. 4.7a). This may indicate more inorganic (silicates) fouling for

the HFR case, while the fouling of the latter case is more mixed organic (polysaccharides) and inorganic (silicates) material. More elemental and compound specific analysis would have verified or denied this hypothesis, which was out of the scope of this study.

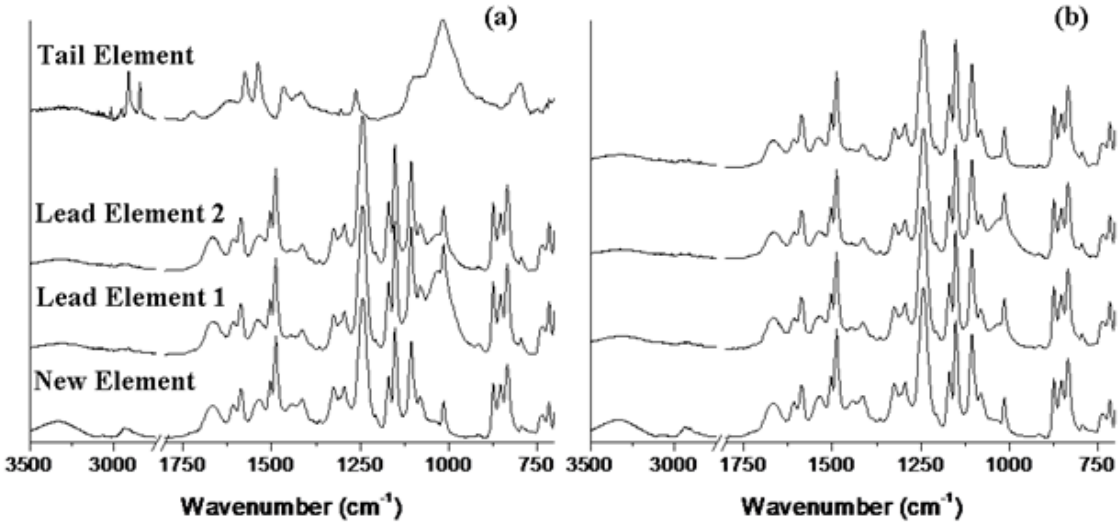

Figure 4.9. Fourier transform infrared spectroscopy (FTIR) spectra of LFC3 elements retired from MU 1 operated with microfiltered MODE water (Pretreatment 1a) at high flux/recovery (HFR); (a) original elements and (b) surface precipitate removed elements by scraping with a soft plastic spatula. Y-axis on the graphs presented is "absorbance"

4.4.4. Elemental Sulfur Deposits

Unexpectedly, the tail membrane elements of both of the high recovery arrays (MU1 and MU3) operated on microfiltered MODE water (pretreatment 1a) and the high recovery array (MU4) operated for nine months on partial lime softened MODE water apparently accumulated elemental sulfur as either the only or a major foulant on membrane surfaces. Figures 4.10, 4.11, and 4.12 all show high sulfur content in SEM–

EDS spot analyses on the tail elements of the arrays. The sulfur weight percent in spots on surface particles is commonly in the 10-50% range.

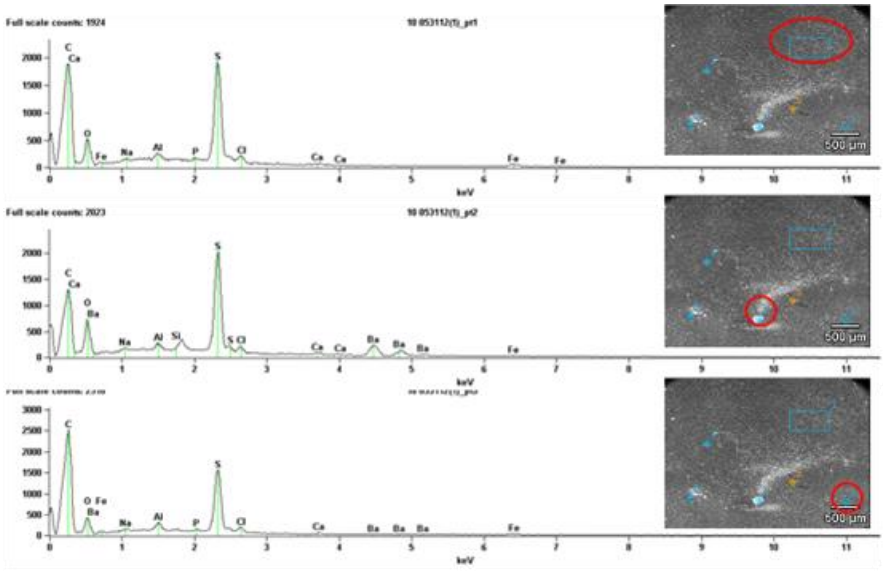

Figure 4.10. SEM-EDS images of LFC3 element (located as Vessel 3 Element 7 – tail element) retired from MU 3 following operation with microfiltered MODE water (Pretreatment 1a) at normal flux/recovery (NFR) during Round 2. Red circles highlight the points examined via EDS

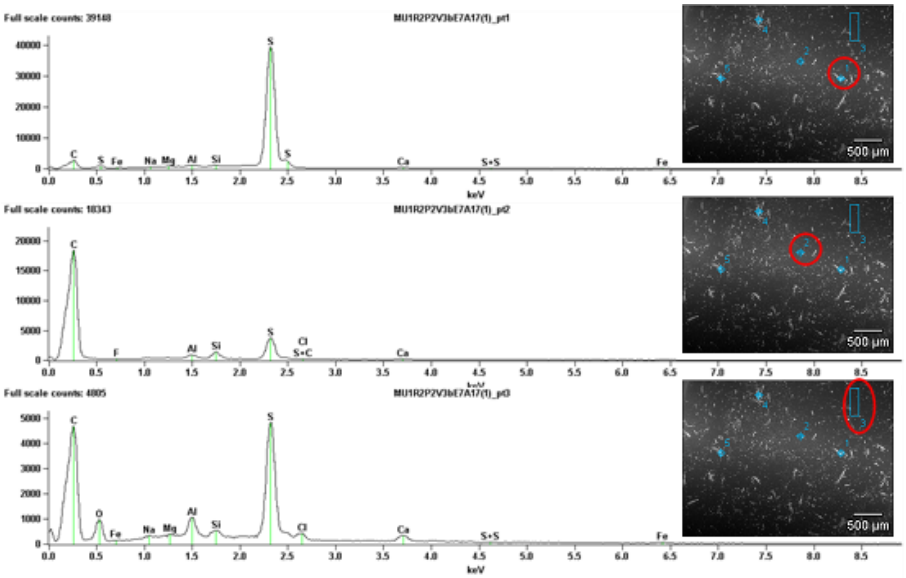

Figure 4.11. SEM-EDS images of LFC3 element (located as Vessel 3 Element 7 – tail element) retired from MU 1 operated with microfiltered MODE water (Pretreatment 1a) at high flux/recovery (HFR) during Round 2 Phase 2. Red circles highlight the points for EDs measurements

XRD spectra from material scraped from the surface of the same tail elements also indicated that elemental sulfur was the primary sulfur-bearing mineralogical species present (Figures 4.13a, 4.13b and 4.13c). Elemental sulfur was not detected by any of the same techniques when applied to the lead elements of high recovery reactors that received MODE water. This suggests that the deposition of the S(0) is concentration-related. That is, the feed/concentrate stream reaches a threshold concentration in S(0) somewhere within the sequence of membrane elements after which the solid element precipitates on membrane surfaces.

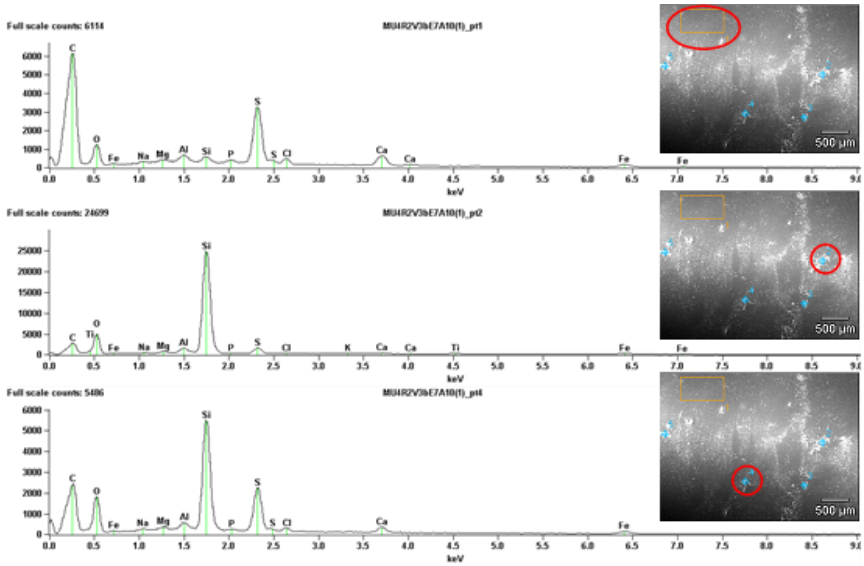

Figure 4.12. SEM-EDS images of LFC3 element (located as Vessel 3 Element 7 – tail element) retired from MU 4 operated with microfiltered MODE water (Pretreatment 1a) at normal flux/recovery (NFR) during Round 2. Red circles highlight the points for EDS readings

Elemental sulfur can be generated under anaerobic conditions from sulfate (SO_4^{2-}) as a two-step process. Sulfate is reduced to sulfide (S^{2-}) by sulfur reducing bacteria and then the sulfide is oxidized abiotically (or in some instances biochemically) to S^0 in the presence of an electron donor such as Fe^{3+} or Mn^{4+}. Given that some sections of the MODE canal are anoxic, it is expected to detect elemental sulfur on the membranes that treated its water, in which the sulfate concentration is high (~850 mg/L) and both oxidized iron and manganese are present.

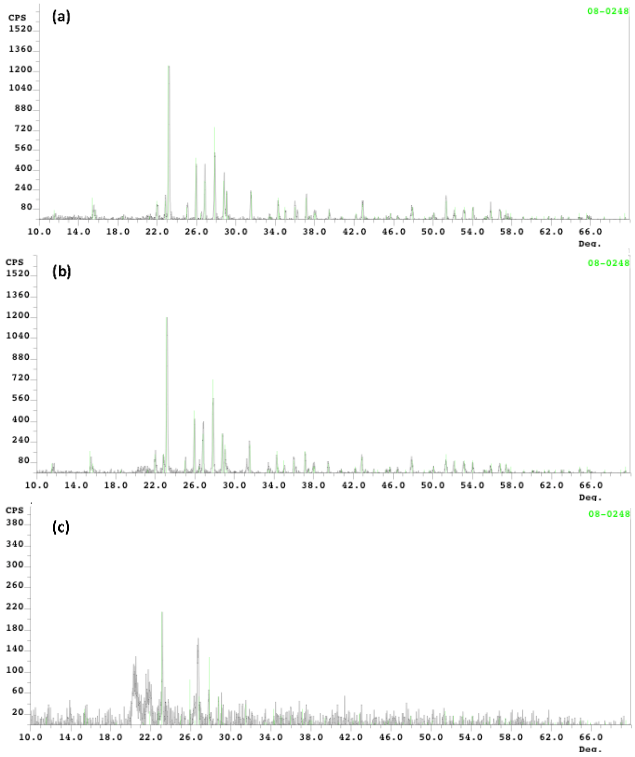

Figure 4.13. The XRD spectra from material scraped from the surface of the tail elements (Vessel 3 Element 7) showing elemental sulfur as the sulfur-bearing mineralogical species present for (a) MU 3, (b) MU 1 – HFR operation during Round 2 Phase 2, and (c) MU 4. MU 3 and MU 1 were operated on Pretreatment 1a, whereas MU 4 was operated on Pretreatment 3

Anaerobic conditions may exist in accumulated sediments within the MODE canal, allowing the products of anoxic microbial metabolism to enter the YDP feed when flow in the canal is perturbed by storms or other events. Alternatively, anaerobic conditions could occur locally at the YDP if the chlorination of MODE water is periodically interrupted or temporarily fails to satisfy chemical demands. With the information available, however, it is not possible to confidently assign a cause-effect relationship that accounts for the deposition of sulfur on the MODE water membranes. There is no literature to suggest that elemental sulfur is more deleterious to membrane performance than other mineral scalants. However, the presence of S(0) is significant in that it indicates there were periods of sub-oxic conditions in the water source. This is a red flag, indicating that other reduced species (e.g., Fe^{2+}, Mn^{2+}) may be present that do have documented negative impacts on membrane material integrity, and that disinfection practices during RO treatment were insufficient to keep microbial growth on the membranes completely in check.

4.4.5. Microfiltration versus Cartridge Filtration Pretreatments for YMC Water

In all cases, the high recovery array (MU) membranes operated on YMC water showed less accumulation of surface materials than those operated on MODE water. However, it is not clear whether this was due to i) higher quality in the YMC water following pretreatment or ii) shorter periods of RO operation prior to post-mortem analyses of RO membranes that were used to treat YMC water. Although both operational results and membrane autopsies both suggest that membrane fouling/scaling is less problematic with YMC than MODE water, conclusions are tentative in light of differences in operational periods preceding membrane autopsies for membranes treating

the two water types. Nevertheless, direct comparisons based on autopsies of RO membranes that received YMC water following (i) microfiltration (MF) and (ii) cartridge filtration (CF) pretreatments is entirely appropriate. Results clearly show that CF is less efficient than MF for protecting downstream membranes from particulate accumulation. Evidence includes both visual inspection and SEM imaging of membranes fed microfiltered and cartridge filtered YMC water (Figures 4.14 and 4.15). When MF pretreatment was provided, SEM inspection showed large particle-free areas on the RO membranes.

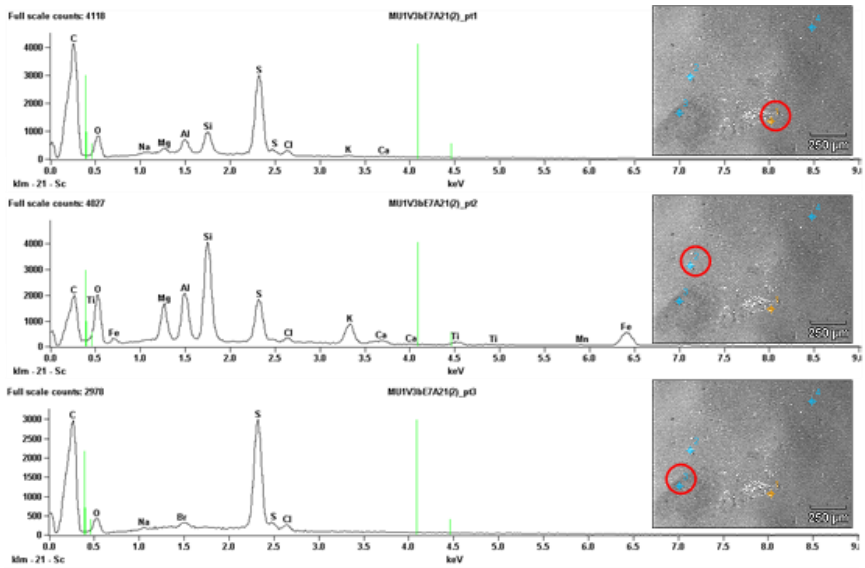

Figure 4.14. SEM-EDS images of LFC3 element (located as Vessel 3 Element 7 – tail element) retired from MU 1 after operation with microfiltered YMC water (Pretreatment 1b) at normal flux/recovery (NFR) during Round 2 Phase 1. Red circles highlight the points for EDS inspections

Figure 4.14 shows a patch of particles imaged on the surface of the tail membrane of the array receiving MF pretreated water. Based on SEM-EDS, the particles are primarily either aluminosilicates (clays) or metal sulfates (e.g., calcium sulfate). Figure

4.15 indicates that particulate deposits on membranes receiving CF-pretreated water were more concentrated and included metal chlorides in addition to aluminosilicates and metal sulfates. SEM-EDS also detected some iron on the CF membrane surface. For neither of these YMC water alternatives was there sufficient material on the membrane surface to allow XRD analysis for more specific identification of mineral species.

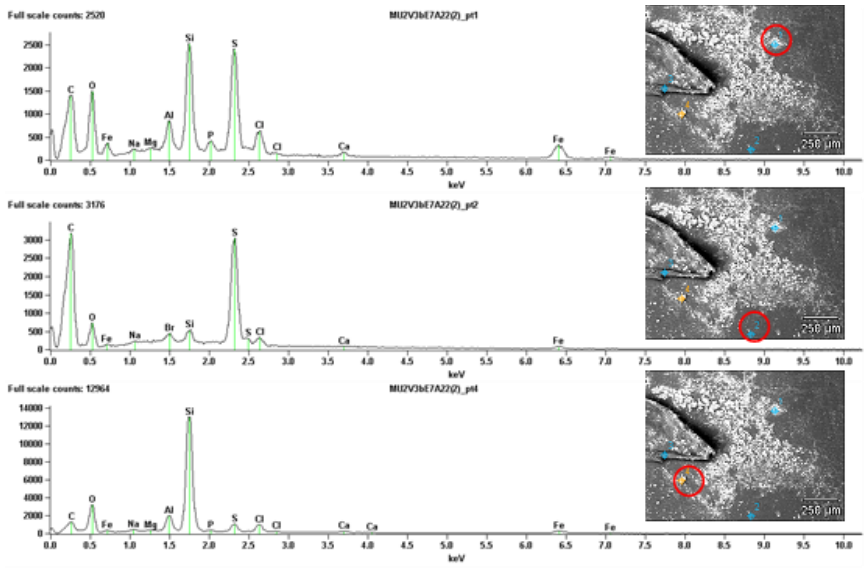

Figure 4.15. SEM-EDS images of LFC3 element (located as Vessel 3 Element 7 – tail element) retired from MU 2 operated with cartridge-filtered YMC water (Pretreatment 2) at normal flux/recovery (NFR) during Round 2 Phase 1. Red circles highlight the points for EDS readings

FTIR spectra were obtained as a part of post mortem analyses on RO membranes that received YMC water following microfiltration (Figure 4.16) and cartridge filtration (Figure 4.17). Each figure contains FTIR scans corresponding to the original filter surface, two lead membrane elements, and one tail element. The lead and tail element membranes were used in the high-recovery arrays. The loss of all spectral peaks in the 1750-1250 cm^{-1} range and the broad, undifferentiated peak at 1250-850 cm^{-1} indicate that

a substantial surface layer (greater than 300nm thickness) accumulated only on the surface of the CF-pretreatment tail element membrane (Figure 4.17a). There was little if any change in the FTIR peaks in the MF water tail element membrane as a consequence of use (Figure 4.16a). The broad peak in the 1250-850 cm^{-1} range (CF pretreatment, tail element, Figure 4.17a) is most likely from silicon-oxygen stretching and/or carbon-carbon stretching, suggesting that the deposited layer is composed of clays, polysaccharides (biological detritus) or a combination of the two.

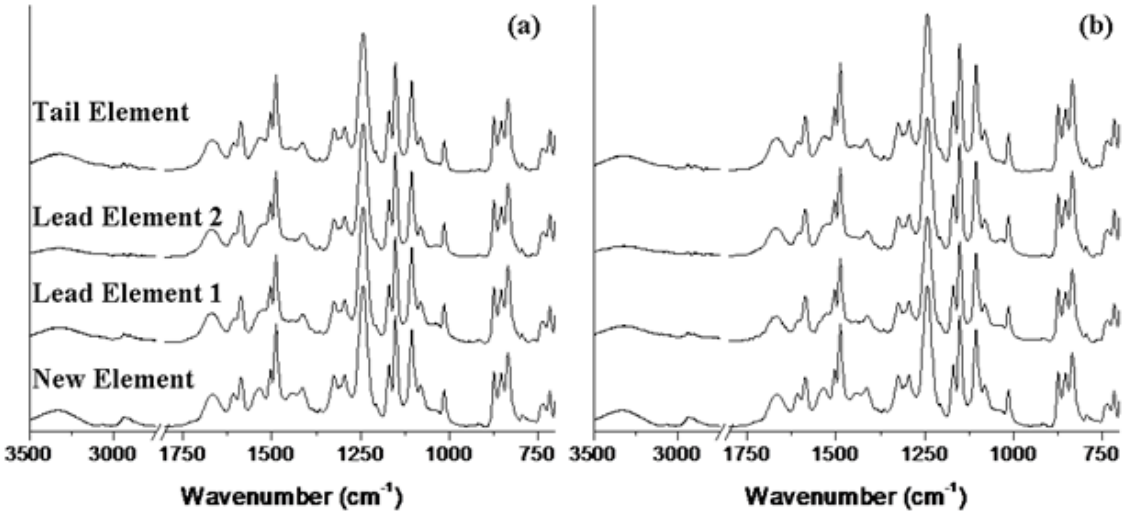

Figure 4.16. Fourier transform infrared spectroscopy (FTIR) spectra of LFC3 elements retired from MU 1 operated with microfiltered YMC water (Pretreatment 1b) at normal flux/recovery (NFR); (a) original elements and (b) surface precipitate removed elements by scraping with a soft plastic spatula. Y-axis on the graphs presented is "absorbance"

The lead elements of the CF-pretreated water array apparently experienced considerably less particle accumulation than the tail element. However, modest loss of definition and increase in absorbance at ~1,050 cm^{-1} suggest that these elements are not entirely free from particle deposition. Furthermore, comparison of the scraped (b) and

unscraped (a) spectra in Figure 4.17 indicate that the material on the lead elements is easily removed by the light scraping with a rubber spatula, whereas the material on the tail element is more tightly bound to the membrane and is not as easily removed.

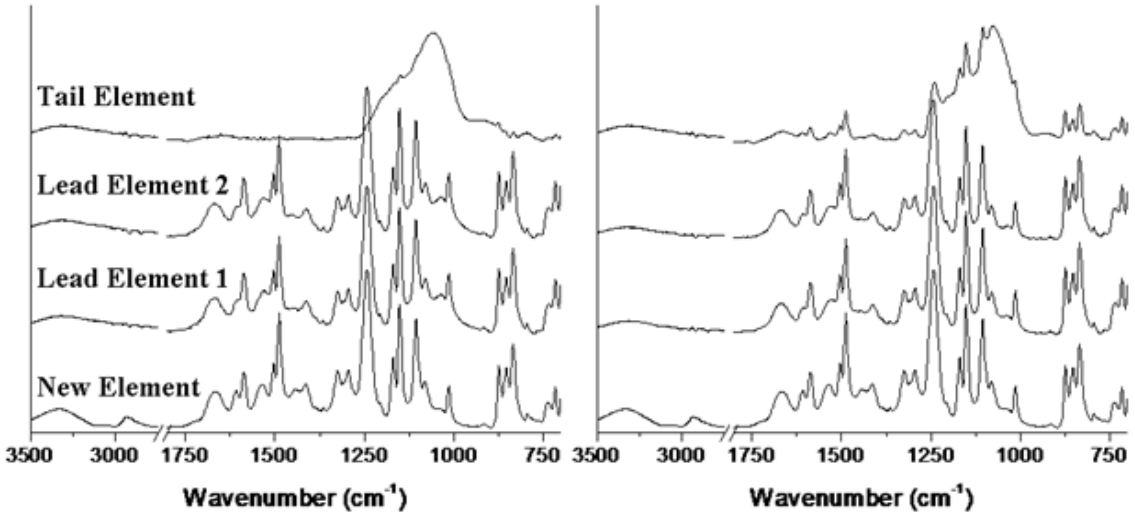

Figure 4.17. Fourier transform infrared spectroscopy (FTIR) spectra of LFC3 elements retired from MU 2 operated with cartridge-filtered YMC water (Pretreatment 2) at normal flux/recovery (NFR); (a) original elements and (b) surface precipitate removed elements by scraping with a soft plastic spatula. Y-axis on the graphs presented is "absorbance"

4.4.6. Chlorination of Polyamide Structure

The presence of an amide II peak at 1,540 cm^{-1} in the FTIR spectra for the virgin Hydranautics LFC membranes used in the round 2, high recovery array tests indicates that the original membrane surface layer contains a fully aromatic polyamide. Attack by free chlorine can result in either ring chlorination or chlorine substitution in the amide group of the polyamide polymer chain (Figure 4.18). Ring chlorination is evidenced by a decrease in the C=C ring vibration peak at 1,610 cm^{-1}, whereas chlorine in the amide group causes a decrease in the (amide II) N-H bending peak at 1,540 cm^{-1}. Changes in

FTIR spectra for Hydranautics ESPA2 membranes during Round 1, low recovery studies were apparently due to both ring and amide group substitutions with chlorine (Figure 4.19). Comparable levels of chlorine substitution were seen in all membranes operated in the low recovery apparatus in rounds 1 and 2. Chlorine substitution into the polyamide polymer is masked when materials build-up on the surface of the membrane. Therefore, to investigate the degree of chlorination in the round 2, high recovery arrays, it is best to consider the FTIR spectra for elements experiencing the least accumulation of particles. As such, analyses of membranes receiving MF-pretreated YMC water (Figure 4.19a) indicate that, although ring and amide chlorine substitution are evident in both lead and tail membranes, the degree of chlorine substitution is greater in the lead elements. Although masked to some extent by surface deposition on other membranes, data suggest that the degree of chlorine substitution decreased from lead to tail elements in all membrane arrays, including those operated on both YMC and MODE waters.

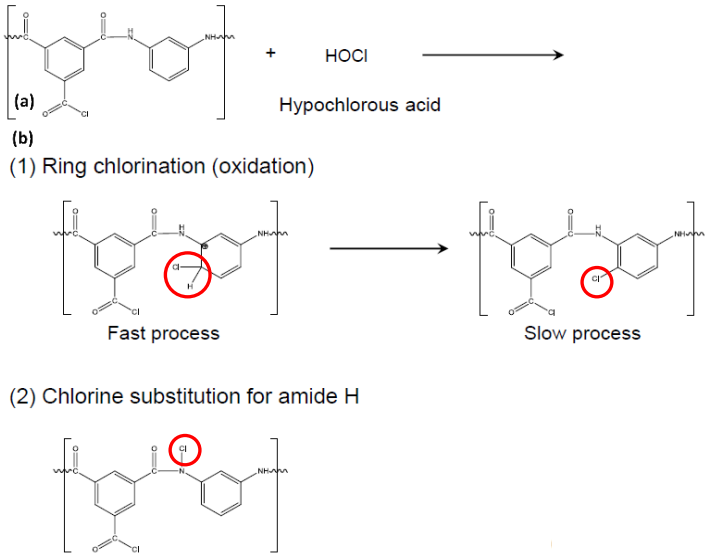

Figure 4.18. (a) The polyamide functional (thin film) surface layer, a fully aromatic polyamide and; (b) the ring chlorination (1) or chlorine substitution (2) in the amide

group of the polyamide polymer chain are illustrated via attack by free chlorine. The chlorine substitutions are highlighted by red circles

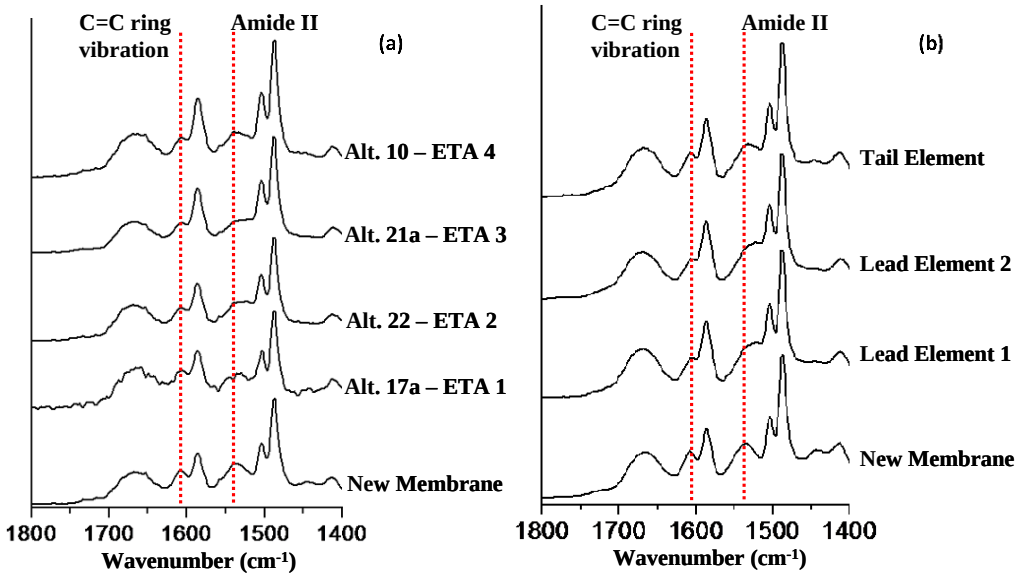

Figure 4.19. Fourier transform infrared spectroscopy (FTIR) spectra changes seen in (a) Hydranautics ESPA2 membranes operated in the Round 1 low recovery apparatus study and (b) Hydranautics LFC3 membranes operated in the Round 2 Phase 1 (Pretreatment 1b – MF treated YMC water) high recovery apparatus study due to both ring and amide group chlorination. Y-axis on the graphs presented is "absorbance"

4.5. Conclusions

Comparing the post-mortem results for membranes treating partial lime-softened MODE water (Pretreatment 3) and microfiltered MODE water (Pretreatment 1a), the following general conclusions can be drawn: i) deposition of polysaccharides (indicative of general biofouling) is much greater with Pretreatment 3 than Pretreatment 1a; ii) deposition of inorganics is greater for Pretreatment 3 and for both alternatives is dominated by aluminum silicates (clays) and silicon oxides with traces of iron; and iii) palmitate deposits (indicative of degraded organic tissues) are significant on Pretreatment

3 and slight on Pretreatment 1a. The autopsy results suggest that YMC water leads to less deposition of material on the membrane surface than MODE water, but this result is not conclusive since the YMC water alternatives operated for a significantly shorter duration than the MODE water alternatives. For the YMC water pre-treatment alternatives, MF versus CF, there was significantly greater material build-up with CF pre-treatment, particularly on the tail element in the high recovery array. Finally, for both source waters and all pre-treatment alternatives, the low recovery, single element testing showed chlorine substitution (both ring and amide group) with all membrane types evaluated. In the high recovery membrane arrays (Round 2), the chlorine substitution was evident in both lead and tail elements, but decreased from lead to tail element.

CHAPTER 5

ECONOMICS OF ION EXCHANGE VS. VIBRATORY SHEAR ENHANCED PROCESSING (VSEP®) FOR MINIMIZATION OF REVERSE OSMOSIS CONCENTRATE VOLUME

Inland water desalination schemes are uniformly handicapped by brine disposal costs. A significant percentage of the overall cost of an inland desalination project arises from brine disposal measures. This study examined aimed to determine the long-term feasibility of the Vibratory Shear Enhanced Processing (VSEP®) for RO brine minimization.

The study compared Ion Exchange (IX) pre-treatment VSEP® post-treatment for RO as alternative measures to increase overall water recovery. Experiments were designed to establish the efficiency of VSEP® and support an economic comparison of between the two options.

The experimental design consisted 24 to 48-hr experiments to determine the characteristics of VSEP® performance. The feed water for VSEP® consisted of brine developed via RO of CAP water and was about five times the total dissolved solid (TDS) concentration of CAP water (~3750 mg/L). Water lost during desalination was reduced from 20% to 2-4% via post-RO VSEP treatment. Under optimal conditions, VSEP treatment alone achieved >80% recovery of water from the RO brine.

My share responsibilities during this study included aspects of the experimental design and execution, the preparation of chemicals, equipment set-up and cleaning, data acquisition and analysis. Finally, I was part of the process that led to the publication of results as a peer-reviewed journal article. The results of this study were published online in the *Journal of Environmental Engineering* in March 2014.

5.1. Abstract

Balancing water supply/demand in Arizona depends on full utilization of the regional allotment of Central Arizona Project (CAP) water. The total dissolved solids (TDS) concentration at the CAP turnout to Cortaro Marana Irrigation District (CMID) in Tucson, AZ (~790 mg/L) is more than three times that of native groundwater. As a consequence, 200,000 metric tons/yr of salt accumulates creating a major long-term issue. Reverse osmosis (RO) was evaluated for salt management. Pilot-scale studies indicated that scaling limits water recovery to 75-80% during conventional RO desalination of CAP water. To increase water recovery (i) ion exchange (IX) pretreatment of the RO influent and (ii) post-treatment of RO brine using the vibratory shear enhanced processing (VSEP®) were evaluated.

If scale-forming cations barium and calcium are removed via IX pretreatment, the expected maximum water recovery is >95% based on solubility product calculations. Alternatively, the water lost as brine can be reduced to 2-4% of the raw CAP water via post-RO VSEP treatment. Estimated costs for a hypothetical 15 MGD treatment plant were compared in three scenarios. Use of VSEP with RO was estimated to save $5M/yr relative to RO treatment alone. At operating conditions near optimal, the total annualized

cost of VSEP operation was insensitive to variation in the operational variables analyzed (VSEP recovery and time between VSEP membrane cleanings).

Although the maximum long-term recovery using a combination of IX/RO treatment has not yet been established experimentally, ~$6M/yr savings was estimated relative to a hypothetical overall recovery of 99% using an optimal combination of IX/RO.

5.2. Introduction

Arizona law mandates achievement of a balance between groundwater withdrawal and replenishment by year 2025 in "active management areas" around major population centers [103]. In the Tucson Active Management Area (TAMA), consisting of 3,866 square miles that is roughly centered on Tucson in southern Arizona, projected compliance is based on full utilization of regional rights to Central Arizona Project (CAP) water and a degree of reclamation/reuse of municipal wastewater effluent [61, 104, 105]. Uncertainty regarding the long-term availability of Colorado River water to the CAP, however, is a major impediment to water resources security [106, 107]. Water users in the TAMA have rights to ~250,000 AFY of CAP water, subject to availability constraints. The current water demand in the TAMA is about 400,000 AFY. The difference can be made up through a combination of groundwater withdrawals (up to 60,000 AFY, the estimated rate of natural groundwater renewal in the TAMA), and greater reliance on reuse of treated wastewater, as shown in Figure. 5.1.

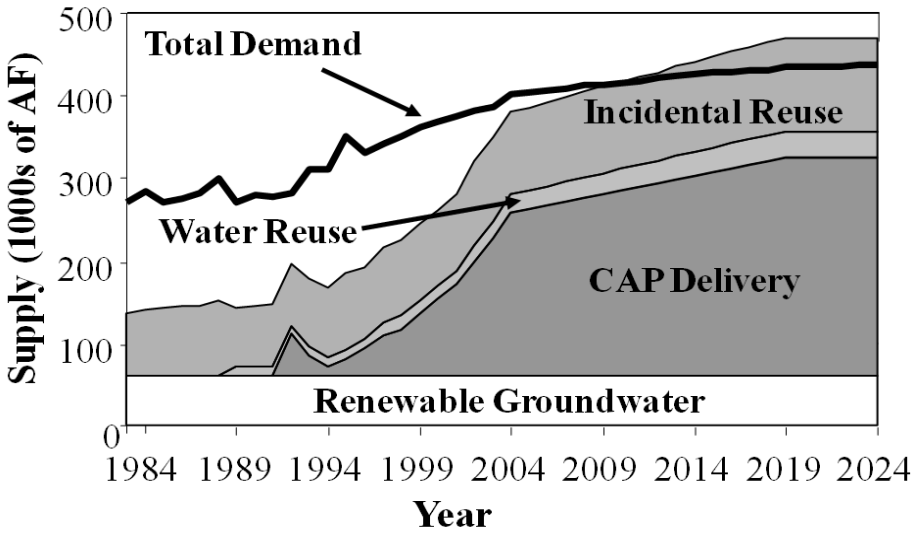

Figure 5.1. Water demand/supply projections in the TAMA [61]. Water reuse consists of planned reuse of reclaimed water for landscape irrigation. Incidental reuse occurs as a consequence of inadvertent infiltration of effluent to the regional aquifer

Reliance on CAP water to satisfy a major fraction of the regional water demand has consequences for the quality of delivered water (Table) 1 [61, 107]. Full use of the area's entitlement to CAP water will bring ~200,000 metric tons of salt into the TAMA each year. Without active steps to manage salt, the average salt content of the regional aquifer will increase by ~5 mg/L-yr, doubling the salt content of the regional aquifer over the next 50 years [61]. CAP water is introduced into Tucson's regional water supply by temporary underground storage, mixing with native ground water and recovery, thus ensuring that salinity levels in delivered water will not rise abruptly to that of CAP water. Nevertheless, delivered water in portions of the city has TDS concentrations of ~600 mg/L and will continue to increase.

Table 5.1- Comparison of Tucson groundwater and CAP water quality. Data for Tucson production wells represent the regional average prior to introduction of CAP water into the regional aquifer

Water Quality Constituent (mg/L)	**Tucson Water Production Wells**	**CAP Water[(a)]**
Total Dissolved Solids	259	787
Hardness (as $CaCO_3$)	119	313
Sodium	40	102
Chloride	17	94
Calcium	39	75
Magnesium	5	30
Sulfate	45	256
Alkalinity (as $CaCO_3$)	126	194
TOC	<1	3

[(a)]Average values observed throughout pilot-scale testing (March 2006-May 2009)

While an essential component of salt management, RO treatment consumes energy and produces brine. It has been estimated that recovery during RO treatment of CAP water is limited to 75-80% to avoid membrane scaling [107] so that the value of water lost as brine contributes to the overall motivation for brine minimization should RO treatment of CAP water be deployed. The solubilities of calcium sulfate, calcium carbonate and barium sulfate, for example, are likely to be exceeded in brines derived from RO treatment of CAP water as (Table 5.2). CAP water arrives in Tucson oversaturated with respect to barium sulfate, and it has been suggested that $BaSO_4$ precipitation limits recovery during RO treatment [108].

Table 5.2 - Concentration/solubility data for CAP ion pairs that may contribute to membrane scaling. Ion products were based on the concentrations shown, uncorrected for the ionic strength of CAP water

Precipitate	Ion Concentration in CAP water	Ion Concentration in RO reject[(b)]	Log of ion product[(c)]	log K_{S0}[(d)]	Qso/Kso Degree of Saturation[(e)]
$BaSO_4$(s)	$[Ba^{+2}] = 1.11 \times 10^{-6}$ M $[SO_4^{-2}] = 2.66 \times 10^{-3}$ M	$[Ba^{+2}] = 5.55 \times 10^{-6}$ M $[SO_4^{-2}] = 1.33 \times 10^{-2}$ M	-7.13	-9.96	673.20
$CaSO_4$(s)	$[Ca^{+2}] = 1.87 \times 10^{-3}$ M	$[Ca^{+2}] = 9.35 \times 10^{-3}$ M	-3.91	-4.85	8.81
$CaCO_3$(s)	$[CO_3^{-2}] = 6.88 \times 10^{-6}$ M[(a)]	$[CO_3^{-2}] = 3.44 \times 10^{-5}$ M	-6.49	-8.48	97.19

(a) based on 118.05 mg/L carbonate alkalinity as HCO_3^- and pH = 7.88.
(b) calculated as 5 times the ion concentration in CAP water with the assumption of RO running at 80% recovery.
(c) calculated by using the ion concentration in RO reject.
(d) [79, 80]
(e) calculated as Q_{SO}/K_{SO}. The value represents the approximate degree of oversaturation in the RO brine produced from CAP water.

If even a third of the regional CAP allotment is RO treated without additional efforts to increase recovery, the value of water lost as brine will be ~ \$20 M·yr^{-1} (based on a unit value of \$1000 per acre foot). The analysis does not include the cost of brine disposal, which is particularly relevant among inland communities like Phoenix and Tucson. Methods for increasing water recovery during salt removal include (i) pre-treatment of CAP water to remove specific components of hardness (here Ca^{2+} and Ba^{2+}) or (ii) post-treatment of CAP brines to separate additional water using the vibratory shear enhanced processing (VSEP).

5.3. Materials and Methods

5.3.1. Reverse Osmosis

The pilot-scale RO unit consisted of 6 pressure vessels containing a total of 18 elements in a two-stage, 2:2:1:1 configuration (Figure 5.3). Membrane elements were 2.5-inch diameter by 40-inch length polyamide thin film composite (PTFC) membranes (ESPA1-2540, Hydranautics). RO pressure requirements depend on the salinity of the feed water, water temperature, the membrane water transport coefficient (A, defined in equation 5.1), the design membrane flux (gallons of permeate per square foot of membrane per day [gfd]), and the target water recovery. Recovery is the percentage of influent that is recovered as permeate. Calculation of the osmotic pressure of a dilute solution follows the van't Hoff equation [30].

$$\pi=\phi \sum C_i R\, T \tag{5.1}$$

where, π, osmotic pressure [Pa], ϕ is the osmotic coefficient [-], ΣC_i is the sum of concentrations of individual ions [moles/L], R is the ideal gas constant [8.314472×10^3 L.Pa/mol.K] and T is the absolute temperature [K]

The water transport coefficient is defined in Eq. 5.2 as follows [30].

$$A=\frac{{Q_p}/{S}}{P_f - P_p - \left[\pi_f - \pi_p\right]} \times \mathrm{TCF} \tag{5.2}$$

where, A, water transport coefficient for water flux [m/s.Pa], Q_p, permeate flow rate [m^3/s], S, nominal membrane interfacial area [m^2], TCF, unitless temperature correction factor [used here as $1.03^{(25\text{-}T)}$] [30], P_f and P_p, pressures on the feed and permeate sides of

the membrane, respectively [Pa], π_f and π_p, osmotic pressure on the feed and permeate sides of the membrane, respectively, [Pa].

CAP water was pretreated via slow sand filtration and fed to the RO unit at an average flow rate of 4.73 gpm. The feed pressure was between 80 and 110 psi adjusted to maintain a consistent permeate flux. The flow of reject water (brine) was maintained at 0.92 gpm to provide an adequate crossflow velocity (~2.95 in/s) in the final pressure vessel [64]. The permeate flux from each element was adjusted to the design water flux, 10.9 gfd [64, 109]. Each element nominally contained 25.5 ft^2 of membrane surface for a permeate flow of 0.21 gpm per element [110]. The six pressure vessels together produced a permeate flow of 3.80 gpm. RO design and operational data are summarized in Table 5.3.

Table 5.3 - Reverse osmosis design and operational data

Parameter	Value
Number of stages (-)	2
Number of vessels (3 elements per vessel)	6
Manufacturer specified membrane area (ft^2/element)	25.5
Membrane type (Hydranautics)	ESPA 1-2540
Water flux (gfd)	10.9
Influent flow rate (gpm)	4.73
Feed salinity ($\mu S\ cm^{-1}$)	1000-1100
Feed pressure (psi)	80-110

5.3.2. Ion Exchange

Removal of hardness cations from CAP water prior to RO treatment was investigated with the objective of achieving recoveries well above 80 percent without precipitating $BaSO_4$(s) or $CaSO_4$(s) – the two most sparingly soluble salts in the feed water. Ion exchange itself produces brine for disposal, but may be justified by decreasing the net brine volume produced by the combined IX and RO system. Bench-scale IX experiments designed to confirm the feasibility of pre-softening CAP water via IX involved a strong acid cation (SAC) synthetic polymeric resin, C-8 L sodium resin from United States Resin Company. C-8 L is a high-capacity, conventional gel, polystyrene (8% cross-linked with divinylbenzene) strong acid cation exchange resin designed for use in residential or industrial water softening equipment.

The bench-scale ion-exchange reactor was too small to allow field testing for the long-term feasibility of enhanced recovery during IX/RO treatment of CAP water. Therefore, the subsequent economic analysis assumed that post-IX recoveries during RO would not be limited by membrane scaling. This assumption is based solely on appropriate equilibrium calculations using ion concentrations measured in water treated by the bench-scale IX system and remains to be confirmed by long-term field testing.

The City of Tucson provided a bench-scale ion exchange reactor system (Tomar Water Systems, Inc.) to the project. The system consisted of 4 IX columns, each with dimensions of a 2-in diameter and 32-in length. Resin capacity per vessel was 0.061 ft^3. The flow for each column was 0.25 gpm, for a hydraulic loading rate of ~11.5 gpm/ft^2. This is well within the norms for field-scale operation of ion exchange processes [30]. The resin bed volume was approximately 0.53 gallons, and the regenerant solution

consisted of 200 g/L NaCl. Regeneration was conducted by applying 7 empty bed volumes of the regenerant solution during a one-hour period.

A Dionex DX500 ion chromatograph and a high-capacity carboxylate-functionalized cation exchange column (IonPac CS16) were used with a CD20 conductivity detector for anion and cation analyses. A 30 mM methane sulfonic acid (MSA) solution buffered the mobile phase. Flows were regulated using an IP25 Isocratic gradient pump system. The software, PeakNet, for the Dionex DX500 consisted of the DX LAN program, data processing, method editor, and various other configuration/driver programs.

5.3.3. Vibratory Shear Enhance Processing VSEP®

VSEP (New Logic Research, Inc.) (Figure 5.2), is a membrane separation system in which high-pressure RO or nanofiltration is used to extract additional water from highly saline solutions. The VSEP reactor was a pilot-scale, LP Series unit containing 16.44 ft^2 of ESPA1 membrane (Hydranautics). The feed flow (RO brine) was provided at 500 psi based on preliminary testing to select an operating pressure. The unit was operated by automatically cycling the brine retention valve between its closed and open positions. With the valve closed, fluid left the reactor only as permeate. In the open-valve position, brine was flushed from the unit and completely replaced with reactor influent (RO brine). During each cycle, the valve was opened (flush position) for six seconds. The length of the closed valve period was adjusted to yield target permeate recoveries. In general, the permeate flow rate progressively decreased throughout the closed-valve period, although longer closed valve periods resulted in greater recoveries. Thus, average permeate flow rate is inversely related to recovery and elapsed time of operation

following VSEP membrane cleaning. Design and operational parameters for the VSEP in P-mode (pilot mode) are presented in Table 5.4.

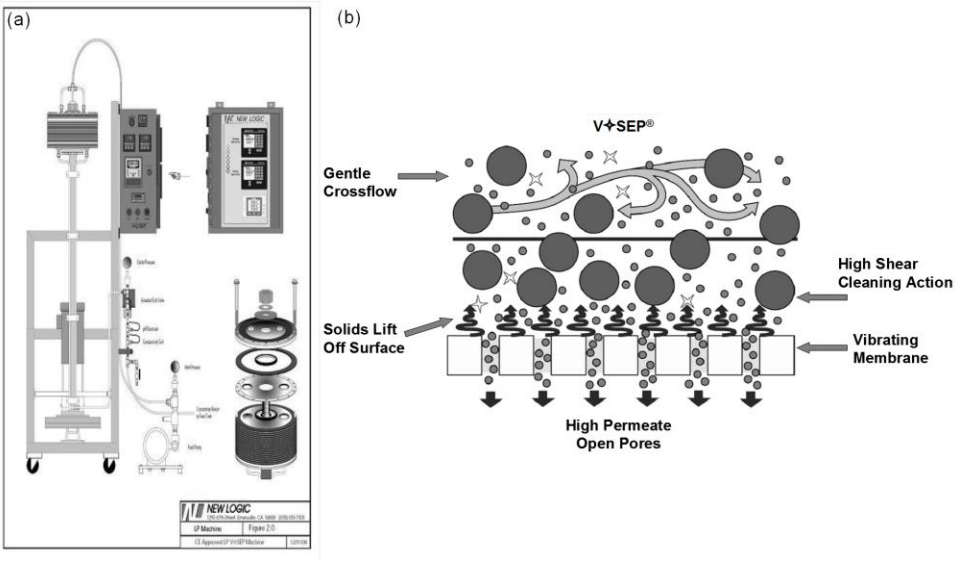

Figure 5.2. (a) VSEP LP shown in pilot-scale (P) mode (b) Principle of VSEP operation—mechanical vibration at the membrane surface produces a shear wave preventing solids formation on membrane surfaces while forcing additional water from brines via high pressure RO [111]. Figures adapted from New Logic Research, Inc. [112]

Table 5.4 - Vibratory shear enhanced processing operational parameters

Parameter	Value
Membrane type	ESPA1
Membrane surface area (ft^2)	16.44 (P-mode)
Influent brine conductivity (μScm^{-1})	3000 – 5000
Operating pressure (psi)	500
Vibration frequency (Hz)	52.0 – 52.5
Flow rate (gpm)	~1.0
Recovery rate for VSEP alone (%)	75 – 90

Cleaning of the VSEP membranes involved five steps. The first was a 15-minute fresh water flush with cold water in a single-pass mode at 50 psi. The second step was a low-pH cleaning with 3% NLR 404 solution [113], a citric acid based solution formulated to remove metallic-based foulant and scaling components. The optimum pH was between 2.0 and 3.0 [113]. The third step was another 15-minute cold water flush, and the fourth was high-pH cleaning with 3% NLR 505 solution [114], a blend of surfactants and chelating agents in a caustic liquid. Best results for the high-pH cleaning are generally obtained between pH 11.0 and 11.5 [114]. The temperature of the cleaning solutions in steps 2 and 4 was maintained at 50 ^{o}C and the solution was continuously recycled through the membrane pack for 45 minutes. The last step of the cleaning process was another 15-minute cold water flush. Throughout the process, the VSEP filter pack was vibrated at 3/4" amplitude (~52 Hz). At the end of each water flush, the pressure was increased to 300 psi while the vibration frequency and amplitude were maintained. Cleaning adequacy was evaluated on the basis of the post-cleaning permeate flux. Irreversible deterioration in VSEP performance due to membrane scaling or fouling as a

result of long cycle times was not observed. At the end of each experiment conducted, recommended membrane cleaning procedures restored the clean water membrane flux.

5.4. Results and Discussion

5.4.1. IX Performance – Pretreatment for RO

Cation concentrations in IX-treated CAP water in Table 5.5 indicated that downstream RO recoveries on the order of 97% should be possible without mineral precipitation and membrane scaling [109]. Barium ion has greater affinity for ion exchange media than calcium or magnesium ions. Hence, barium ion break through occurs after that of calcium and magnesium ions in cation-exchange water softening resins. Therefore, the limiting solid phase was assumed to be calcium sulfate. As the worst case scenario in RO operation, free magnesium and calcium ions in IX treated CAP water were assumed to be at the detection limit (10 µM). The reject concentrations of the ions in such treated water (~33 times higher than corresponding RO feed concentrations) were estimated at 3.3×10^{-4} M for free calcium ion and 8.9×10^{-2} M for free sulfate ion based on measured IX product concentrations. Thus, the ion product for calcium sulfate would be about 2.1 times its solubility product. The acceptable level of oversaturation for calcium sulfate is assumed to be 2.3 in the concentrate [109]. Provision of anti-scalant should permit RO recoveries up to 99% [115, 116].

Table 5.5 – Average concentrations of limiting ions in raw CAP water and bench-scale IX treated CAP water

Source	Sodium[c] (mM)	Magnesium[c] (mM)	Calcium[c] (mM)	Sulfate[b] (mM)	Carbonate[b] (mM)	pH[b] (-)
Raw CAP Water	3.79	1.01	1.27	2.66	6.9×10^{-3}	7.88
IX Treated CAP Water	6.68	ND[a]	ND[a]	2.66	6.9×10^{-3}	7.88

[a] ND = non-detect. Quantity was below the method detection limit of 10 µM.
[b] Average values observed throughout the pilot-scale testing.
[c] Average values observed throughout the bench-scale IX testing. Dilution factor of 10 was used during IC measurement.

The operational space in which IX/RO combination is economically favored over RO/VSEP depends on the feasibility of achieving sustainable RO recoveries >97% following the IX treatment. Although recoveries of that magnitude might be possible without precipitating calcium sulfate (based on post IX concentrations measured here), it must not be assumed without piloting that barium sulfate precipitation or silica scale formation will not occur in the resultant brines. Our own membrane autopsies (not shown) indicated that at 80-85% recovery during RO treatment of CAP water there was minimal $BaSO_4$(s) scaling despite the degree of super-saturation predicted (>670 at 80% recovery). This suggests that following IX pretreatment, scaling with $BaSO_4$(s) may be avoidable using antiscalant even at the higher recovery values.

A pilot-scale research facility was constructed 20 miles northwest of Tucson in a collaborative effort between the University of Arizona, U.S. Bureau of Reclamation (USBR), a consortium of utilities in northwest Pima County—the Northwest Water Providers (NWWP) and the City of Tucson. The project was designed to establish the

long-term (inter-seasonal) performance of RO for salt separation from CAP water at 80% recovery and provide operational data with which to determine the economic feasibility of VSEP as a post-treatment for RO brine. IX performance was not tested in the field but, nevertheless, a sequential treatment consisting of IX/RO was analyzed based on bench-scale studies and solubility product calculations that suggest reverse osmosis is not limited by scaling up to 99% recovery following IX pre-treatment. This led to economic comparisons among RO treatment (alone), RO/VSEP and IX/RO salt management alternatives.

5.4.2. RO Performance

The extended record of RO performance for desalting CAP water in Figure 5.3, suggests that membrane scaling or fouling occurred on a time-scale of months. Impaired hydraulic performance was first observed in vessels 5 and 6, where ion concentrations were highest, suggesting precipitation of sparingly soluble ions as the cause. However, high total coliform counts in the reject stream provided an indication of biofouling, as well. Therefore, a four-step high-pH membrane cleaning occurred in April 2008, indicated as (1) in Figure 5.3. This cleaning consisted of one-hour low-flow flush in recycle mode followed by two hours soak, two hours high-flow flush in recycle mode and a clean water flush at pH ~7.0 for half an hour. Sodium hydroxide (NaOH) and hydrochloric acid (HCl) were used to adjust the chlorine-free (<0.01 mg/L) cleaning solution pH to ~12.0. Since no heating was used, the temperature of the cleaning solution fluctuated between 23 and 26 ^{o}C throughout the process. The cleaning temporarily restored membrane permeability, but downstream (stage 2) recovery again declined precipitously after a short period of steady operation. When the stage 2 recovery fell to

25% (from an initial 55%) in early August 2008, the membranes in stage 2 (only) were replaced with new ESPA 3 membranes. The point of change is indicated as (2) in Figure 5.3. The system was operated to achieve a slightly higher overall recovery (80-85%) for the next three months. Near the end of that period, there was again preferential loss of permeability in the downstream RO vessels. At the end of October 2008, the second stage membranes were again replaced, this time with new ESPA 4 membranes, indicated as (3) in Figure 5.3. The unit was thoroughly cleaned and subsequent operation at an overall recovery of ~75% led to reasonably stable performance for the next 9 months. During the last three and a half months of this period, the pre-treatment for the RO unit was switched from slow sand filtration to 0.2-micron polypropylene microfiltration (MEMCOR CMF Unit – Model 3M10C), indicated as (4) in Figure 5.3. All the membranes were removed from the unit at this stage for post-mortem analyses. A new set of membranes from Koch (ULP-2540) was installed in early August 2009 for a comparison study, indicated as (5) in Figure 5.3. Neither the results of the post-mortem analyses nor the outcome of the comparison studies are within the scope of this paper. In summary, the record of performance suggests that long-term, satisfactory RO performance is possible at recoveries approaching 80% without pre-treatment to remove hardness cations. Higher recovery without water softening ahead of RO is inadvisable.

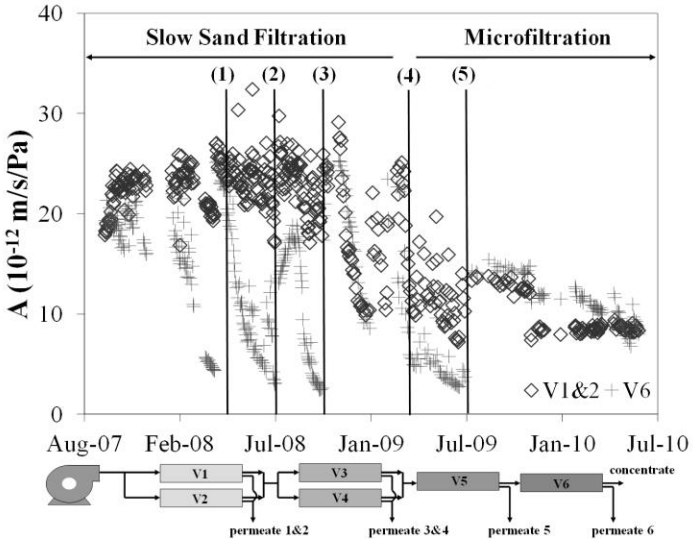

Figure 5.3. Water transport coefficient (A) profile for RO operation (for gfd/psi, multiply y–scale by 0.0146). RO consisted of a 2-stage array (2:2:1:1) with each pressure vessel containing three 2.5-in spiral wound membranes. The RO processed 5 gpm of CAP water. All values are adjusted to 25°C. (1) High-pH membrane cleaning; (2) high-pH membrane cleaning, installation of new membranes in stage 2 and beginning of 80-85% recovery; (3) installation of new membranes in stage 2 and the end of 80-85% recovery; (4) beginning of microfiltration as the pre-treatment method; and (5) installation of new Koch membranes in both stages 1 and 2

5.4.3. VSEP Performance—Post-Treatment of RO Brine

A series of VSEP runs were carried out between May 2008 and July 2009. VSEP recovery and the operation time between each reactor cleaning were decision variables for VSEP operation. It was postulated that some combination of these variables could lead to economically optimal VSEP performance. Increased VSEP recovery produces additional potable water and decreases the cost of brine disposal, but also lowers the average permeate flux so that more reactors are necessary to treat the same brine flow. Similarly, less frequent reactor cleaning saves on cleaning costs but, again, lowers the average VSEP permeate flux leading to purchase and operation of additional reactors.

VSEP recoveries of 89.2%, 85.7 % and 82.4 % were selected for this phase of study (overall recoveries of 98%, 97% and 96.5%, including the RO running at 80% recovery), and 24-hour pilot experiments were run to establish the time-dependent permeate flux at each recovery level (Figure 5.4). Based on these results, linear relationships were established between the temperature-corrected water flux and the length of operation between membrane cleanings. Simple linear regression results are summarized.

In the 89.2% recovery experiment, for example, the duration of the closed-valve period necessary to maintain recovery increased from 4.7 minutes to 6.9 minutes over 23 hours of operation without cleaning. The temperature-corrected water flux dropped from 59.5 gfd to 33.9 gfd over the same period. Other VSEP operating conditions were as follows: 3/4-inch amplitude of torsional vibration, 500 psi operating pressure (during the closed-valve period), and 0.1 minute open-valve time. The influent TDS concentration was about 2,300 mg/L, and the product water had an average TDS of 46.5 mg/L. The TDS of the VSEP concentrate was ~20,000 mg/L. A salt balance, defined in equation 5.3, around the reactor produced a positive salt mass balance deviation (MBD_S) ≤+5%. The temperature of the water varied between 12^{o}C and 20^{o}C during the day-long study, averaging 15.3 ^{o}C. The results of day-long experiments at the other recoveries were similar as shown in Figure 5.4.

$$\text{Salt Mass Balance Deviation } (MBD_s) = \frac{[Salt_{in} - \sum Salt_{out}]}{Salt_{in}} \times 100\% \qquad (5.3)$$

where, $Salt_{in}$ is the salt mass flux entering the RO unit [mg/min], $Salt_{out}$ is the sum of salt mass fluxes leaving the reactor in permeate and brine streams [mg/min]

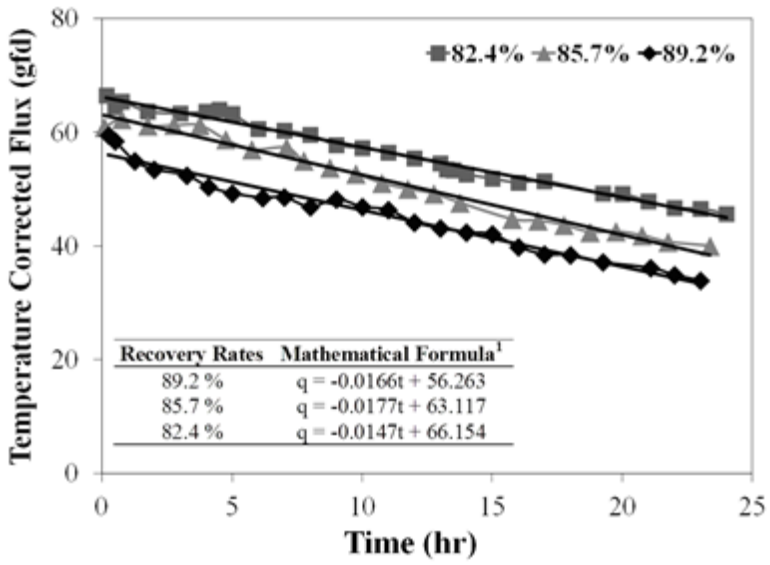

Figure 5.4. The temperature-corrected (20°C) permeate flux as a function of overall VSEP recovery and time of continuous operation following membrane cleaning. 1Linear regression lines of best fit are shown

5.4.4. Economic Analysis

Three cases were selected for economic comparison—(i) RO alone, with brine disposal via augmented evaporation, (ii) IX before RO to achieve higher recoveries without scaling during RO, and (iii) RO followed by VSEP to minimize the volume of brine for evaporative disposal. Process schematics for each of the three treatment scenarios as well as typical flow rates for each process are presented in Figure 5.5. Augmented evaporation was chosen as a find brine disposal step for its smaller footprint and lower cost advantages compared to solar evaporation, which is one of the most common brine disposal techniques for inland desalination. Water spraying or misting are among the most common augmentation methods. Average pan evaporation and precipitation rates of 107 and 11.7 inches per year, respectively, were selected based on

local measurements [107]. Economic and performance data for VSEP operation were derived from experiments or provided by New Logic Research, Inc. Economic comparisons were based on treatment of 15 MGD of CAP water as RO feed. The period of the economic analysis was 30 years (the assumed service life of the RO vessels), and the discount operator was 0.06 yr^{-1}. All costs are in January 2010 dollars. The unit value of water was assumed to be $1000/AF, a fairly conservative estimate considering the current price of raw CAP water in the Tucson area and future regional water demand/supply scenarios.

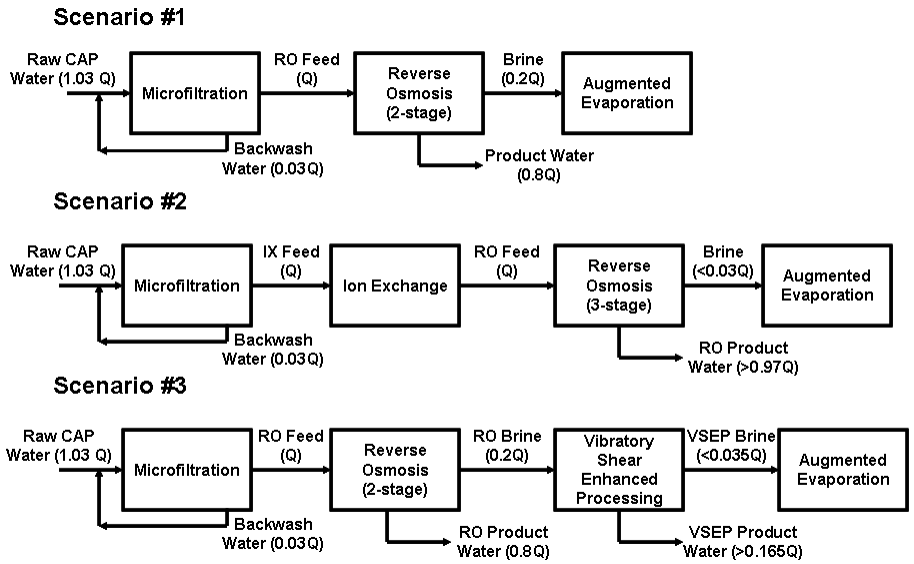

Figure 5.5. Process schematics for each of the three treatment scenarios that were selected for economic comparison and typical flow rates for each process are shown. RO feed flow is represented by Q for ease of interpreting the RO and VSEP recovery rates. The recovery displayed in the figure for MF was the observed recovery throughout pilot testing. However, 100% recovery is assumed for MF during the economic analysis

5.4.5. RO Treatment / Brine Disposal

Considered in the cost analysis were the capital and operating costs of microfiltration (pre-treatment for RO), chemical addition, reverse osmosis and brine treatment/disposal. 100% recovery was assumed for microfiltration (Observed recoveries for microfiltration during pilot experiments were ~97%). The extended record of performance shown in Figure 5.3, suggests that long-term, satisfactory RO performance is possible at recoveries approaching 80% without pre-treatment to remove hardness cations. Therefore, the entire 15 MGD feed flow was (hypothetically) treated by RO at 80% recovery (Scenario #1). The resultant brine (3 MGD) was treated using augmented evaporation ponds and the salt residual was landfilled. Operation and maintenance (O&M) costs included chemicals added for pH control, disinfection and scale prevention; chemical cleaning reagents; disposal of membrane cleaning residuals and personnel costs.

Relevant cost functions are provided in Table B.1 of the supplementary material. The costs of MF pre-treatment, RO treatment up to a recovery of 80% and the associated O&M costs are essentially the same for all three scenarios investigated. As such, they should affect the total but not the relative costs of the alternatives. Scenario-dependent costs are broken down into capital and O&M costs for source water purchase, MF, chemical addition, RO and brine treatment/disposal. The incremental cost for the RO treatment option ($12.3M/yr, Table 5.6) was more or less evenly distributed between water purchase cost and the capital and O&M costs of the evaporation ponds. Total annual cost for this option (calculations not shown) is ~$18.7M/yr.

Table 5.6 Summary of scenario dependent annualized costs above those of the baseline scenario (pretreatment via microfiltration plus RO with 80% recovery). For the RO treatment column, costs are those of brine disposal. The unit costs are based on the water produced. The percentages represent overall, scenario-dependent recoveries

RO Treatment	VSEP as Post-treatment of RO			IX as Pre-treatment of RO		
	96.5%	**97.1%**	**97.8%**	**96.5%**	**97.1%**	**97.8%**
$12.3M/yr ($2.81/kgal)	$7.11M/yr ($1.35/kgal)	$7.30M/yr ($1.37/kgal)	$7.61M/yr ($1.42/kgal)	$7.16M/yr ($1.35/kgal)	$6.80M/yr ($1.28/kgal)	$6.44M/yr ($1.20/kgal)

5.4.6. IX / RO

Incremental costs attributable to the IX/RO alternative (Scenario #2) include capital and/or operational costs arising from (i) IX pre-treatment; (ii) addition of a third RO stage, necessary to satisfy crossflow requirements at postulated recoveries; (iii) energy required to overcome osmotic pressure in the third RO stage; (iv) disposal of the residual (reduced volume) RO brine and spent IX regenerant by augmented evaporation and (v) cost of sodium chloride for preparing the regenerant solution. The entire 15 MGD flow was to be treated by IX. Osmotic pressure was calculated based on the recovery-dependent ion composition of the brine. Components of IX reactor costs are as summarized in Table B.2. The recovery-dependent incremental costs for Scenario #2 are as illustrated in Figure 5.6.

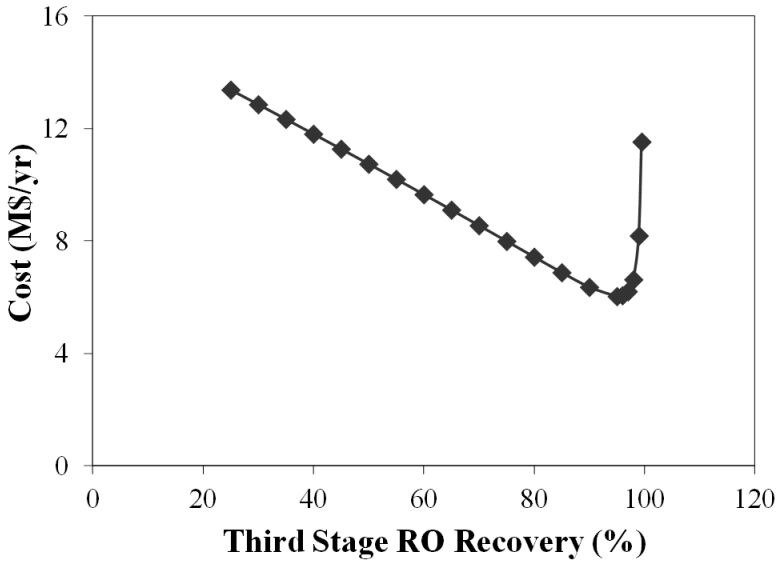

Figure 5.6. The combined incremental cost for IX, RO and enhanced evaporation as a function of third-stage RO recovery during reverse osmosis treatment of IX-pretreated CAP water

IX reactor design was based on an assumed resin bed depth of 8 ft. The reactor diameter was assumed to be 12 ft, so that 12 IX units were required to treat 15 MGD at a hydraulic loading rate of 7.7 gpm/ft^2 [30]. The calculated bed capacity for specific ions and volume to breakthrough were then determined based on an assumed resin capacity of 1.9 equivalents per liter and the major ion composition of CAP water shown in Table 5.1. Results suggest that about 221 bed regenerations (total) would be necessary per year. The lab-scale experiments showed that 5 regeneration cycles are achievable with the same regenerant solution provided that the NaCl concentration is brought back up to 200 g/L after each regeneration cycle. Hence, 44 new regenerant solutions need to be prepared in a year. At 10 bed volumes per regeneration [30], the IX process will produce 100k gallons of brine per day (all reactors). This was ignored in calculating the overall

recovery, although it was added to the recovery-dependent RO brine production rate to estimate the cost of augmented evaporation for the IX/RO alternative. Chlorine disinfection was assumed to be unnecessary ahead of IX treatment.

Sources of incremental cost in Scenario #2 are functions of a single independent variable– the anticipated recovery during RO treatment of pre-softened water. Functions used to calculate the annualized cost for treatment of the same 15 MGD flow using IX/RO are summarized in Table B.2. A plot of annualized (incremental) cost versus recovery shown in Figure 5.6, indicates that reduction of cost is achieved by increasing RO recovery up to 99%. Savings originate in (i) reduced brine volume for treatment and disposal and (ii) water conserved. Beyond that point, however, the energy necessary to overcome osmotic pressure in the final stage of RO dominates the calculation, and the total annualized cost increases rapidly. IX ahead of RO treatment was predicted to increase power costs for operation of the first two stages of RO by <<1%. At the total recovery of 99%, the capital costs for MF, IX, RO and augmented evaporation are the primary sources (50%) of the overall cost for the IX pre-softening alternative. The total annualized scenario #2 cost was estimated at ~$12.4M/yr at the same recovery.

5.4.7. RO / VSEP

Incremental costs attributable to the RO/VSEP option (Scenario #3) include the capital plus operation and maintenance costs for (i) VSEP treatment for brine reduction, (ii) augmented evaporation of reduced-volume (post-VSEP) brine and (iii) water lost as brine through augmented evaporation treatment. A near-optimum period of VSEP operation between membrane cleanings was determined as a function of VSEP recovery as follows: Fitted curves (Figure 5.4) were used to express the permeate flow rate as a

function of time of operation without cleaning at each level of VSEP recovery. The total volume of permeate produced between cleaning operations, divided by the operational period plus cleaning time, yields the average permeate production rate for a single VSEP device as defined as equation 5.4. That is,

$$Q_i = \frac{(a_i \times t + 2b_i) \times A \times t}{2(t + t_c)} \tag{5.4}$$

where, Q_i is the average permeate flow rate for a single VSEP unit at VSEP recovery rate i [gpd], t is the VSEP run time between cleanings [days], t_C time required for membrane cleaning [days], a_i, slope of the fitted relationship between flux and run time [gfd/day], b_i intercept (vertical axis) of the same fitted relationship [gfd], A membrane area for a single VSEP unit [ft^2].

The number of VSEP units required (N_i) at VSEP recovery R_i is then given by Eq. 5.5:

$$N_i = \frac{Q_B \times R_i}{Q_i} \tag{5.5}$$

where, Q_B is the total rate of brine flow from the RO process [gpd].

Operational costs that were considered include (i) VSEP power costs– 500 psi feed pressure and generation of torsional vibration (manufacturer's data), (ii) membrane cleaning and replacement costs and (iii) personnel costs. The details of the VSEP related cost functions are presented in Table B.3. The value of water lost as VSEP brine was again taken as a system cost, estimated at $1000 per acre foot of unrecovered brine. The service life for VSEP reactors was assumed to be 10 years. For evaporation ponds and

related equipment, service life was assumed to be 30 years. The largest VSEP unit manufactured by New Logic Research, Inc., the I-84, was used for the economic analysis. The membrane area of the I-84 unit is 1500 ft^2, and the cost is $250,000 per unit.

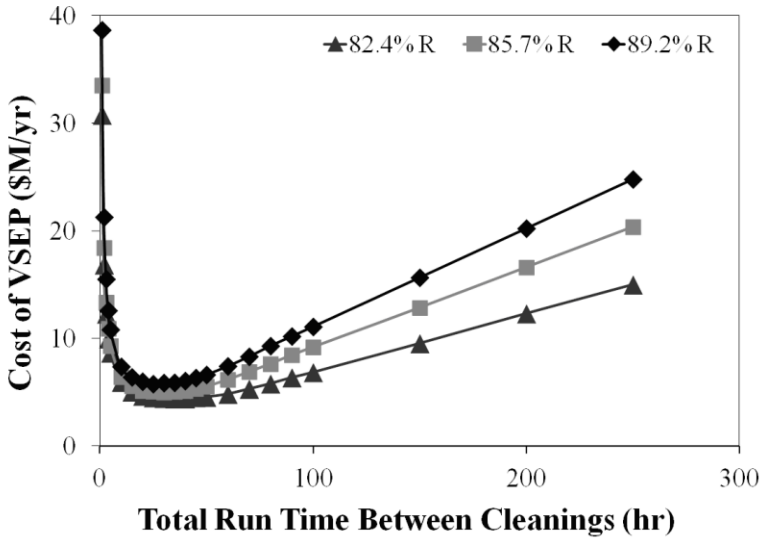

Figure 5.7. Annualized VSEP capital/O&M costs as a function of VSEP recovery and time between cleanings

At each recovery rate for which there were pilot data (R_i), the annualized cost for treating 3 MGD of RO brine was calculated as a function of the period of VSEP operation between membrane cleanings shown in Figure 5.7. The global optimum was found at the combination of recovery and cleaning frequency that provided the lowest total annualized cost. Results suggest that there is a broad operational region in which VSEP operation is near optimal—that total annualized cost is fairly insensitive to recovery in the range 80-90 percent and period between cleanings in the range of 25-40

hrs. In those ranges, the total annualized cost for the VSEP system was significantly lower ($7.11-7.61 M/yr) than the cost of the no-VSEP option ($12.3 M/yr) (Table 5.6). In the RO/VSEP system, only 2-4% of the CAP water treated would be lost as brine. The total incremental cost of the RO/VSEP option is $423 per acre foot of water treated (influent to the RO unit). The cost of additional treatment per unit of water recovered from RO brine is about $2,500 per acre foot. The total annual scenario #3 cost is estimated at ~$13.5M/yr at 96.5% overall recovery. The breakdown of the total annual cost for each scenario is presented in Figure 5.8.

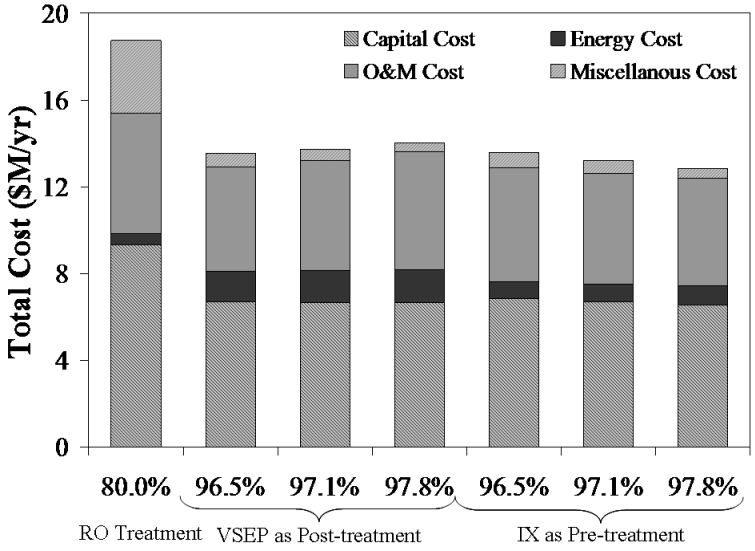

Figure 5.8. Economic summary and break down of the total costs (in $/yr) of treatment options – percentages represent overall, scenario-dependent recoveries

5.5. Conclusions

Water loss during desalination was reduced from 20% to 2-4% via post-RO VSEP treatment. Under optimal conditions, VSEP treatment alone achieved >80% recovery of water from RO brine. The total annualized cost of brine treatment was fairly insensitive

to VSEP recovery in the range 80-90% and the period between cleanings in the range 25-40 hrs. These values define a fairly broad window for near optimal VSEP operation under the conditions of the study. The cost of VSEP treatment to decrease overall brine loss to 3.5% (82.5% recovery during VSEP) was estimated at $423 per acre foot ($1.30 per 1000 gal) assuming 15 MGD CAP water is treated. For a hypothetical 3 MGD RO brine flow, the use of VSEP to recover water and reduce the volume of brine for disposal results in savings of more than $5M/year compared to the no-VSEP brine disposal alternative.

IX pre-treatment is predicted to do slightly better than RO/VSEP at overall recoveries of 97% or higher, but there are no field data to confirm the feasibility of the assumed IX/RO recoveries. At these recoveries, IX used as pre-treatment for RO is predicted to save more than $0.5M/yr compared to VSEP post-treatment of RO brine. Overall recoveries >>80% might be achievable if IX removes essentially all the divalent cations and no other precipitation reactions occur during RO treatment. These values should not be accepted without experimental support for IX/RO recovery assumptions.

CHAPTER 6

SUMMARY AND FUTURE WORK

6.1. Summary

6.1.1. Mass and Heat Transfer Mathematical Modeling for Vacuum Membrane Distillation in a Hollow Fiber Contactor

The development of a finite difference mass and heat transfer model for a hollow fiber reactor allowed us to predict the permeate production based on membrane characteristics during VMD operation. The model also was capable of determining that Knudsen diffusion was the prevailing mass transfer mechanism.

The model accounted for the effect of the brine temperature drop at the interface, T_i, as water vapor diffuses across the membrane. The effect of brine temperature, vacuum on the permeate side of the membrane, and brine velocity were analyzed and modeled. Modeled results are in good agreement with the experimental data obtained. Modeling also supports the following conclusions:

- Increasing the brine feed temperature results in an increase in permeate production due to an increase the driving force –gradient in vapor pressure.
- A lower absolute pressure on the permeate side of the membrane results in an increase in the permeation flux.

- The permeation flux is a function of the brine velocity. Higher brine velocities reduce the difference between inlet and outlet temperature.
- Larger pore size results in a higher permeation flux, however this is limited by other membrane characteristics like porosity and tortuosity.

6.1.2. Comparison of Slow Sand Filtration and Microfiltration as Pretreatment for Inland Desalination via Reverse Osmosis

- An effective pre-treatment of RO feed water is essential for an optimal operation of an RO desalination system. The results from a 2-year pilot plant study compared slow sand filtration and microfiltration as pretreatments for RO. Results of this study show:
- RO performance was more stable when MF pretreatment was used to treat the RO feed water.
- Post-mortem membrane inspections, confirmed by SEM-EDS images, showed that significantly more material accumulated on the membrane surface during SSF pretreatment, reducing the water transport coefficient due to a combination of fouling and scaling reactions.
- Economic analysis suggests that the costs of MF and SSF pretreatments are comparable, but MF pretreatment should be economically preferred when RO membrane cleaning and replacement costs are considered.

6.1.3. Post-mortem Study of Membranes from the Yuma Desalting Plant Polyamide Assessment Study

Comparing the pre-treatments in both the YMC and MODE waters the following general conclusions can be drawn:

- Deposition of polysaccharides (indicative of general biofouling) is much greater with lime-softening as pretreatment than when microfiltration is used.
- Deposition of inorganics is greater for lime-softened MODE water and for both pretreatments is by aluminum silicates (clays) and silicon oxides with traces of iron
- Palmitate deposits (indicative of degraded organic tissues) are significant on the lime-softened water and slight on microfiltered water.
- Post-mortem study results suggest that YMC water leads to less deposition of material on the membrane surface than MODE water, but this result is not conclusive since the YMC water alternatives operated for a significantly shorter duration than the MODE water alternatives.
- For the YMC water pre-treatment alternatives, MF versus CF, there was significantly greater material build-up with CF pre-treatment, particularly on the tail element in the high recovery array.
- Finally, for both source waters and all pre-treatment alternatives, the low recovery, single element testing showed chlorine substitution (both ring and amide group) with all membrane types evaluated. In the high recovery membrane arrays the chlorine substitution was evident in both lead and tail elements, but decreased from lead to tail element.

6.1.4. RO Brine Minimization Study via Vibratory Shear Enhanced Processing (VSEP®)

The study compared Ion Exchange (IX) pre-treatment VSEP® post-treatment for RO as alternative measures to increase overall water recovery. Experiments were designed to establish the efficiency of VSEP® and support an economic comparison of between the two options.

- Water loss during desalination was reduced from 20% to 2-4% via post-RO VSEP treatment. Under optimal conditions, VSEP treatment alone achieved >80% recovery of water from RO brine.
- The cost of VSEP treatment to decrease overall brine loss to 3.5% (82.5% recovery during VSEP) was estimated at $423 per acre foot ($1.30 per 1000 gal) assuming 15 MGD CAP water is treated. For a hypothetical 3 MGD RO brine flow, the use of VSEP to recover water and reduce the volume of brine for disposal results in savings of more than $5M/year compared to the no-VSEP brine disposal alternative.
- IX pre-treatment is predicted to do slightly better than RO/VSEP at overall recoveries of 97% or higher, but there are no field data to confirm the feasibility of the assumed IX/RO recoveries.
- At these recoveries, IX used as pre-treatment for RO is predicted to save more than $0.5M/yr compared to VSEP post-treatment of RO brine. Overall recoveries >>80% might be achievable if IX removes essentially all the divalent cations and no other precipitation reactions occur during RO treatment. These values should not be accepted without experimental support for IX/RO recovery assumptions.

6.2. Future Work

Despite all the results and findings of this study on inland desalination, there is still a need for further investigation and experimentation especially in the area of MD which are beyond the scope of this study [13, 15, 37]. Below is a list of some of the areas that future research needs to focus on:

- MD use of realistic solutions (multiple components solutions e.g. wastewater) including volatile and non-volatile compounds.
- Membrane module configuration to optimize heat and mass transfer
- Development of membranes specifically for MD.
- Optimization of MD systems to increase product water and reduce energy consumption.
- To reduce the likelihood of biological fouling, future work of this nature should regulate free chlorine contact time and chloramine residual in the RO feed to maintain HPCs below 100 CFU/mL in the RO reject.
- IX pre-treatment pilot study to confirm the feasibility of the assumed IX/RO recoveries.

APPENDIX A – SUPPLEMENTARY DATA – Comparison of Slow Sand Filtration and Microfiltration as Pretreatments for Inland Desalination via Reverse Osmosis

The supporting material presented includes turbidity data following SSF or MF pretreatment and results of the SEMS and XRD analyses for the membranes autopsied during this study.

A.1. SDI Values for Slow Sand Filter Effluent

Table A.1. Mean and standard deviation for SDI measurements in SSSF and NSSF product waters during August 2009 to November 2010. SDI values for the raw CAP water could not be obtained since the PF routinely exceeded 75% prior to the end of the 15-min test. Mean and standard deviation values are in %/min

Overflow Rate	**SSSF**			**NSSF**		
[m^3/m^2 d]	μ	σ	n	μ	σ	n
1.6	3.4	0.5	50	2.4	1.0	52
3.1	4.2	1.0	17	3.0	0.9	17
4.7	3.8	0.5	23	3.4	1.1	24
6.3	4.2	0.2	32	3.8	1.0	32

A.2. Turbidity Data for Slow Sand Filter Effluent

The turbidity data for the SSFs are shown in Table A.2. The MF unit product water showed turbidity average values of 0.24 NTU (S.D. = 0.12, n = 25). It is apparent

that turbidity is a poor measure of pretreatment efficiency due to the lack of sensitivity among the effluent data.

Table A.2. Turbidity values of product waters from the north and south slow sand filters. Data were obtained from August 2009 to November 2010. Mean and standard deviation values are in NTUs

Overflow Rate [m/d]	**SSSF**			**NSSF**		
	μ	σ	n	μ	σ	n
1.6	0.3	0.1	50	0.2	0.1	52
3.1	0.3	0.1	17	0.2	0.1	17
4.7	0.3	0.1	23	0.3	0.1	24
6.3	0.5	0.1	30	0.2	0.1	26

A.3. Membrane Post- Mortem Analyses

SEM Analyses for ESPA 2 Reverse Osmosis Membranes

Autopsies were performed on the tail element of the RO unit operating with SSF pretreatment. The period of operation preceding the autopsy was six months and during which recovery was 80%.SEM images of membrane autopsies and the results of EDS elemental analyses of materials collected from membrane surfaces are provided. Accumulation of material on the membrane surface is shown in Figure A.1. The dark cracks between the dried material represent the membrane itself.

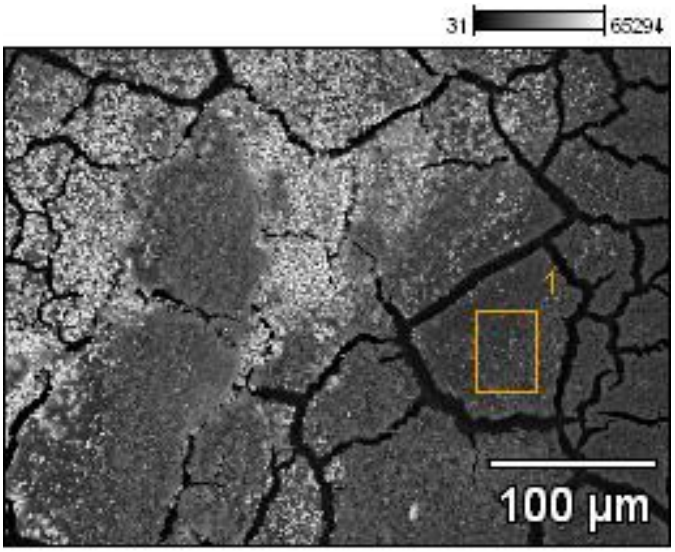

Figure A.1. SEM image of ESPA2 RO membrane fed SSF pretreated water. The membranes were in operation for 6 months running at 80% recovery. The rectangle indicates the area analyzed leading to data shown in Figure A.2 and Table A.2

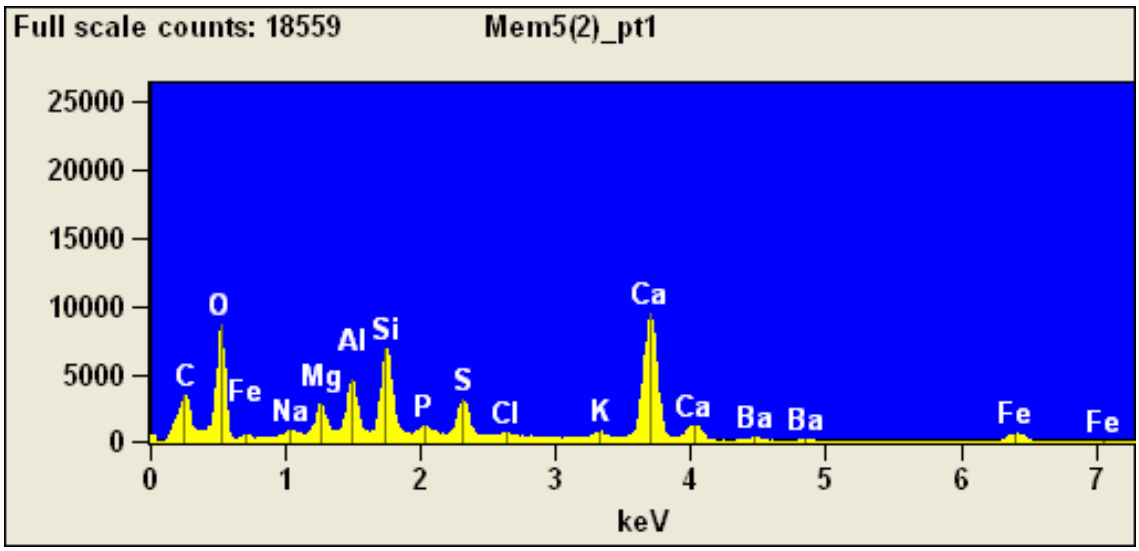

Figure A.2. EDS analysis for the ESPA2 RO membrane fed SSF pretreated water

Fractional elemental compositions (Table A.2) from the EDS analysis (Figure A.2) of the membrane sample suggest that both fouling and scaling reactions contributed

to the loss of membrane permeability. Silicon-to-aluminum ratios ranged from 1.6 to 2.5. Figure A.3 contains maps of specific elements over the membrane surface. Notice that Si, Al, K and some Fe are co-dispersed. The same is true for S and Ba. Together, these observations suggest that the dark areas in Figure A.1 are dominated by a mixture of aluminum-silicate (mixed ratio) clays and the light areas contain a significant fraction of barium sulfate or barium sulfite. Calcium and sulfur are not, however, co-distributed, so that formation of gypsum was probably not a major scaling reaction. It is apparent that both scaling reactions and inorganic fouling may have contributed to the time-dependent loss of membrane performance.

Table A.3. Atom Percentage of Major Elements on ESPA2 Membrane

Atom % Error (± 1 Sigma)												
C	O	Na	Mg	Al	Si	P	S	Cl	K	Ca	Fe	Ba
0.48	0.32	0.04	0.03	0.04	0.03	0.01	0.02	0.01	0.02	0.03	0.03	0.01

Atom %												
C	O	Na	Mg	Al	Si	P	S	Cl	K	Ca	Fe	Ba
40.29	42.38	0.75	1.42	2.19	3.46	0.32	1.47	0.17	0.23	6.30	0.85	0.17

The spatial distribution of major elements was determined via EDS for a membrane fragment is shown in Figure A.3.

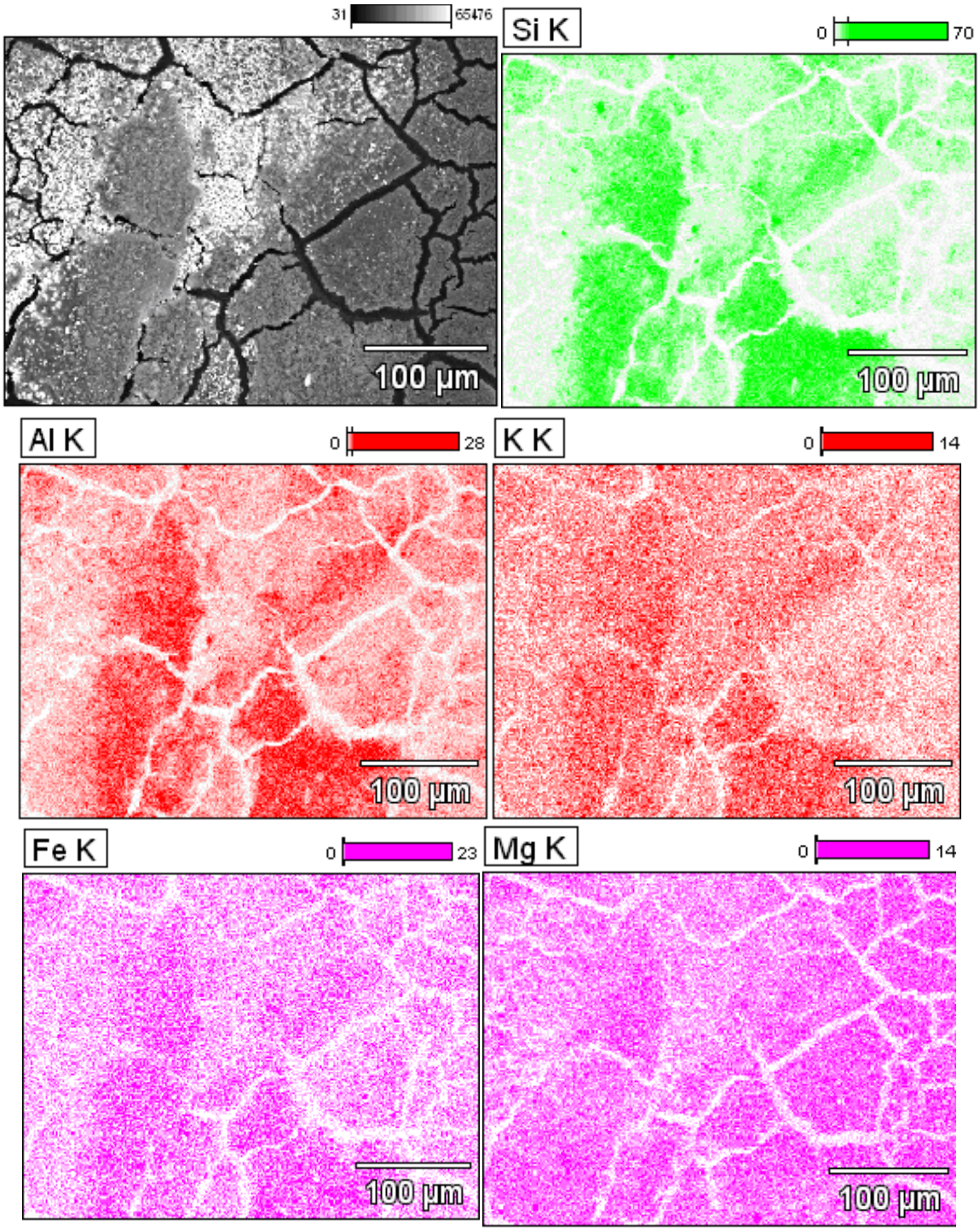
31
65476
100 µm
Si K
0
70
100 µm
Al K
0
28
100 µm
K K
0
14
100 µm
Fe K
0
23
100 µm
Mg K
0
14
100 µm

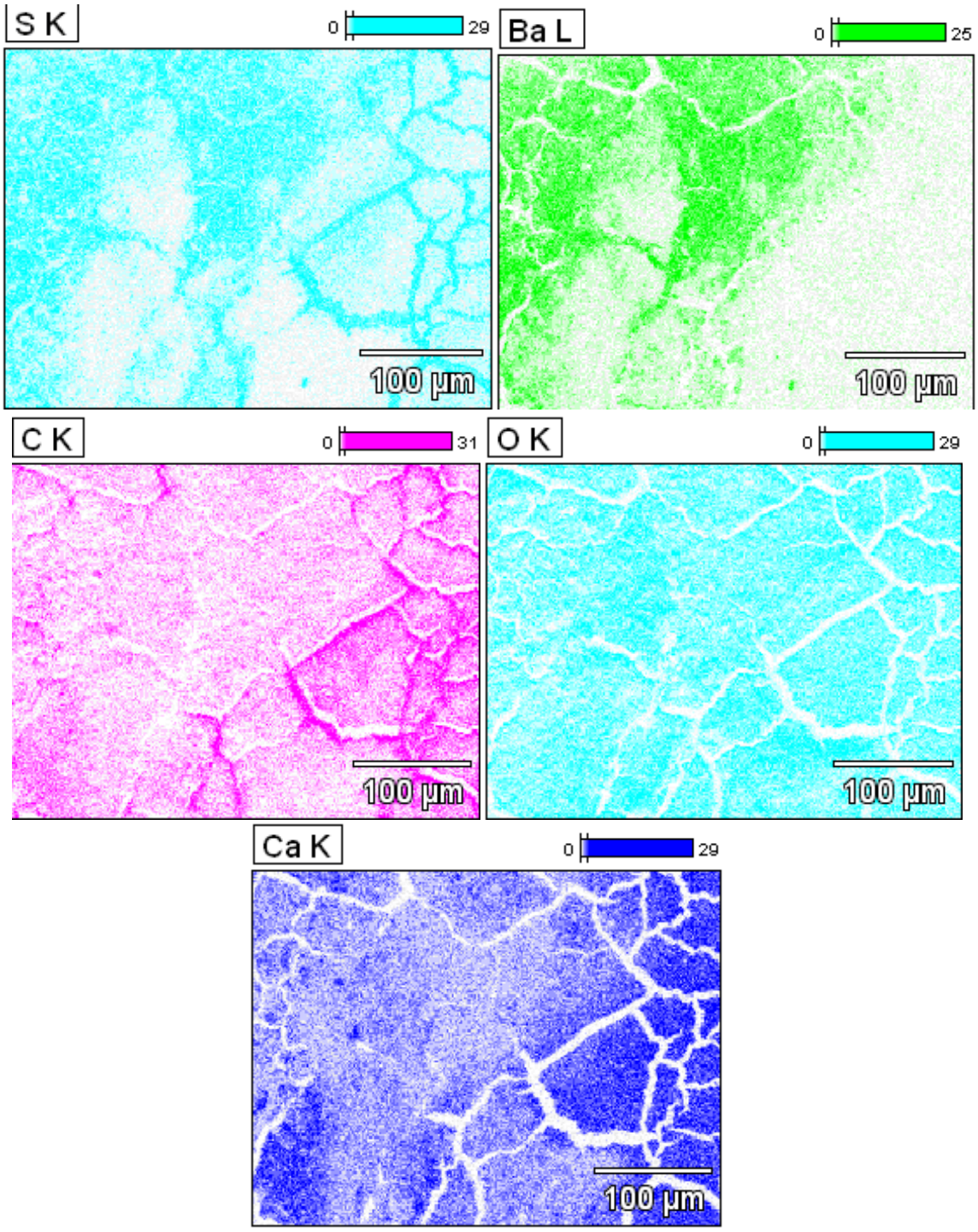

Figure A.3. Element distribution by EDS mapping on an ESPA2 membrane fragment. Notice that sulfur and barium are co-distributed, as are aluminum, potassium, iron and magnesium

XRD Analyses ESPA 2 Reverse Osmosis Membrane

Material scraped from of the tail element membrane of the RO unit was analyzed for mineral content via X-ray diffraction (XRD). The top rectangle of all XRD figures (A.4-A.9) reflects the background corrected graph (baseline normalized to zero), the middle rectangle shows the peaks that are generated from the graph above, and ranked, with 100% peak the largest, and the bottom rectangle represents an International Centre for Diffraction Data (ICDD) data card peak solution. The clays identified were silicon oxide (Figure A.4), potassium aluminum silicate (Figure A.5), sodium magnesium aluminum silicate hydroxide hydrate (Figure A.6) and sodium calcium aluminum silicate (Figure A.7). Additional peaks corresponded to calcium phosphide (Figure A.8) and phosphorus oxide sulfide (Figure A.9). Neither calcite ($CaCO_3$) nor barite ($BaSO_4$) was detected even though barium and sulfur were co-dispersed as shown in corresponding elemental maps (Figure A.3). The sensitivity of the technique was estimated at 5% mass of analyte phase/total mass.

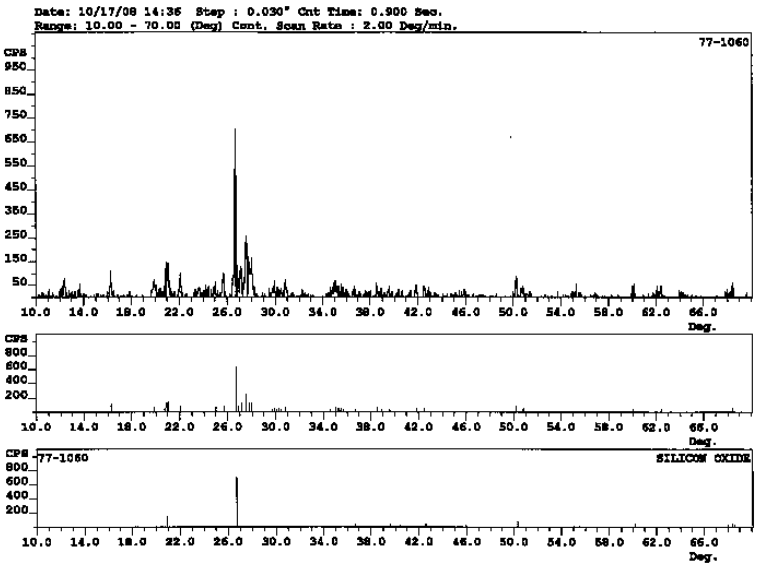

Figure A.4. Silicon oxide peaks in the X-ray diffraction pattern for material scraped from one of the tail elements of ESPA2

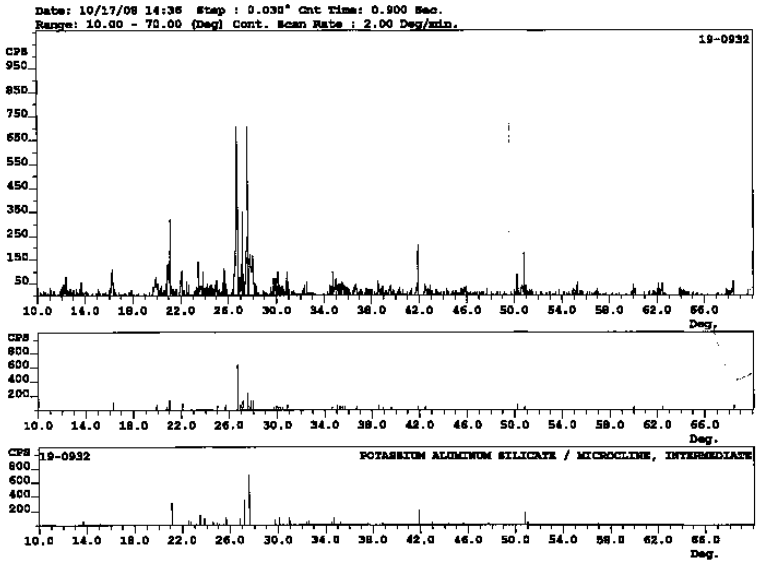

Figure A.5. Potassium Aluminum Silicate peaks in the X-ray diffraction pattern for material scraped from one of the tail elements of ESPA2

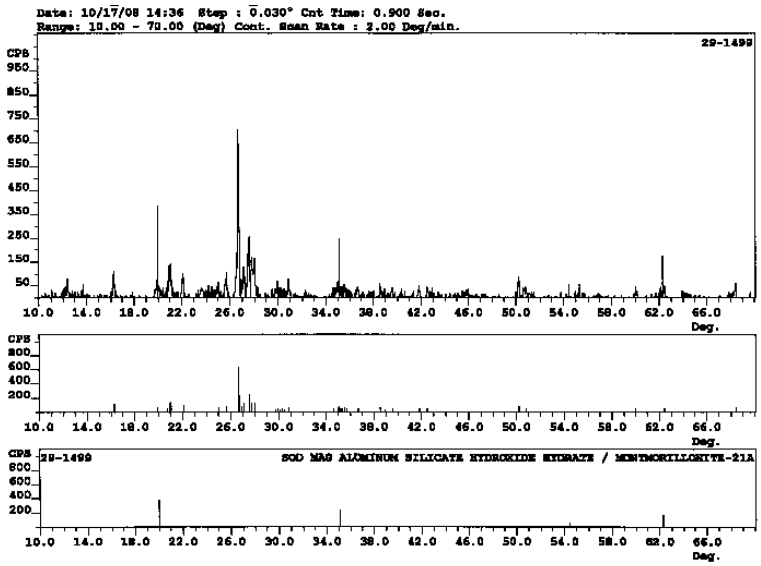

Figure A.6. Sodium magnesium silicate hydroxide hydrate peaks in the X-ray diffraction pattern for material scraped from ESPA2

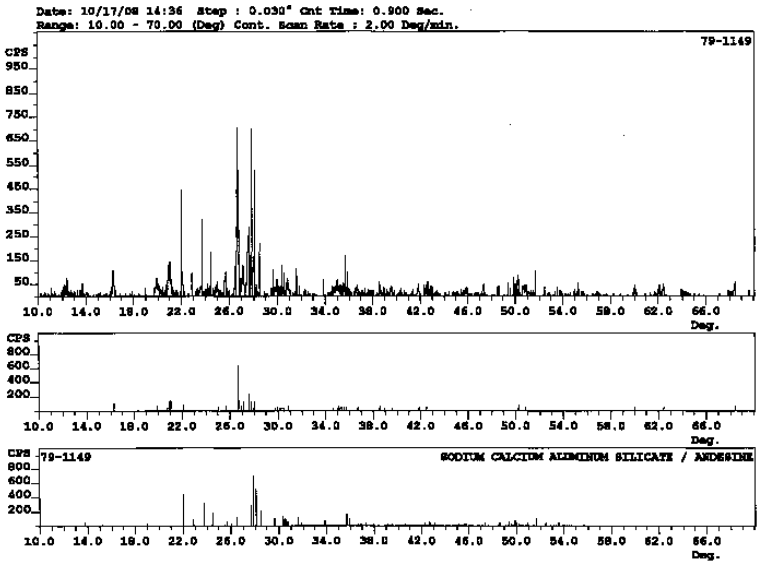

Figure A.7. Sodium calcium aluminum silicate peaks in the X-ray diffraction pattern for material scraped from ESPA2

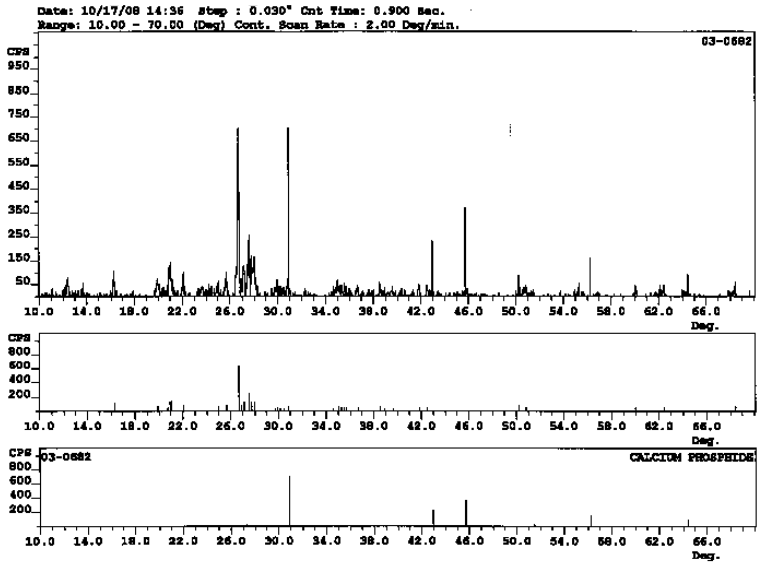

Figure A.8. Calcium phosphide peaks in the X-ray diffraction pattern for material scraped from ESPA2

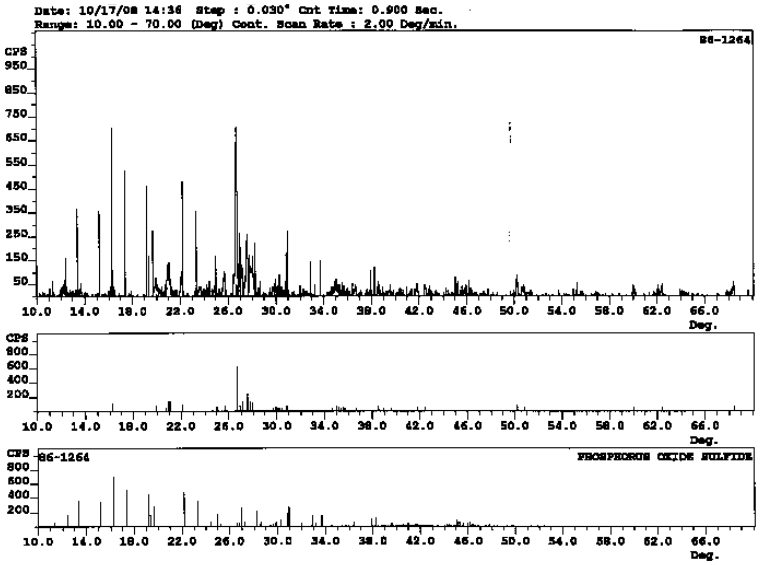

Figure A.9. Phosphorus oxide sulfide peaks in the X-ray diffraction pattern for material scraped from membrane from ESPA2

SEM Analyses of Koch ULP Reverse Osmosis Membrane

Autopsies were also performed on the tail element of the RO unit after operating for 15 months using water pretreated via MF. Corresponding SEM images and results of EDS elemental analyses follow.

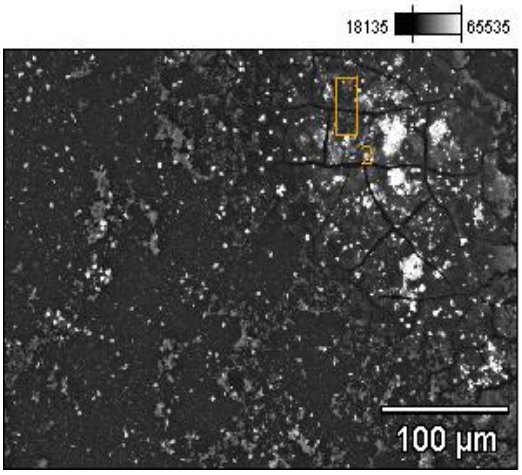

Figure A.10. SEM image of Koch ULP RO membrane fed with SSFs pretreated water. The membrane were in operation for 15 months running at 80% recovery. The rectangle shows the section analyzed via EDS to produce Figure A.11 and Table A.3

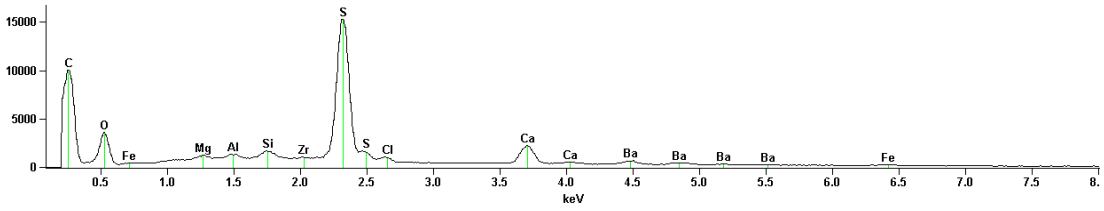

Figure A.11. EDS analysis for the Koch ULP RO membrane fed with MF pretreated water

The fractional elemental compositions (Table A.3) from the EDS analysis (Figure A.11) of the membrane sample suggest that scaling reactions contributed to the loss of

membrane permeability. Barium and sulfur were present in relatively high concentrations on the membrane surface.

Table A.4. Atom Percentage of Major Elements on Koch ULP Membrane

Atom %										
C	O	Mg	Al	Si	S	Cl	Ca	Fe	Zr	Ba
76.02	15.79	0.13	0.13	0.30	5.97	0.22	1.01	0.16	0.00	0.28

Atom % Error ± 2 sigma										
C	O	Mg	Al	Si	S	Cl	Ca	Fe	Zr	Ba
0.64	0.26	0.03	0.02	0.03	0.06	0.03	0.02	0.0.3	0.01	0.02

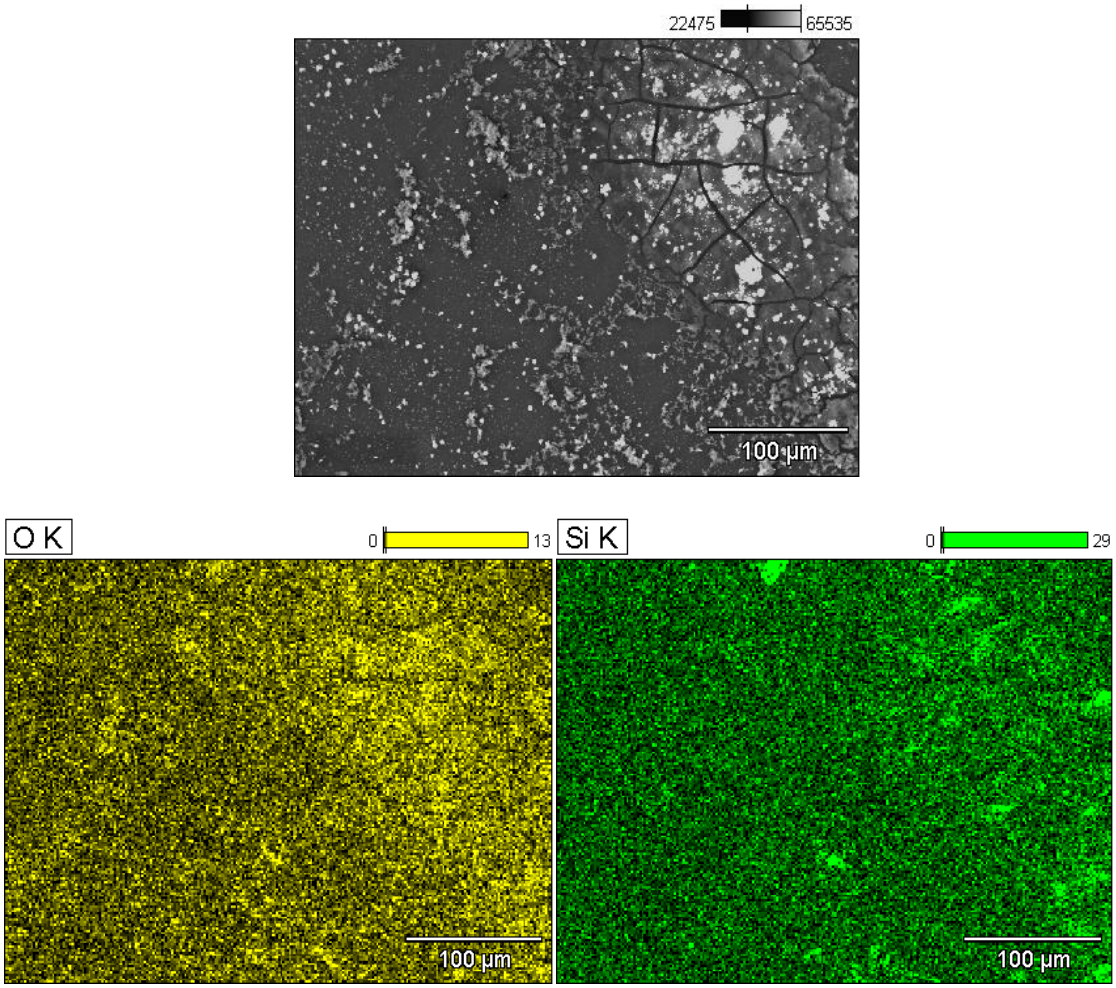

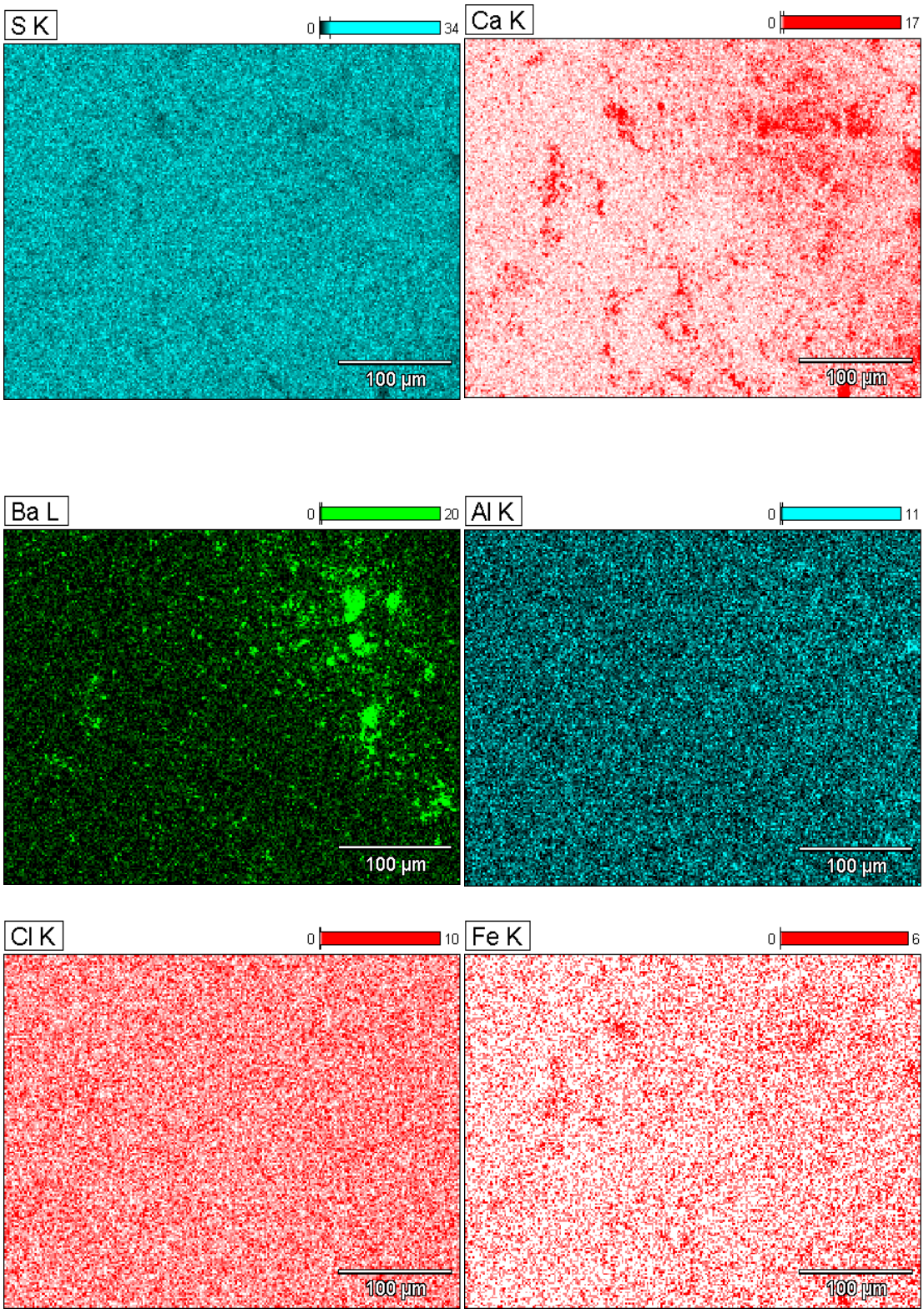
S K
0
34
100 µm
Ca K
0
17
100 µm
Ba L
0
20
100 µm
Al K
0
11
100 µm
Cl K
0
10
100 µm
Fe K
0
6
100 µm

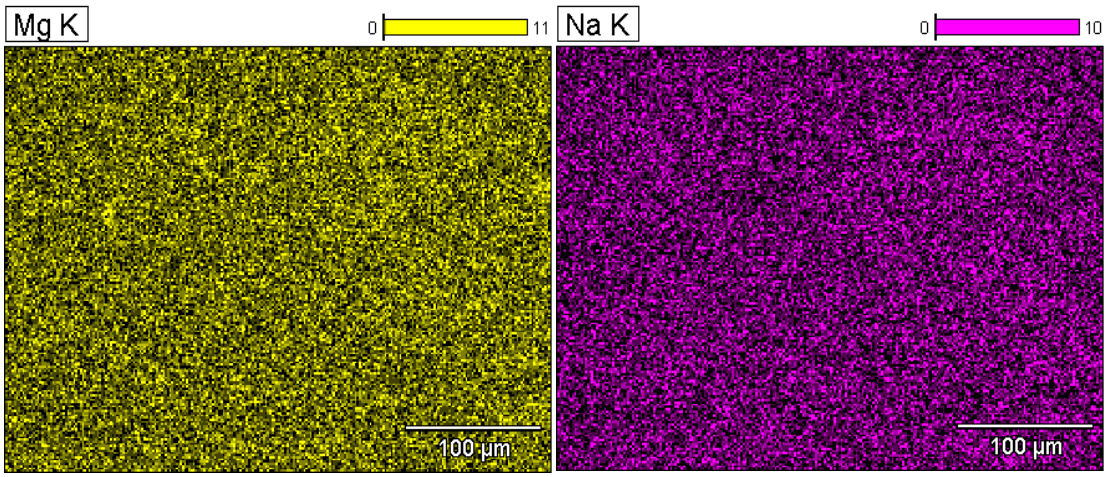

Figure A.12. Element distribution by EDS mapping on Koch ULP membrane surface

XRD Analyses Koch ULP Reverse Osmosis Membrane

Material scraped from the tail element membrane of the RO unit was analyzed for mineral content via XRD as shown in Figures A.13 to A.16. The minerals identified were barium strontium sulfate (Figure A.13), barium sulfate (Figure A.14), barium sulfite (Figure A.15) and silicon oxide (Figure A.16). The sensitivity of the technique was estimated at 5% mass of analyte phase/total mass.

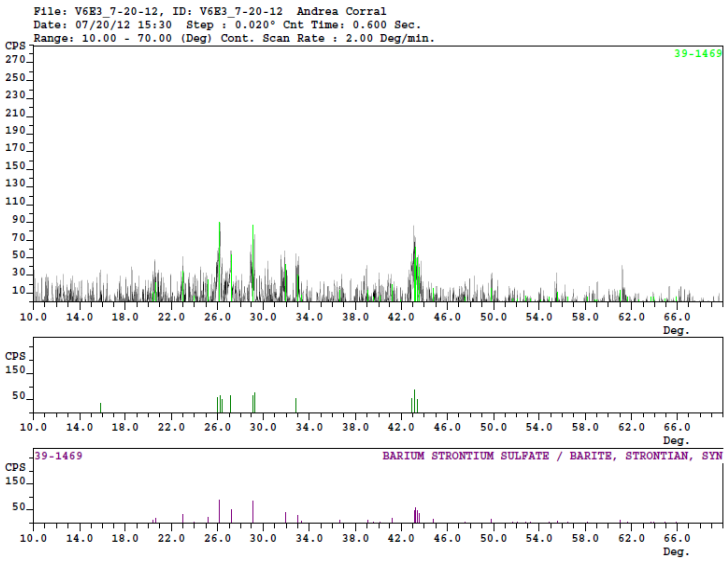

Figure A.13. Barium strontium sulfate peaks in the X-ray diffraction pattern for material scraped from Koch ULP

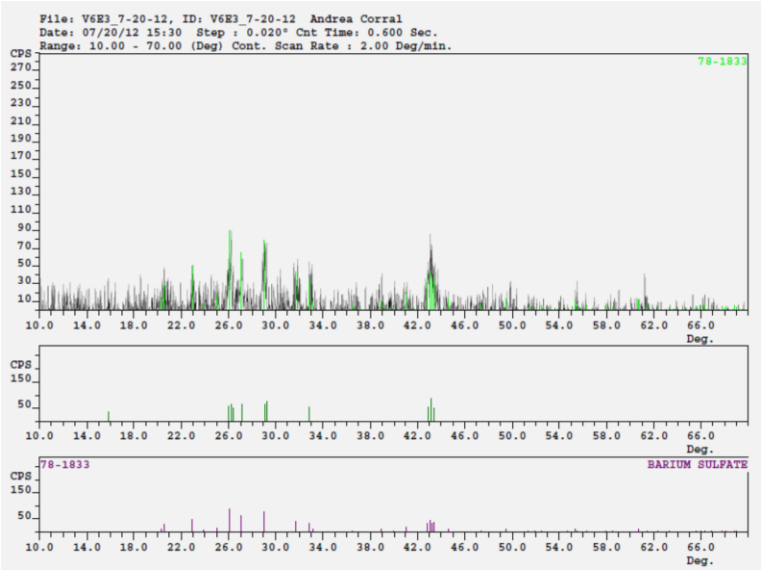

Figure A.14. Barium sulfate peaks in the X-ray diffraction pattern for material scraped from Koch ULP

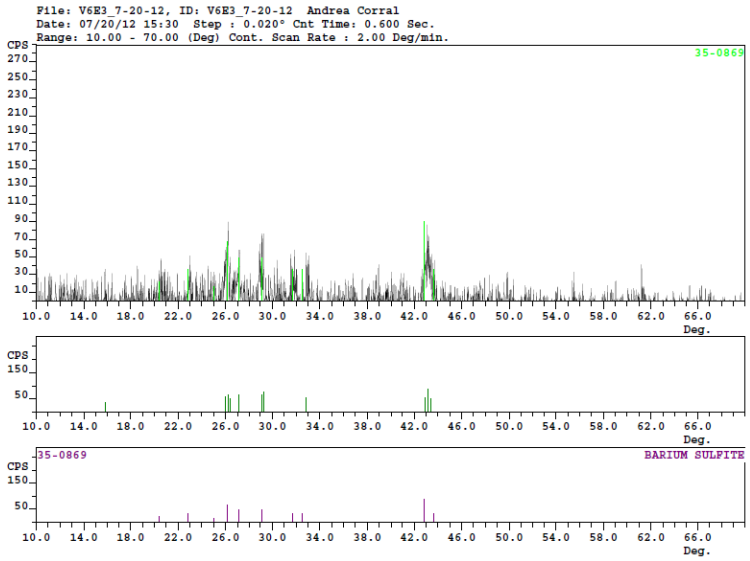

Figure A.15. Barium sulfite peaks in the X-ray diffraction pattern for material scraped from Koch ULP

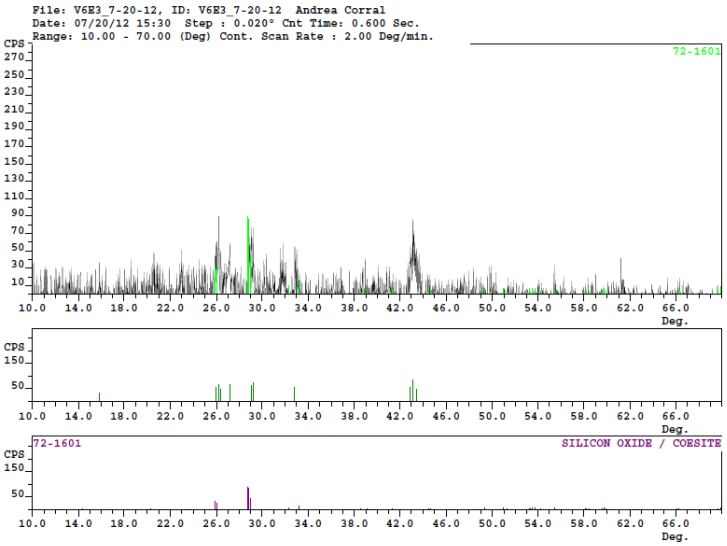

Figure A.16 Silicon oxide peaks in the X-ray diffraction pattern for material scraped from Koch ULP

A.4. Membrane Characteristics

Table A.5. Membrane Characteristics

Manufacturer	Membrane	Max. Operating Pressure [kPa]	Permeate Flow rate [m/d]	Salt Rejection [%]	Active Membrane Area [m^2]
Koch Membranes	TCF – ULP	2415	1.1	98.00	2.5
Hydranautics	ESPA2 2540	2068	1.2	98.0 - 99.4	2.4

For the Koch Membranes the test conditions were: mixed feed with 700 mg/L TDS, of which at least 45% was monovalent, at 760 kPa, 15 % recovery, 25 °C and pH 7 ± 0.5. For the ESPA2 2540 membranes the test conditions were: 1500 mg/L of NaCl solution, at 1034 kPa, 10% recovery, 25°C and pH between 6.5 – 7.0.

APPENDIX B – SUPPLEMENTARY DATA – Economics of Ion Exchange vs. Vibratory Shear Enhanced Processing (VSEP®) For Minimization of Reverse Osmosis Concentrate Volume

The supporting material present in the following document contains the detailed mathematical model and formulas used to calculate the economics of the three scenario different scenarios presented in the paper.

Table B.1. Cost components for Scenario 1 (x is process capacity in mgd)

Item	Basis of Calculation	Assumptions & Explanations	Contribution to Annualized Cost
Capital costs:			
Microfiltration units	$3.011\times10^6 \times (Q_{TP})^{0.872} \times F_{30}$	The capital cost for MF units is adapted from "Cost Estimating Manual for Water Treatment Facilities".	12.3%
RO units	$2.1M\$ \times Q_{TP}\times(R_{RO}/100) \times F_{30}$	Construction cost for two stage RO running at 80% recovery.	12.2%
Disposal of brine cost (augmented evaporation ponds)	$(21.182 \times [Q_{TP} \times (1 - R_{RO}/100)]^{0.953}) \times 1.0M\$ \times F_{30}$	The capital cost curve is adapted from "Technical Memorandum: Evaluation of Water Treatment Options for TDS Control".	25.3%
Energy costs:			
Pumping cost	$Q_{TP} \times (\Sigma\Pi_{RO2R} + \Delta Pnet) \times$ 0.12\$/kWh / 3.6M Nm/kWh × 24hrs/d × 365 days/yr × $(1/P_E)$	The shaft efficiency of the pump is 80% and salt rejection is 100%.	2.7%
O&M Costs:			
O&M Cost for microfiltration	$4.441\times10^5 \times (Q_{TP})^{0.4323}$	O&M cost for MF is linearly related with capital cost of MF.	3.6%
Membrane replacement cost for RO	$[Q_{TP}\times(R_{RO}/100) / J_W] / S \times C_{memb.RO} \times P_{V,3} \times F_{30}$	A single set of membranes lasts for 3 years. 10 sets of membranes are needed.	2.4%
O&M Cost for augmented evaporation ponds	$(1.769 \times [Q_{TP} \times (1 - R_{RO}/100)]^{0.709}) \times 1.0M\$$	The O&M cost curve is adapted from "Technical Memorandum: Evaluation of Water Treatment Options for TDS Control".	22.3%
Personnel cost	$N_P \times 100K\$/yr/personnel$	The personnel works with 8 hours shifts around the clock at the facility.	1.3%
Miscellaneous Costs:			
Water cost due to loss of water	$(C_{w,unit} / 0.33$ Mgal/AF) × $[Q_{TP} \times (1 - R_{RO}/100)] \times 365$days/yr	Unit value of water ($C_{w,unit}$) is 1000\$/AF.	17.9%

Table B.2. Functional relationships used to calculate IX and three-stage RO costs

Item	Basis of Calculation	Assumptions & Explanations	Contribution to Annualized Cost
Capital costs:			
Microfiltration units	$3.011\times10^{6} \times (Q_{TP})^{0.872} \times F_{30}$	The capital cost for MF units is adapted from "Cost Estimating Manual for Water Treatment Facilities" [21].	18.6%
IX units construction cost	$(314{,}215.7Q_{TP} + 655{,}103.9) \times F_{30}$	30-year service life.	3.1%
RO units	$2.1M\$ \times Q_{TP}\times(R_{RO}/100) \times F_{30}$	Construction cost for two stage RO running at 80% recovery [19].	18.3%
Third stage RO units	$2.1M\$ \times Q_{RO3} \times(R_{RO3}/100) \times F_{30}$	Linear relation between the water treated in MGD and the capital cost of RO	4.4%
Disposal of brine cost (augmented evaporation ponds)	$(21.182 \times [Q_{RO3} \times (1 - R_{RO3}/100)]^{0.953}) \times 1.0M\$ \times F_{30}$	The capital cost curve is adapted from "Technical Memorandum: Evaluation of Water Treatment Options for TDS Control" [6].	3.6%
Energy costs:			
Pumping cost	$Q_{TP} \times (\Sigma\Pi_{RO2R} + \Delta Pnet) \times$ 0.12\$/kWh / 3.6M Nm/kWh × 24hrs/d × 365 days/yr $\times (1/P_E)$	The shaft efficiency of the pump is 80% and salt rejection is 100%.	4.0%
Pumping cost (addition to the first two stages of RO)	$Q_{TP} \times \Delta\Pi_{RO1\&2} \times$ 0.12\$/kWh / 3,6M Nm/kWh × 24hrs/d × 365 days/yr	Increase in the concentration of divalent cations due to the operation of IX.	0.05%
Pumping cost (third stage RO)	$Q_{RO3} \times [(J_W / A_{avg}) + (M_{ions\ in\ reject} \times R \times T \times 14.7\ psi/atm)] \times 6894.8$ $((N/m^2)/psi)$ / 3,6M Nm/kWh × 0.12\$/kWh × 24hrs/d × 365 days/yr	It is required to overcome the osmotic pressure at the last element.	6.1%
O&M Costs:			
O&M Cost for microfiltration	$4.441\times10^{5} \times (Q_{TP})^{0.4323}$	O&M cost for MF is linearly related with capital cost of MF.	5.4%
Resin cost	$4{,}240\$/m^3 \times V_{bed} \times P_{V,5} \times F_{30}$	The lifetime of the resin is estimated as 5 years.	2.4%
Regenerant cost	$[(R_{BS} \times MW_{NaCl} \times 10^{-6}\ tons/g) \times N_{RRS} \times C_{NaCl}] + [V_{bed} \times N_{BV} \times N_{NRS} \times \rho_{NaCl} \times 10^{-6}\ tons/g \times C_{NaCl}]$	The regenerant solutions are used 5 times before preparing a new one. During the reuse, salt concentration is topped off.	18.7%
Membrane replacement cost for RO	$([Q_{TP}\times(R_{RO}/100) / J_W] / S) \times C_{memb,RO} \times P_{V,3} \times F_{30}$	A single set of membranes lasts for 3 years. 10 sets of membranes are needed.	4.4%
O&M Cost for augmented evaporation ponds	$(1.769 \times [Q_{RO3} \times (1 - R_{RO3}/100) + Q_{IX,brine}]^{0.709}) \times 1.0M\$$	The O&M cost curve is adapted from "Technical Memorandum: Evaluation of Water Treatment Options for TDS Control" [6].	5.7%
Personnel cost	$N_P \times 100K\$/yr/personnel$	The personnel works with 8 hours shifts around the clock at the facility.	2.8%
Miscellaneous Costs:			
Water cost due to loss of water	$(C_{w,unit} / 0.33\ Mgal/AF) \times [Q_{TP} \times (1 - R_{RO}/100)] \times 365 days/yr$	Unit value of water ($C_{w,unit}$) is 1000\$/AF.	2.2%

*The percent values are presented at the optimum operating conditions of Scenario 2, which supplies 99% overall recovery.

Table B.3. Summary of VSEP related cost functions and contribution to annual cost

Item	Basis of Calculation	Assumptions & Explanations	Contribution to Annualized Cost
Capital costs:			
Microfiltration units	$3.011\times10^{6} \times (Q_{TP})^{0.872} \times F_{30}$	The capital cost for MF units is adapted from "Cost Estimating Manual for Water Treatment Facilities".	17.1%
RO units	$2.1M\$ \times Q_{TP}\times(R_{RO}/100) \times F_{30}$	Construction cost for two stage RO running at 80% recovery.	16.9%
VSEP units	$C_{VSEP} \times N_{VSEP} \times P_{V,10} \times F_{30}$	10-year service life is estimated for each VSEP unit by the manufacturer.	8.8%
Disposal of brine cost (augmented evaporation ponds)	$(21.182 \times [Q_{VSEP} \times (1 - R_{VSEP}/100)]^{0.953}) \times 1.0M\$ \times F_{30}$	The capital cost curve is adapted from "Technical Memorandum: Evaluation of Water Treatment Options for TDS Control".	6.7%
Energy costs:			
Pumping cost for RO	$Q_{TP} \times (\Sigma\Pi_{RO2R} + \Delta Pnet) \times$ 0.12\$/kWh / 3.6M Nm/kWh × 24hrs/d × 365 days/yr × $(1/P_E)$	The shaft efficiency of the pump is 80% and salt rejection is 100%.	3.7%
Pumping cost for VSEP	$[(Q_{VSEP} \times \rho_W \times g \times P_{VSEP})$ / 3.6M j/h/kW] × 0.12\$/kWh × 24hrs/d × 365 days/yr × $(1/P_E)$	The shaft efficiency of the pump is 80%.	4.4%
Vibration cost for VSEP	$P_{vibration} \times N_{VSEP} \times$ 0.12\$/kWh × 24hrs/d × 365 days/yr	Power requirement for vibrating each VSEP unit is supplied as 12 hp by the manufacturer.	2.4%
Cleaning costs for VSEP units:			
Chemical cost	$C_{chem} \times [24hrs/d \times 365days / (\check{T}+T_C)] \times N_{VSEP}$	Cost of chemicals is supplied by manufacturer.	6.0%
Water cost	$[(V_{w,cleaning} \times [24hrs/d \times 365days / (\check{T}+T_C)] \times N_{VSEP}) / 3.3\times10^{5}$ gal/AF] × $C_{w,unit}$	Unit value of water ($C_{w,unit}$) is 1K\$/AF.	0.2%
O&M Costs:			
O&M Cost for microfiltration	$4.441\times10^{5} \times (Q_{TP})^{0.4323}$	O&M cost for MF is linearly related with capital cost of MF.	5.0%
Membrane replacement cost for RO	$[Q_{TP}\times(R_{RO}/100) / J_W] / S \times C_{memb.RO} \times P_{V,3} \times F_{30}$	A single set of membranes lasts for 3 years. 10 sets of membranes are needed.	3.3%
Membrane replacement cost for VSEP	$C_{memb.VSEP} \times N_{VSEP} \times P_{V,2} \times F_{30}$	A single set of membranes lasts for 2 years. 15 sets of membranes are needed.	9.9%
O&M Cost for augmented evaporation ponds	$(1.769 \times [Q_{VSEP} \times (1 - R_{VSEP}/100)]^{0.709}) \times 1.0M\$$	The O&M cost curve is adapted from "Technical Memorandum: Evaluation of Water Treatment Options for TDS Control".	9.0%
Personnel cost	$N_P \times 100K\$/yr/personnel$	The personnel works with 8 hours shifts around the clock at the facility.	2.2%
Miscellaneous Costs:			
Water cost due to loss of water	$(C_{w,unit}$ / 0.33 Mgal/AF) × $[Q_{VSEP} \times (1 - R_{VSEP}/100)] \times 365days/yr$	Unit value of water ($C_{w,unit}$) is 1K\$/AF.	4.4%

Abbreviations for Tables B.1 – B.3

$\Delta\Pi_{RO1\&2}$	sum of all divalent cation concentrations that get replaced by sodium ions
$\Sigma\Pi_{RO2R}$	total osmotic pressure of the sum of all major ions concentrations in the reject stream of the second stage RO, psi
ρ_{NaCl}	concentration of NaCl for the regenerant solution, g/L
ΔP_{net}	net pressure needs to be overcome to produce the desired amount of water flux, psi
ρ_W	density of water, kg/m^3
A_{avg}	average water transport coefficient, m/s.Pa (gfd/psi)
C_{chem}	chemical cost, $/cleaning
$C_{memb,VSEP}$	cost of single set of VSEP membranes, $/set
$C_{memb.RO}$	cost of single set of RO membranes, $/set
C_{NaCl}	cost of NaCl, $/ton
C_{VSEP}	capital cost of each VSEP unit, $/unit
$C_{w,unit}$	unit value of water, $/AF
F_{30}	annuity factor for 30 years
g	gravitational acceleration, m/s^2
IX	ion exchange
J_W	average water flux, gfd
$M_{ions\ in\ reject}$	total ion concentration in the reject of third stage RO, mol/L
MW_{NaCl}	molecular weight of sodium chloride, g/mol
N_{BV}	number of bed volumes needed for each regeneration cycle

N_{NRS}	number of times new regenerant solution is prepared in a year
N_P	number of personnel working around the clock
N_{RRS}	number of times regenerant solution is reused in a year
N_{VSEP}	number of VSEP units
P_E	pump efficiency
PV	conversion factor for present value
$P_{V,n}$	annuity immediate factor, n = number of years
$P_{vibration}$	power for vibration for each VSEP unit, hp
P_{VSEP}	operating pressure of VSEP, psi
$Q_{IX,brine}$	volume of regenerant solution disposed into the evaporation pond, MGD
Q_{RO3}	feed flow for third stage RO, MGD
Q_{TP}	treatment plant flow rate, MGD
Q_{VSEP}	VSEP flow rate, MGD
R	ideal gas constant, $L.atm.mol^{-1}.K^{-1}$
R_{BS}	total number of binding sites on the resin in the amount of V_{bed}
RO	reverse osmosis
R_{RO2}	2-stage RO recovery, %
R_{RO3}	third stage RO recovery, %
R_{VSEP}	VSEP recovery, %
S	single membrane area, ft^2
T	temperature, K
$\breve{T}$	VSEP operating time between each cleaning, hr
T_C	VSEP cleaning time, hr

V_{bed}	total resin volume used in the IX columns, m^3
VSEP	vibratory shear enhance processing
$V_{w,cleaning}$	volume of water used for each VSEP cleaning, gal

REFERENCES

[1] B.D. Richter, D. Abell, E. Bacha, K. Brauman, S. Calos, A. Cohn, C. Disla, S.F. O'Brien, D. Hodges, S. Kaiser, M. Loughran, C. Mestre, M. Reardon, E. Siegfried, Tapped out: how can cities secure their water future?, Water Policy, 15 (2013) 335-363.

[2] P. World Water Assessment, Water for people, water for life a joint report by the twenty three UN agencies concerned with freshwater, in, UNESCO Pub. : Berghahn Books, New York, 2003.

[3] E.H. Oelkers, J.G. Hering, C. Zhu, Water: Is There a Global Crisis?, Elements, 7 (2011) 157-162.

[4] W.R. Bidlack, W. Wang, R. Clemens, Water: The world's most precious resource, Journal of Food Science, 69 (2004) R55-R60.

[5] D.I.W.M.I.C.A.o.W.M.i.A. Molden, Water for food, water for life : a comprehensive assessment of water management in agriculture, Earthscan, London; Sterling, VA, 2007.

[6] U.N. Water, Water For Food, in: U. Nations (Ed.), 2013.

[7] J.M. Tarjuelo, J.A. De-Juan, M.A. Moreno, J.F. Ortega, Review. Water resources deficit and water engineering, Spanish Journal of Agricultural Research, 8 (2010) S102-S121.

[8] L. Horrigan, R.S. Lawrence, P. Walker, How sustainable agriculture can address the environmental and human health harms of industrial agriculture, Environmental Health Perspectives, 110 (2002) 445-456.

[9] M. Brewer, Current U.S. Drought Monitor, in: Monthly, 2013.

[10] A. Al-Karaghouli, L.L. Kazmerski, Energy consumption and water production cost of conventional and renewable-energy-powered desalination processes, Renewable & Sustainable Energy Reviews, 24 (2013) 343-356.

[11] T. Younos, The Economics of Desalination, Journal of Contemporary Water Research & Education, 132 (2005) 39-45.

[12] R. Hochstrat, T. Wintgens, C. Kazner, T. Melin, J. Gebel, Options for water scarcity and drought management-the role of desalination, Desalination and Water Treatment, 18 (2010) 96-102.

[13] M.S. El-Bourawi, Z. Ding, R. Ma, M. Khayet, A framework for better understanding membrane distillation separation process, Journal of Membrane Science, 285 (2006) 4-29.

[14] L.M. Camacho, L. Dumee, J. Zhang, J.-d. Li, M. Duke, J. Gomez, S. Gray, Advances in Membrane Distillation for Water Desalination and Purification Applications, Water, 5 (2013) 94-196.

[15] M. Khayet, Membranes and theoretical modeling of membrane distillation: A review, Advances in Colloid and Interface Science, 164 (2011) 56-88.

[16] A. Kullab, A. Martin, Membrane distillation and applications for water purification in thermal cogeneration plants, Separation and Purification Technology, 76 (2011) 231-237.

[17] S. Ben Abdallah, N. Frikha, S. Gabsi, Simulation of solar vacuum membrane distillation unit, Desalination, 324 (2013) 87-92.

[18] M. Khayet, M.P. Godino, J.I. Mengual, Possibility of nuclear desalination through various membrane distillation configurations: a comparative study, International Journal of Nuclear Desalination, 1 (2003) 30-46.

[19] R. Sarbatly, C.-K. Chiam, Evaluation of geothermal energy in desalination by vacuum membrane distillation, Applied Energy, 112 (2013) 737-746.

[20] P.K. Tewari, R.K. Verma, B.M. Misra, H.K. Sadhukhan, Iaea, Iaea, Low temperature vacuum evaporation process for sea water desalination using waste heat from PHWRs, in: Nuclear Desalination of Sea Water, Int Atomic Energy Agency, Vienna, 1997, pp. 307-313.

[21] A. Zrelli, B. Chaouchi, S. Gabsi, Simulation of vacuum membrane distillation coupled with solar energy: Optimization of the geometric configuration of a helically coiled fiber, Desalination and Water Treatment, 36 (2011) 41-49.

[22] E. Curcio, E. Drioli, Membrane distillation and related operations - A review, Sep. Purif. Rev., 34 (2005) 35-86.

[23] K.W. Lawson, D.R. Lloyd, Membrane distillation, Journal of Membrane Science, 124 (1997) 1-25.

[24] A.M. Alklaibi, N. Lior, Membrane-distillation desalination: status and potential, Desalination, 171 (2005) 111-131.

[25] H. Susanto, Towards practical implementations of membrane distillation, Chemical Engineering and Processing: Process Intensification, 50 (2011) 139-150.

[26] A. Alkhudhiri, N. Darwish, N. Hilal, Membrane distillation: A comprehensive review, Desalination, 287 (2012) 2-18.

[27] A. Criscuoli, P. Bafaro, E. Drioli, Vacuum membrane distillation for purifying waters containing arsenic, Desalination, 323 (2013) 17-21.

[28] M.S.M.T. Khayet, Membrane distillation principles and applications, in, Elsevier, Amsterdam; Boston, 2011.

[29] K.W. Lawson, D.R. Lloyd, Membrane distillation .1. Module design and performance evaluation using vacuum membrane distillation, Journal of Membrane Science, 120 (1996) 111-121.

[30] J.C. Crittenden, Montgomery Watson Harza (Firm), MWH's water treatment principles and design, in, John Wiley & Sons, Hoboken, N.J., 2012, pp. 1 online resource (xviii, 1901 p.).

[31] L. Malaeb, G.M. Ayoub, Reverse osmosis technology for water treatment: State of the art review, Desalination, 267 (2011) 1-8.

[32] C. Fritzmann, J. Lowenberg, T. Wintgens, T. Melin, State-of-the-art of reverse osmosis desalination, Desalination, 216 (2007) 1-76.

[33] R.W. Baker, Membrane technology and applications, in, J. Wiley, Chichester; New York, 2004.

[34] L. Huisman, W.E. Wood, Slow sand filtration, World Health Organization; sold by Q Corp., Geneva Albany, 1974.

[35] M.L. Weber-Shirk, R.I. Dick, Biological mechanisms in slow sand filters, American Water Works Association Journal, 89 (1997) 72-83.

[36] M.L. Weber-Shirk, R.I. Dick, Physical-chemical mechanisms in slow sand filters, American Water Works Association Journal, 89 (1997) 87-100.

[37] C.-K. Chiam, R. Sarbatly, Vacuum membrane distillation processes for aqueous solution treatment-A review, Chemical Engineering and Processing, 74 (2013) 27-54.

[38] A.C. Sun, W. Kosar, Y. Zhang, X. Feng, Vacuum membrane distillation for desalination of water using hollow fiber membranes, Journal of Membrane Science, 455 (2014) 131-142.

[39] B. Li, K.K. Sirkar, Novel membrane and device for vacuum membrane distillation-based desalination process, Journal of Membrane Science, 257 (2005) 60-75.

[40] A. Criscuoli, M.C. Carnevale, E. Drioli, Modeling the performance of flat and capillary membrane modules in vacuum membrane distillation, Journal of Membrane Science, 447 (2013) 369-375.

[41] E. Drioli, A. Ali, S. Simone, F. Macedonio, S.A. Al-Jlil, F.S. Al Shabonah, H.S. Al-Romaih, O. Al-Harbi, A. Figoli, A. Criscuoli, Novel PVDF hollow fiber membranes for vacuum and direct contact membrane distillation applications, Separation and Purification Technology, 115 (2013) 27-38.

[42] M. Khayet, T. Matsuura, Preparation and Characterization of Polyvinylidene Fluoride Membranes for Membrane Distillation, Industrial & Engineering Chemistry Research, 40 (2001) 5710-5718.

[43] L.Z. Zhang, An Analytical Solution to Heat and Mass Transfer in Hollow Fiber Membrane Contactors for Liquid Desiccant Air Dehumidification, J. Heat Transf.-Trans. ASME, 133 (2011) 8.

[44] T.K. Sherwood, R.L. Pigford, Absorption and extraction, McGraw-Hill, New York, 1952.

[45] G.A. Mannella, V. La Carrubba, V. Brucato, Evaluation of vapor mass transfer in various membrane distillation configurations: an experimental study, Heat and Mass Transfer, 48 (2012) 945-952.

[46] Z. Jianhua, L. Jun-De, M. Duke, H. Manh, X. Zongli, A. Groth, T. Chan, S. Gray, Influence of module design and membrane compressibility on VMD performance, Journal of Membrane Science, 442 (2013) 31-38.

[47] Z. Jianhua, L. Jun-De, M. Duke, H. Manh, X. Zongli, A. Groth, T. Chan, S. Gray, Modelling of vacuum membrane distillation, Journal of Membrane Science, 434 (2013) 1-9.

[48] M. Khayet, T. Matsuura, Vacuum Membrane Distillation, 2011.

[49] H. Fan, Y. Peng, Application of PVDF membranes in desalination and comparison of the VMD and DCMD processes, Chemical Engineering Science, 79 (2012) 94-102.

[50] J.-P. Mericq, S. Laborie, C. Cabassud, Vacuum membrane distillation of seawater reverse osmosis brines, Water Research, 44 (2010) 5260-5273.

[51] J.I. Mengual, M. Khayet, M.P. Godino, Heat and mass transfer in vacuum membrane distillation, International Journal of Heat and Mass Transfer, 47 (2004) 865-875.

[52] X. Wang, L. Zhang, H. Yang, H. Chen, Feasibility research of potable water production via solar-heated hollow fiber membrane distillation system, Desalination, 247 (2009) 403-411.

[53] G.C. Sarti, C. Gostoli, S. Bandini, Extraction of Organic-Components from Aqueous Streams by Vacuum Membrane Distillation, Journal of Membrane Science, 80 (1993) 21-33.

[54] M. Gryta, M. Tomaszewska, A.W. Morawski, Membrane distillation with laminar flow, Separation and Purification Technology, 11 (1997) 93-101.

[55] F. Banat, F. Abu Al-Rub, K. Bani-Melhem, Desalination by vacuum membrane distillation: sensitivity analysis, Separation and Purification Technology, 33 (2003) 75-87.

[56] T. Mohammadi, M.A. Safavi, Application of Taguchi method in optimization of desalination by vacuum membrane distillation, Desalination, 249 (2009) 83-89.

[57] M. Safavi, T. Mohammadi, High-salinity water desalination using VMD, Chemical Engineering Journal, 149 (2009) 191-195.

[58] W.S. National Research Council, N.R.C.C.o.t.S.B.o.C.R.B.W.M. Technology Board, Colorado River Basin water management evaluating and adjusting to hydroclimatic variability, in, National Academies Press, Washington, D.C., 2007.

[59] U.S.D.o.t.I.B.o. Reclamation, Colorado River Basin Water Supply and Demand Study in: C.R.B.W.S.a.D.S.S. Team (Ed.), Phoenix, 2001.

[60] U.S.D.o.t.I.B.o. Reclamation, Quality of Water Colorado River Basin, in, Phoenix, 2005.

[61] R.G. Arnold, K.P. Arnold, Integrated Urban Water Management in the Tucson, Arizona Metropolitan Area, in: L. Mays (Ed.) Integrated urban water management : arid and semi-arid regions, CRC Press UNESCO Pub., Boca Raton, USA Paris, France, 2009, pp. 113-138.

[62] E.P. Agency, Drinking Water Contaminants, in, 2013.

[63] U.S.D.o.t.I.B.o. Reclamation, Central Arizona Salinity Study, Phase II - Salinity Control in Waste Water Treatment Plants, in, Phoenix, 2006.

[64] C.D. Moody, B. Garret, F.E. Holler, Pilot Investigation of Slowsand Filtration and Reverse Osmosis Treatment of Central Arizona Project Water, in, Phoenix, 2002.

[65] X. Zheng, M. Ernst, M. Jekel, Pilot-scale investigation on the removal of organic foulants in secondary effluent by slow sand filtration prior to ultrafiltration, Water Research, 44 (2010) 3203-3213.

[66] X. Zheng, R. Mehrez, M. Jekel, M. Ernst, Effect of slow sand filtration of treated wastewater as pre-treatment to UF, Desalination, 249 (2009) 591-595.

[67] C.D. Moody, M.D. Norris, F.E. Holler, C.H. McCaughey, Evaluation of Slow Sand Filtration for Reducing Costs of Desalination by Reverse Osmosis, in, Phoenix, 2007, pp. 1-10.

[68] J.P. van der Hoek, J. Hofman, P.A.C. Bonne, M.M. Nederlof, H.S. Vrouwenvelder, RO treatment: selection of a pretreatment scheme based on fouling characteristics and operating conditions based on environmental impact, Desalination, 127 (2000) 89-101.

[69] M. Abdel-Jawad, E.E.F. El-Sayed, S. Ebrahim, A. Al-Saffar, M. Safar, M. Tabtabaei, G. Al-Nuwaibit, Fifteen years of R&D program in seawater desalination at KISR Part II. RO system performance, Desalination, 135 (2001) 155-167.

[70] S. Ebrahim, M. Abdel-Jawad, S. Bou-Hamad, M. Safar, Fifteen years of R&D program in seawater desalination at KISR Part I. Pretreatment technologies for RO systems, Desalination, 135 (2001) 141-153.

[71] M. Karime, S. Bouguecha, B. Hamrouni, RO membrane autopsy of Zarzis brackish water desalination plant, Desalination, 220 (2008) 258-266.

[72] G.K. Pearce, The case for UF/MF pretreatment to RO in seawater applications, Desalination, 203 (2007) 286-295.

[73] G.K. Pearce, UF/MF pre-treatment to RO in seawater and wastewater reuse applications: a comparison of energy costs, Desalination, 222 (2008) 66-73.

[74] N. Prihasto, Q.-F. Liu, S.-H. Kim, Pre-treatment strategies for seawater desalination by reverse osmosis system, Desalination, 249 (2009) 308-316.

[75] J.A. Redondo, Brackish-, sea- and wastewater desalination, Desalination, 138 (2001) 29-40.

[76] D. Vial, G. Doussau, The use of microfiltration membranes for seawater pre-treatment prior to reverse osmosis membranes, Desalination, 153 (2003) 141-147.

[77] R.W. Baker, NetLibrary Inc., Membrane technology and applications, in, J. Wiley, Chichester ; New York, 2004, pp. x, 538 p.

[78] A.D.o.W.R.T.A.M. Area, Third management plan, 2000-2010 : Tucson Active Management Area, Arizona Dept. of Water Resources, Phoenix, Ariz., 1999.

[79] M.M. Benjamin, Water chemistry, McGraw-Hill, Boston, 2002.

[80] W.M.L.D.R. Haynes, CRC handbook of chemistry and physics : a ready-reference book of chemical and physical data, CRC ; Taylor & Francis [distributor], Boca Raton, Fla.; London, 2010.

[81] O.N.I.S. Inc., Cost of Silica Sand Filter Media ES 0.27 - 0.33 mm UC 1.7, in, 2006.

[82] A.D.o.E. Quality, Guidelines for the Construction fo Water Systems, in, Phoenix, AZ, 1978.

[83] M. Group, 3M10C CMF Unit Operation and Maintenance Manual, in, 1997.

[84] S.G. Yiantsios, A.J. Karabelas, An assessment of the Silt Density Index based on RO membrane colloidal fouling experiments with iron oxide particles, Desalination, 151 (2003) 229-238.

[85] A. Alhadidi, A.J.B. Kemperman, J.C. Schippers, B. Blankert, M. Wessling, W.G.J. van der Meer, SDI normalization and alternatives, Desalination, 279 (2011) 390-403.

[86] A. Alhadidi, A.J.B. Kemperman, B. Blankert, J.C. Schippers, M. Wessling, W.G.J. van der Meer, Silt Density Index and Modified Fouling Index relation, and effect of pressure, temperature and membrane resistance, Desalination, 273 (2011) 48-56.

[87] R.G.N.J.D.C.M.R. Gimbel, Recent progress in slow sand and alternative biofiltration processes, IWA Pub., London, 2006.

[88] W.H.O.I.R.C.f.C.W. Supply, Slow sand filtration for community water supply in developing countries : a selected and annotated bibliography, The Centre, Voorburg (The Hague), the Netherlands, 1977.

[89] T. Grogan, Construction Cost IndexBuilding Cost IndexMaterials Cost IndexIndex Review, in, 2013, pp. Construction Economics; Pg. 71.

[90] Z. Donohew, Property rights and western United States water markets, Australian Journal of Agricultural and Resource Economics, 53 (2009) 85-103.

[91] L.F. Greenlee, D.F. Lawler, B.D. Freeman, B. Marrot, P. Moulin, Reverse osmosis desalination: Water sources, technology, and today's challenges, Water Research, 43 (2009) 2317-2348.

[92] R.P. Schneider, L.M. Ferreira, P. Binder, J.R. Ramos, Analysis of foulant layer in all elements of an RO train, Journal of Membrane Science, 261 (2005) 152-162.

[93] L.D. Nghiem, A.I. Schäfer, Fouling autopsy of hollow-fibre MF membranes in wastewater reclamation, Desalination, 188 (2006) 113-121.

[94] M. Pontié, A. Thekkedath, K. Kecili, H. Habarou, H. Suty, J.P. Croué, Membrane autopsy as a sustainable management of fouling phenomena occurring in MF, UF and NF processes, Desalination, 204 (2007) 155-169.

[95] M. Herzberg, M. Elimelech, Biofouling of reverse osmosis membranes: Role of biofilm-enhanced osmotic pressure, Journal of Membrane Science, 295 (2007) 11-20.

[96] T. Tran, B. Bolto, S. Gray, M. Hoang, E. Ostarcevic, An autopsy study of a fouled reverse osmosis membrane element used in a brackish water treatment plant, Water Research, 41 (2007) 3915-3923.

[97] M. Pontié, S. Rapenne, A. Thekkedath, J. Duchesne, V. Jacquemet, J. Leparc, H. Suty, Tools for membrane autopsies and antifouling strategies in seawater feeds: a review, Desalination, 181 (2005) 75-90.

[98] R.A. Al-Juboori, T. Yusaf, Biofouling in RO system: Mechanisms, monitoring and controlling, Desalination, 302 (2012) 1-23.

[99] T. Darton, U. Annunziata, F. del Vigo Pisano, S. Gallego, Membrane autopsy helps to provide solutions to operational problems, Desalination, 167 (2004) 239-245.

[100] E.M.V. Hoek, J. Allred, T. Knoell, B.-H. Jeong, Modeling the effects of fouling on full-scale reverse osmosis processes, Journal of Membrane Science, 314 (2008) 33-49.

[101] A. Plottu, B. Houssais, C. Democrate, D. Gatel, J. Cavard, Autopsies of membranes fouled on Mery-sur-Oise pilot units: Many lessons for the behaviour of the water treatment plant, Desalination, 157 (2003) 367.

[102] Y. Zhao, L. Song, S.L. Ong, Fouling of RO membranes by effluent organic matter (EfOM): Relating major components of EfOM to their characteristic fouling behaviors, Journal of Membrane Science, 349 (2010) 75-82.

[103] Arizona Land and Water Trust, Citron A. , G. D., Benefiting Landowners and Desert Rivers: A Water Rights Handbook for Conservation Agreements in Arizona, in, Arizona Land and Water

Trust, 2009.

[104] J. Gelt, Water in the Tucson area : seeking sustainability : a status report, Water Resources Research Center, Tucson, A, 1999.

[105] C.o.T.W. Department, Water Plan: 2000-2050, Final Report, in, Tucson, AZ, 2004.

[106] P.D.W. Barnett Tp, Sustainable water deliveries from the Colorado River in a changing climate, Proceedings of the National Academy of Sciences of the United States of America, 106 (2009) 7334-7338.

[107] M.P. Inc.;, S.P. Inc., Evaluation for Water Treatment Options for TDS Control, Draft Technical Memorandum, in, , , Tempe, AZ, 2008.

[108] D.o.W.R.T.A.M.A. Arizona, Third management plan, 2000-2010 : Tucson Active Management Area, Arizona Dept. of Water Resources, Phoenix, Ariz., 1999.

[109] Hydranautics, Design Limits, in, 2001.

[110] Hydranautics, Membrane Characteristics, (2001).

[111] R.Y.K.W.Y. Bian, The effect of shear rate on controlling the concentration polarization and membrane fouling, DESALINATION, 131 (2000) 225-236.

[112] I.R. New Logic Research, Vibratory Shear Enhanced Processing VSEP, in, 2001.

[113] I.R. New Logic Research, 404–Acidic Liquid Membrane Cleaner & Cleaning instructions, in.

[114] I.R. New Logic Research, 505–Alkaline Liquid Membrane Cleaner & Cleaning instructions, in.

[115] Z. Amjad, Applications of antiscalants to control calcium sulfate scaling in reverse osmosis systems, DES</cja:jid> Desalination, 54 (1985) 263-276.

[116] A.L.J.H.G.S.C.A.E.L.-C.P.L.G. Antony, Scale formation and control in high pressure membrane water treatment systems: A review, Journal of Membrane Science, 383 (2011) 1-16.